Aggregate Structures and Magnetorheological Characteristics of a Suspension Composed of Magnetic Cubic Particles (Monte Carlo and Brownian Dynamics Simulations)

キューブ状磁性粒子分散系の凝集構造と磁気粘性効果 (モンテカルロおよびブラウン動力学シミュレーション)

Kazuya Okada

Akita Prefectural University

March 2021

This page intentionally left blank.

Contents

Nomenclature

a	:	radius of a sphere
d	:	side length of a cube
d_{center}, d_{edge}, d_{corner}	:	three diameters for the sphere-connected model
d_{ia}	:	diameter of a sphere i_a
D^T, D^R	:	translational and rotational diffusion coefficients
$\boldsymbol{e}_1$, $\boldsymbol{e}_2$, $\boldsymbol{e}_3$	:	three plane direction vectors of a cubic particle
$\boldsymbol{e}_{\perp 1}(t)$, $\boldsymbol{e}_{\perp 2}(t)$	:	orthogonal unit vectors normal to the magnetic moment of a cubic particle
$f_{o.c.}^{(e)}(r)$	:	orientational pair correlation function
$\boldsymbol{F}$	:	force acting on the ambient fluid by a particle
$\boldsymbol{F}^P$	:	force acting on a particle
$\boldsymbol{F}_{ij}^{(m)}$	:	magnetic force due to the magnetic particle-particle interaction
$\boldsymbol{F}^{(V)}$, $\boldsymbol{F}_{ij}^{(V)}$, $\boldsymbol{F}_{iajb}^{(V)}$	:	repulsive force due to the overlap of steric layers
$g(r)$	:	radial distribution function
$\boldsymbol{h}$	:	unit vector of a magnetic field $\boldsymbol{H}$
$\boldsymbol{H}$	:	external magnetic field
$\boldsymbol{I}$	:	unit tensor
k	:	Boltzmann's constant
L_x, L_y, L_z	:	size of a simulation region in each axis direction
$\boldsymbol{m}$	:	magnetic moment of a particle
$\boldsymbol{n}$	:	unit vector of a magnetic moment $\boldsymbol{m}$
$\hat{\boldsymbol{n}}$	:	unit projection vector of a magnetic moment

n_s	:	number of surfactant molecules per unit area
n_0	:	particle number density
N	:	total number of particles
N_{pair}	:	number of pairs of particles
N_s	:	number of clusters for describing a cluster size distribution
N_{smplmx}	:	total MC steps for a MC simulation
N_{sph}	:	number of spherical particles per cube side for Donaldson model
N_{timemx}	:	total number of time steps per simulation run for BD simulation
N_{up}, N_{dwn}	:	number of particles with upward and downward pointing magnetic moments
Pe	:	Peclet number
$P_2(-)$	:	second Legendre polynomial
$P_4(-)$	:	fourth Legendre polynomial
r	:	radial distance for a radial distribution function $g(r)$
r_{coff}	:	cutoff distance
r_{clstr}	:	criterion distance for the assessment of cluster formation
$\boldsymbol{r}_i$	:	position vector of particle i
$\boldsymbol{r}_{ij}$	:	relative position vector from particle j to particle i
$\boldsymbol{R}$	:	resistance matrix
$\boldsymbol{R}_a$, $\boldsymbol{R}_b$, $\boldsymbol{R}_c$, $\boldsymbol{R}_d$	:	resistance matrices
R_{updwn}	:	composition ratio regarding the number of two types of particles
Re	:	Reynolds number

s	:	number of particles that make up each cluster for a cluster size distribution
$S_1^{(m)}$, $S_2^{(m)}$, $S_3^{(m)}$	:	order parameter of magnetic moments
$S_4^{(e)}$	:	order parameter of particle directions
S_{ny}, S_{nz}	:	order parameter regarding the components of magnetic moments
t	:	time
$\boldsymbol{t}_{ij}$	:	unit vector of vector $\boldsymbol{r}_{ij}$
T	:	absolute temperature of a liquid
$\boldsymbol{T}$	:	torque acting on the ambient fluid by a particle
$\boldsymbol{T}^P$	:	torque acting on a particle
$\boldsymbol{T}_i^{(H)}$	:	magnetic torque due to the magnetic particle-field interaction
$\boldsymbol{T}_{ij}^{(m)}$	:	magnetic torque due to the magnetic particle-particle interaction
$\boldsymbol{T}^{(V)}$, $\boldsymbol{T}_{ij}^{(V)}$, $\boldsymbol{T}_{iajb}{}^{(V)}$	:	torque due to the overlap of steric layers
$u_i^{(H)}$	:	interaction energy of the magnetic particle-field interaction
$u_{ij}^{(m)}$	:	interaction energy of the magnetic particle-particle interaction
$u_{iajb}{}^{(V)}$	:	interaction energy due to the overlap of steric layers
U	:	total system potential energy
$\boldsymbol{U}$	:	inflowing uniform velocity
$\boldsymbol{v}$	:	velocity of a particle
V	:	volume of a system
α_{cube}^T, α_{cube}^R	:	modification coefficients
$\dot{\gamma}$	:	shear rate

δ	:	thickness of a uniform steric layer
$\Delta N_i(r)$	:	number of particles existing in an infinitesimal area at a radial distance r
Δr	:	width of an infinitesimal area
Δr_{MC}	:	maximum random translational distance for Monte Carlo procedures
$\Delta \boldsymbol{r}^B$	:	random displacement inducing translational Brownian motion
ΔS	:	infinitesimal area
Δt	:	time interval
ΔV	:	infinitesimal shell volume
$\Delta \theta_{MC}$	:	maximum random rotation angle for Monte Carlo procedures
$\Delta \boldsymbol{\phi}^B$	:	random displacement inducing rotational Brownian motion
η	:	liquid viscosity
η_{yx}^{F}, η_{yx}^{TH}, η_{yx}^{FT}	:	viscosity components
η_{yx}^{total}	:	net viscosity
θ	:	polar angle from the z-axis
$\theta_{ij}^{(n)}$	:	angle between $\hat{\boldsymbol{n}}_i$ and $\hat{\boldsymbol{n}}_j$
λ	:	non-dimensional parameter representing the strength of the magnetic particle-particle interaction
λ_V	:	non-dimensional parameter representing the strength of the repulsive interaction relative to the thermal energy
μ_0	:	permeability of free space
v	:	kinematic viscosity
ξ	:	non-dimensional parameter representing the strength of the magnetic particle-field interaction
ξ^T, ξ^R	:	translational and rotational friction coefficients

ρ	:	density
τ_{yx}^{total}	:	total shear stress
ϕ	:	azimuthal angle from the x-axis
ϕ_V	:	volumetric fraction of particles
$\psi_{ij}^{(p)}$, $\psi_{ij}^{(n)}$	:	angle between magnetic moment directions $\boldsymbol{n}_i$ and $\boldsymbol{n}_j$
$\psi_{ij}^{(\boldsymbol{e}_k, \boldsymbol{e}_l)}$	:	angle between direction vectors $\boldsymbol{e}_k$ and $\boldsymbol{e}_l$ of cubic particles i and j
$\Psi_{\theta\phi}$	:	orientational distribution function
$\boldsymbol{\omega}$	:	angular velocity of a particle
$\boldsymbol{\Omega}$	:	angular velocity of a flow field
$\langle - \rangle$	:	ensemble average

Chapter 1 Introductory remarks

A magnetic particle suspension has a significant potential for application in a variety of engineering fields, and therefore numerous studies have been conducted up to the present time.

In the field of fluid engineering, typical applications are magnetically-controlled fluid devices such as mechanical dampers and actuators [1-3], where the magnetorheological properties of a suspension are controlled by means of an external magnetic field. Magnetic particle suspensions with a large magnetorheological effect are required for the development of effective magnetically-controlled devices. The magnetorheological properties of a suspension are significantly dependent on the particle aggregates formed in the system and therefore it is required that the internal structure of the particle aggregates should be controlled in an appropriate manner by means of an external magnetic field.

In the field of biomedical engineering, numerous studies are currently being conducted with regard to the development of a magnetically guided drug delivery system [4-19], whereby drug-loaded magnetic particles are guided to the targeted tissues or cells. In this research field, three main areas of study are required to develop the application of the drug delivery system, (1) a technique for loading drugs onto a magnetic particle [4-6], (2) a technique for controlling the behavior of the particle by an external non-uniform magnetic field [7-9] and (3) a technique for releasing drugs at a targeted position [10-13]. A variety of studies have been conducted in the fields of material science and biomedical engineering in order to generate highly functionalized particles for the efficient loading of drugs onto a magnetic particle. On the other hand, many fluid engineering researchers have conducted both simulation [14-17] and experimental studies [18, 19] on the behavior of magnetic particles in a blood vessel in order to elucidate the attachment and trapping characteristics of the magnetic particles to a targeted position under the influence of a non-uniform magnetic field.

Currently, a large number of researchers have focused on the application of a magnetic particle suspension to a magnetic particle hyperthermia treatment [20-30]. Magnetic hyperthermia is a new medical treatment designed to kill targeted tumor or cancer cells by means of the heating effect arising from the relaxation of magnetic moments in a time-dependent magnetic field, such as, an alternating magnetic or a rotating magnetic field. In a magnetic particle suspension, there are two main relaxation mechanisms for the magnetic moment [24-27] which are (1) the Brownian relaxation mode and (2) the Néel relaxation mode. The Brownian relaxation mode is the heating mechanism for relatively large magnetic particles where the magnetic moment is fixed within the particle body and gives rise to heat production as the whole particle rotates to follow a time-dependent magnetic field. In contrast, in the Néel relaxation mode, heat production arises as the magnetic moment rotates within the particle while the particle as a whole remains fixed. Although a

variety of studies [21-23] regarding the application to magnetic hyperthermia have been performed for the smaller magnetic particles that produce a heating effect due to the Néel relaxation mechanism, however, several researchers have recently focused on the heat production due to the Brownian relaxation mechanism [28-30].

In the engineering field of environmental resource, magnetic particles are attractive from the viewpoint of new adsorption agents for improving the visibility of water in small lakes and ponds. There are a variety of techniques for improving the visibility of water [31-48], such as the method of stimulating a self-cleaning action by an aeration process [31], an adsorption method that employs active carbon and zeolite as the porous materials [32, 33], a filtering technique [34], and a coagulating sedimentation technique that employs flocculating agents such as aluminum sulfates [35]. The most appropriate technique is dependent on the conditions of the water pollution and the dimensions of the river, lake or pond and is typically adopted from one of the above methods. Currently, as indicated above, magnetic particles have been applied in the industrial field of adsorption agents. In this field, the process of a visibility-improving method is generally made up of two stages: (1) the generation of functionalized magnetic particles designed to adsorb water-borne metal ions or pollutants [36-40], and (2) the recovery of the absorbing magnetic particles by means of an external non-uniform magnetic field [41-48]. The main task has been the generation of highly multi-functionalized magnetic particles with the facility to adsorb specific heavy metal ions such as copper, lead, cadmium and mercury. However, after the absorption of the heavy metals or pollutants, an effective technique is then required for collecting the magnetic particles using a gradient magnetic field.

Nowadays, material scientists are able to synthesize magnetic particles with various magnetic properties and various geometric shapes such as rod-like [49-55], disk-like [56-60], cube-like [61-66] and peanut-like particles [62, 67-69]. In the cases of magnetite Fe_3O_4, maghemite γ-Fe_2O_3, or Barium ferrite $BaFe_{12}O_{19}$, particles, the particles have a significantly strong magnetization and they tend to aggregate and sediment quickly unless their surface is coated with a surfactant layer. Moreover, we can not easily obtain a stable suspension composed of these magnetic particles because it is difficult to re-disperse them in a solvent once they have aggregated together. In contrast, hematite α-Fe_2O_3 particles have a significantly weak magnetization which may be of merit for obtaining a stable suspension without the need for a surfactant treatment. For the case of a coarse hematite particle in the size range of several hundred nanometers to one micrometer, the magnetic interaction acting between particles is no longer negligible, and thus these coarse hematite particles tend to sediment and to form aggregate structures on the sedimentation surface. Hence, research has focused on a suspension composed of coarse hematite particles from the viewpoint of developing a surface modification technology. The objective of these studies has been to clarify the orientational characteristics and aggregation phenomena of magnetic particles on the material surface [63, 65,

70-72].

It is known that ferromagnetic particles and hematite particles have different magnetization properties. For the case of a magnetic rod-like particle, it is known that the ferromagnetic rod-like particles [53] are magnetized in the major axis direction of the particle, whereas the rod-like hematite particles [54, 55] are weakly magnetized in the minor axis direction. For the case of a cubic hematite particle, it was known that the magnetic dipole moment of the particle tends to orient in the diagonal direction of the cube, however, from a recent experimental study, it has been clarified that the magnetic moment is not fully oriented in a diagonal direction [66].

There are a variety of computational micro-analysis methods [73-85] for particle suspensions, such as Monte Carlo (MC), molecular dynamics (MD), Brownian dynamics (BD), lattice Boltzmann (LB), multi-particle collision dynamics (MPCD) and dissipative particle dynamics (DPD). The Monte Carlo method [73, 74] is a powerful technique for simulating particle ensembles in the situation of thermodynamic equilibrium, whereby the microscopic states of a system are generated according to stochastic theory using a series of random numbers. Moreover, this simulation method may be performed for a solid particle system even if the interaction between the steric or repulsive layers is not completely formulated. On the other hand, for non-equilibrium studies such as flow problems and the study of rheological properties, the Brownian dynamics method [77, 78] offers the simplest simulation technique, whereby particle motion is simulated according to the Langevin equation by which the Brownian motion is expressed through stochastic characteristics. Hence, this method requires knowledge of the particle friction or diffusion coefficients and the equation of the repulsive interaction between the steric layers. Moreover, the BD method may be desirable for the simulation of a dilute suspension of magnetic particles where the multi-body hydrodynamic interaction among particles may be neglected. In order to obtain more accurate simulation results, it may be required to employ a more advanced simulation approach such as LB [79-81], MPCD [82, 83] and DPD [84, 85]. These simulation methods are able to treat the hydrodynamic interaction because their methodology is to simultaneously solve for the particle motion and the ambient flow field. Many researchers have conducted simulation studies with respect to the behavior of magnetic particles by means of these simulation methods [79-85]. However, the focus has mainly been on a spherical magnetic particle dispersion, and therefore, it may be desirable to develop the LB, MPCD and DPD methods to accommodate a suspension composed of non-spherical particles such as the rod-like and cube-like particles.

The Brownian dynamics method is considered to be a useful simulation tool for a suspension of axisymmetric particles such as the spherical, rod-like and disk-like particles. However, the Brownian dynamics method is not directly applicable to a suspension composed of non-axisymmetric particles where the relationship between the components of the friction or

diffusion tensor has not fully been clarified at the present, as in the case of cube-like particles.

Many researchers have shown an active interest in the relationship between the magnetorheological properties of a suspension and the particle aggregates, where past studies [86-90] have mainly targeted a suspension composed of magnetic spherical particles. Since the employment of non-spherical particles is expected to yield a suspension that exhibits a larger magneto-rheological effect [91-94], further studies are necessary with regard to magnetic particles with a variety of geometrical shapes.

From this background, several simulation and experimental studies [95-99] have been conducted by our research group in order to investigate the magnetorheological properties of a suspension of ferromagnetic or hematite rod-like particles. For example, in the case of a suspension of ferromagnetic rod-like particles that are magnetized in the major axis direction, it was clarified that an increase in the magnetic field strength induces a regime change from raft-like clusters to chain-like and wall-like clusters that lead to a significant increase in the net viscosity [95]. In contrast, a suspension composed of rod-like hematite particles that are magnetized normal to the particle axis direction, may exhibit a negative magnetorheological effect under certain conditions [96]. The appearance of this effect had been previously predicted from a theoretical analysis based on the orientational distribution function [99] and has been verified by an experimental study [97].

The magnetorheological effect is significantly dependent on the internal structure of the particle aggregates formed in the system, and since the geometrical shape of a magnetic particle has a significant influence on the formation of the aggregate structure, a suspension composed of cubic particles may be expected to exhibit relatively complex magnetorheological properties. Therefore, the purpose of the task here is to employ the Brownian dynamics method and develop a simulation for a cubic particle suspension in order to investigate the relationship between magnetorheological properties and aggregation phenomena.

In Chapters 2 to 4, we will address a system in thermodynamic equilibrium and investigate the internal structure of the particle aggregates and regime change phenomena by means of 2D and 3D Monte Carlo simulations.

In Chapter 5, we will analyze the flow field around a cube via commercial software ANSYS CFX in order to elucidate the features of the resistance component matrices.

In Chapter 6, we will propose a new repulsive layer model for evaluating the repulsive interaction due to the overlap of the steric layers and will verify the validity of this interaction model by performing 3D Brownian dynamics simulations for comparison with a corresponding Monte Carlo simulation.

In Chapter 7, we will treat a suspension composed of cubic magnetic particles in the situation of a simple shear flow and investigate the relationship between the magnetorheological effects and the aggregate structures by means of Brownian dynamics simulations.

In Chapter 8, we will summarize the progress of the current study and will introduce a possible direction for the future research of cubic magnetic particle suspensions.

References

[1] W. A. Bullough, (ed.), *Electro-Rheological Fluids, Magneto-Rheological Suspensions and Associated Technology* (World Scientific, Singapore, 1996).

[2] N. M. Wereley, (ed.), *Magnetorheology: Advances and Applications* (Royal Society of Chemistry, London. 2013).

[3] R. E. Rosensweig, *Ferrohydrodynamics* (Cambridge University Press, Cambridge, 1985).

[4] S. Patra, E. Roy, P. Karfa, S. Kumar, R. Madhuri and P. K. Sharma, Dual-responsive polymer coated superparamagnetic nanoparticle for targeted drug delivery and hyperthermia treatment, ACS Appl. Mater. Interfaces 7 (2015) 9235-9246.

[5] R. M. Erb, H. S. Son, B. Samanta, V. M. Rotello and B. B. Yellen, Magnetic assembly of colloidal superstructures with multipole symmetry, Nature 457 (2009) 999-1002.

[6] J. Weingart, P. Vabbilisetty and X.L. Sun, Membrane mimetic surface functionalization of nanoparticles: methods and applications, Adv. Colloid Interface Sci. 197-198 (2013) 68-84.

[7] F. Mishima, S. Fujimoto, S. Takeda, Y. Izumi and S. Nishijima, Development of control system for magnetically targeted drug delivery, J. Magn. Magn. Mater. 310 (2007) 2883-2885.

[8] S. Takeda, F. Mishima, S. Fujimoto, Y. Izumi, S. Nishijima, Development of magnetically targeted drug delivery system using superconducting magnet, J. Magn. Magn. Mater. 311 (2007) 367-371.

[9] B. Shapiro, Towards dynamic control of magnetic fields to focus magnetic carriers to targets deep inside the body, J. Magn. Magn. Mater. 321 (2009) 1594-1599.

[10] S. Kayal and R. V. Ramanujan, Anti-cancer drug loaded iron–gold core–shell nanoparticles (Fe@ Au) for magnetic drug targeting, J. Nanosci. Nanotechnol. 10 (2010) 1-13.

[11] R. O. Rodrigues, G. Baldi, S. Doumett, L. Garcia-Hevia, J. Gallo, M. Bañobre-López, G. Dražić, R. C. Calhelha, I. C. F. R. Ferreira, R. Lima, H. T. Gomes and A. M. T. Silva, Multifunctional graphene-based magnetic nanocarriers for combined hyperthermia and dual stimuli-responsive drug delivery, Mater. Sci. Eng., C 93 (2018) 206-217.

[12] D. H. Kim, D. E. Nikles, D. T. Johnson and C. S. Brazel, Heat generation of aqueously dispersed CoFe2O4 nanoparticles as heating agents for magnetically activated drug delivery and hyperthermia, J. Magn. Magn. Mater. 320 (2008) 2390-2396.

[13] D. Müller-Schulte, T. Schmitz-Rode, Thermosensitive magnetic polymer particles as contactless controllable drug carriers, J. Magn. Magn. Mater. 302 (2006) 267-271.

[14] E. P. Furlani and K. C. Ng, Analytical model of magnetic nanoparticle transport and capture in the microvasculature, Phys. Rev. E 73 (2006) 061919.

[15] S Sharma, VK Katiyar and U Singh, Mathematical modelling for trajectories of magnetic nanoparticles in a blood vessel under magnetic field, J. Magn. Magn. Mater. 379 (2015) 102-107.

[16] O. Pourmehran, M. Rahimi-Gorji, M. Goji-Bandpy and T.B. Gorji, Simulation of magnetic drug targeting through tracheobronchial airways in the presence of an external non-uniform magnetic field using Lagrangian magnetic particle tracking, J. Magn. Magn. Mater. 393 (2015) 380-393.

[17] L. Agiotis, I. Theodorakos, S. Samothrakitis, S. Papazoglou, I.Zegioti and Y. S. Raptis, Magnetic manipulation of superparamagnetic nanoparticles in a microfluid system for drug delivery applications, J. Magn. Magn. Mater. 401 (2016) 956-964.

[18] Y. Yoshida, S. Fukui, S. Fujimoto, F. Mishima, S. Takeda, Y. Izumi, S. Ohtani, Y. Fujitani and S. Nishijima, Ex vivo investigation of magnetically targeted drug delivery system, J. Magn. Magn. Mater. 310 (2007) 2880-2882.

[19] Y. Hirota, F. Mishima, Y. Akiyama and S. Nishijima, Drug delivery using an embedded ferromagnetic needle and external magnets, IEEE Trans. Appl. Supercond. 20 (2010) 826-828.

[20] Y. L. Golovin, S. L. Gribanovsky, D. Y. Golovin, N. L. Klyachko, A. G. Majouga, A. M. Master, S. Marina and A. V. Kabanov, Towards nanomedicines of the future: Remote magneto-mechanical actuation of nanomedicines by alternating magnetic fields, J. Controlled Release 219 (2015) 43-60.

[21] A.M. Schmidt, Thermoresponsive magnetic colloids, Colloid Polym. Sci. 285 (2007) 953-966.

[22] C. S. S. R. Kumar and F. Mohammad, Magnetic nanomaterials for hyperthermia-based therapy and controlled drug delivery, Adv. Drug Delivery Rev. 63 (2011) 789-808.

[23] I. M. Obaidat, B. Issa and Y. Haik, Magnetic properties of magnetic nanoparticles for efficient hyperthermia, Nanomaterials 5 (2015) 63-89.

[24] A. E. Deatsch and B. A. Evans, Heating efficiency in magnetic nanoparticle hyperthermia, J. Magn. Magn. Mater. 354 (2014) 163-172.

[25] J. Landers, S. Salamon, H. Remmer, F. Ludwig and H. Wende, Simultaneous study of Brownian and Néel relaxation phenomena in ferrofluids by mössbauer spectroscopy, Nano Lett. 16 (2016) 1150-1155.

[26] R. Kotitz, W. Weitschies, L. Trahms and W. Semmler, Investigation of Brownian and Néel relaxation in magnetic fluid, J. Magn. Magn. Mater. 201 (1999) 102-104.

[27] R. E. Rosensweig, Heating magnetic fluid with alternating magnetic field, J. Magn. Magn. Mater. 252 (2002) 370-374.

[28] S. Suzuki and A. Satoh, Influence of the cluster formation in a magnetic particle suspension on heat production effect in an alternating magnetic field, Colloid Polym. Sci. 297 (2019) 1265-1273.

[29] Z. Zhao and C. Rinaldi, Magnetization dynamics and energy dissipation of interacting magnetic nanoparticles in alternating magnetic fields with and without a static bias field, J. Phys. Chem. C 122 (2018) 21018-21030.

[30] D. Soto-Aquino and C. Rinaldi, Nonlinear energy dissipation of magnetic nanoparticles in oscillating magnetic fields, J. Magn. Magn. Mater. 393 (2015) 46-55.

[31] T. Okai, Y. Sasada, S. Komino and S. Tanaka, Improvement of water quality and control of blue-green algae growth by aeration, Annual Report of Kagawa Prefectural Research Institute for Environmental Sciences and Public Health 6 (2007) 29-36 (in Japanese).

[32] S. Ismadji and S. K. Bhatia, Characterization of activated carbons using liquid phase adsorption,

Carbon, 39 (2001) 1237-1250.
[33] P. A. Gauden, A. P. Terzyk, P. Kowalczyk, Some remarks on the calculation of the pore size distribution function of activated carbons, J. Colloid Interface Sci. 300 (2006) 453-474.
[34] R. S. Wotton, Water purification using sand, Hydrobiologia 469 (2002) 193-201.
[35] N. Tambo and Y. Watanabe, Physical characteristics of flocs—I. The floc density function and aluminium floc, Water Res. 13 (1979) 409-419.
[36] M. A. Ahmed, S. M. Ali, S. I. El-Dek and A. Galal, Magnetite–hematite nanoparticles prepared by green methods for heavy metal ions removal from water, Mater. Sci. Eng. B 178 (2013) 744-751.
[37] P. I. Girginova, A. L. Daniel-da-Silva, C. B. Lopes, P. Figueira, M. Otero, V. S. Amaral, E. Pereira and T. Trindade, Silica coated magnetite particles for magnetic removal of Hg2+ from water, J. Colloid Interface Sci. 345 (2010) 234-240.
[38] L. Jiang, P. Liu and S. Zhao, Magnetic ATP/FA/Poly(AA-co-AM) ternary nanocomposite microgel as selective adsorbent for removal of heavy metals from wastewater, Colloids Surf. A 470 (2015) 31-38.
[39] K. Lia, Z. Zenga, J. Xionga, L. Yana, H. Guoa, S. Liua, Y. Daia and T. Chen, Fabrication of mesoporous Fe3O4@SiO2@CTAB–SiO2 magnetic microspheres with a core/shell structure and their efficient adsorption performance for the removal of trace PFOS from water, Colloids Surf. A 465 (2015) 113-123.
[40] S. H. Sajjadi and E. K. Goharshadi, Highly monodispersed hematite cubes for removal of ionic dyes, J. Environ. Chem. Eng. 5 (2017) 1096-1106.
[41] S. Kalia, S. Kango, A. Kumar, Y. Haldorai, B. Kumari and R. Kumar, Magnetic polymer nanocomposites for environmental and biomedical applications, Colloid Polym. Sci. 292 (2014) 2025-2052.
[42] H. Tian, F. Liu and J. He, Multifunctional Fe3O4@nSiO2@mSiO2–Fe core–shell microspheres for highly efficient removal of 1,1,1-trichloro-2,2-bis (4-chlorophenyl)ethane (DDT) from aqueous media, J. Colloid Interface Sci. 431 (2014) 90-96.
[43] H. Yang, H. Zhang, J. Peng, Y. Zhang, G. Du and Y. Fang, Smart magnetic ionic liquid-based Pickering emulsions stabilized by amphiphilic Fe3O4 nanoparticles: Highly efficient extraction systems for water purification, J. Colloid Interface Sci. 485 (2017) 213-222.
[44] R. Hasanzadeh, P. N. Moghadam, N. Bahri-Laleh and M. Sillanpää, Effective removal of toxic metal ions from aqueous solutions: 2-Bifunctional magnetic nanocomposite base on novel reactive PGMA-MAn copolymer@Fe3O4 nanoparticles, J. Colloid Interface Sci. 490 (2017) 727-746.
[45] K. Dashtian and R. Zare-Dorabei, Synthesis and characterization of functionalized mesoprous SBA-15 decorated with Fe3O4 nanoparticles for removal of Ce(III) ions from aqueous solution: ICP–OES detection and central composite design optimization, J. Colloid Interface Sci. 494 (2015) 114-123.

[46] W. Konicki, A. Hełminiak, W. Arabczyk and E. Mijowska, Removal of anionic dyes using magnetic Fe@graphite core-shell nanocomposite as an adsorbent from aqueous solutions, J. Colloid Interface Sci. 497 (2017) 155-164.

[47] H. Vojoudi, A. Badiei, S. Bahar, G. M. Ziarani, F. Faridbod and M. R. Ganjali, A new nano-sorbent for fast and efficient removal of heavy metals from aqueous solutions based on modification of magnetic mesoporous silica nanospheres, J. Magn. Magn. Mater. 441 (2017) 193-203.

[48] S. Lan, X. Wu, L. Li, M. Li, F. Guo and S. Gan, Synthesis and characterization of hyaluronic acid-supported magnetic microspheres for copper ions removal, Colloids Surf. A 425 (2013) 42-50.

[49] V. ZÁVIŠOVÁ, N. TOMAŠOVIČOVÁ, J. KOVÁČ, M. KONERACKÁ, P. KOPČANSKÝ and I. VÁVRA, Synthesis and characterisation of rod-like magnetic nanoparticles, Olomouc, Czech Republic, EU, 2010.

[50] J. Wang, Y. Wu and Y. Zhu, Fabrication of complex of Fe3O4 nanorods by magnetic-field-assisted solvothermal process, Mater. Chem. Phys. 106 (2007) 1-4.

[51] E. Cisternas and E. E. Vogel, Inscription and stabilization of ferromagnetic patterns on arrays of magnetic nanocylinders, J. Magn. Magn. Mater. 337 (2013) 74-78.

[52] M. Ozaki and E. Matijević, Preparation and magnetic properties of monodispersed spindle-type γ-Fe2O3 particles, J. Colloid Interface Sci. 107 (1985) 199-203.

[53] A. Mertelj and D. Lisjak, Ferromagnetic nematic liquid crystals, Liq. Cryst. Rev. 5 (2017) 1-33.

[54] D. Zákutná, Y. Falke, D. Dresen, S. Prévost, P. Bender, D. Honecker and S. Disch, Morphological and crystallographic orientation of hematite spindles in an applied magnetic field, Nanoscale (2019) 7149-7156.

[55] N Tomašovičová, S Burylov, V Gdovinová, A. Tarasov, J. Kovac, N. Burylova, A. Voroshilov, P. Kopčanský and J. Jadżyn, Magnetic Freedericksz transition in a ferronematic liquid crystal doped with spindle magnetic particles, J. Mol. Liq. 267 (2018) 390-397.

[56] D. Lisjak and S. Ovtar, The alignment of barium ferrite nanoparticles from their suspensions in electric and magnetic fields, J. Phys. Chem. B 177 (2013) 1644-1650.

[57] S. Ovtar, D. Lisjak and M. Drofenik, The influence of processing parameters on the orientation of barium ferrite platelets during electrophoretic deposition, Colloids Surf., A 403 (2012) 139-147.

[58] D. Primc, D. Makovec, D. Lisjak and M. Drofenik, Hydrothermal synthesis of ultrafine barium hexaferrite nanoparticles and the preparation of their stable suspensions, Nanotechnology 20 (2009) 315605.

[59] M. Ozaki, N. OOkoshi and E. Matijević, Preparation and magnetic properties of uniform hematite platelets, J. Colloid Interface Sci. 137 (1990) 546-549.

[60] K. Kandori, Y. Yamoto and T. Ishikawa, Effects of vinyl series polymers on the formation of hematite particles in a forced hydrolysis reaction, J. Colloid Interface Sci. 283 (2005) 432-439.

[61] M. Ozaki, T. Egami, N. Sugiyama and E. Matijević, Agglomeration in colloidal hematite dispersions due to weak magnetic interactions: II. The effects of particle size and shape, J. Colloid Interface Sci. 126 (1988) 212-219.

[62] J. W. J. de Folter, E. M. Hutter, S. I. R. Castillo, K. E. Klop, A. P. Philipse and W. K. Kegel, Particle shape anisotropy in Pickering emulsions: cubes and peanuts, Langmuir 30 (2014) 955-964.

[63] L. Rossi, S. Sacanna, W. T. M. Irvine, P. M. Chaikin, D. J. Pine and A. P. Philipse, Cubic crystals from cubic colloids, Soft Matter 7 (2011) 4139-4142.

[64] C. Su, H. Wang and X. Liu, Controllable fabrication and growth mechanism of hematite cubes, Cryst. Res. Tehnol. 46 (2011) 209-214.

[65] J. M. Meijer, F. Hagemans, L. Rossi, D.V. Byelov, S. I. R. Castillo, A. Snigirev, I. Snigireva, A. P. Philipse and A. V. Petukhov, Self-assembly of colloidal cubes via vertical deposition, Langmuir 28 (2012) 7631-7638.

[66] L. Rossi, J.G. Donaldson, J.M. Meijer, A.V. Petukhov, D. Kleckner, S.S. Kantorovich, M.T. Lrvine, A.P. Philipse and S. Sacanna, Self-organization in dipolar cube fluids constrained by competing anisotropies, Soft Matter 14 (2018) 1080-1087.

[67] Z. An, J. Zhang, S. Pan and G. Song, Novel peanut-like α-Fe2O3 superstructures: Oriented aggregation and Ostwald ripening in a one-pot solvothermal process, Powder Technol. 217 (2012) 274-280.

[68] D. Shindo, G. S. Part, Y. Waseda and T. Sugimoto, Internal structure analysis of monodispersed peanut-type hematite particles produced by the gel-sol method, J. Colloid Interface Sci. 168 (1994) 478-484.

[69] T. Sugimoto, M. M. Khan and A. Muramatsu, Preparation of monodisperse peanut-type α-Fe2O3 particles from condensed ferric hydroxide gel, Colloids Surf., A 70 (1993) 167-169.

[70] M. Aoshima, M. Ozaki and A.Satoh, Structural analysis of self-assembled lattice structures composed of cubic hematite particles, J. Phys. Chem. C 116 (2012) 17862-17871.

[71] S. I. R. Castillo, C. E. Pompe, J. van Mourik, D. M. A. Verbart, D. M. E. Thies-Weesie, P. E. de Jongh and A. P. Philipse, Colloidal cubes for the enhanced degradation of organic dyes, J. Mater. Chem. A 2 (2014) 10193-10201.

[72] M. V. Kovalenko, M. I. Bodnarchuk, R. T. Lechner, G. Hesser, F. Schäffler, and W. Heiss, Fatty acid salts as stabilizers in size-and shape-controlled nanocrystal synthesis: the case of inverse spinel iron oxide, J. Am. Chem. Soc. 129 (2007) 6352-6353.

[73] N. Metropolis, A. W. Rosenbluth, M. N. Rosenbluth, A. H. Teller and E. Teller, Equation of state calculations by fast computing machines, J. Chem. Phys. 21(1953) 1087-1092.

[74] R. W. Chantrell, A. Bradbury, J. Popplewell, and S. W. Charles, Agglomerate formation in a magnetic fluid, J. Appl. Phys. 53 (1982) 2742-2744.

[75] W. Smith, The computer simulation of liquids by molecular dynamics, Phys. Educ. 22 (1987) 355-3599.

[76] I. Drikis and A. Cebers, Molecular dynamics simulation of the chain of magnetic particles and flexible filament model, Magnetohydrodynamics, 40 (2004) 351-358.

[77] Z. Wang and C. Holm, Structure and magnetic properties of polydisperse ferrofluids: A molecular dynamics study, Phys. Rev. E 68 (2003) 041401.

[78] G. Mériguet, M. Jardat and P. Turq, Structural properties of charge-stabilized ferrofluids under a magnetic field: A Brownian dynamics study, J. Chem. Phys. 121 (2004) 6078-6085.

[79] A. Satoh and R. W. Chantrell, Application of the lattice Boltzmann method to many particle dispersions, J. Fluid Sci. Tech. 6 (2011) 114-127.

[80] Y. Ido, H. Sumiyoshi and H. Tsutsumi, Simulations of behavior of magnetic particles in magnetic functional fluids using a hybrid method of lattice Boltzmann method, immersed boundary method and discrete particle method, Comput. Fluids 142 (2017) 86-95.

[81] K. Han, Y. T. Feng and D. R. J. Owen, Three-dimensional modelling and simulation of magnetorheological fluids, Int. J. Numer. Meth. Engng. 84 (2010) 1273-1302.

[82] A. Satoh, Feasibility of the multi-particle collision dynamics method as a simulation technique for a magnetic particle suspension, Mol. Simul. 46 (2020) 213-223.

[83] D. Zablotsky, Field effect in the viscosity of magnetic colloids studied by multi-particle collision dynamics, J. Magn. Magn. Mater.

[84] A. Satoh and R. W. Chantrell, Application of the dissipative particle dynamics method to magnetic colloidal dispersions, Mol. Phys. 104 (2006) 3287-3302.

[85] A. J. Gharibvand, M. Norouzi and M. M. Shahmardan, Dissipative particle dynamics simulation of magnetorheological fluids in shear flow, J. Braz. Soc. Mech. Sci. Eng. 41 (2019) 103.

[86] M. L. Levin, D. E. Polesskii and I. V. Prokhorov, Some features of the magnetorheological effect, J. Eng. Phys. Thermophys. 70 (1997) 769-772.

[87] E. Lemaire, A. Meunier, G. Bossis, J. Liu, D. Felt, P. Bashtovoi and N. Matoussevitch, Influence of the particle size on the rheology of magnetorheological fluids, J. Rheol. 39 (1995) 1011-1020.

[88] J. M. Ginder, L. C. Davis and L. D. Elie, Rheology of magnetorheological fluids: Models and measurements, Int. J. Mod. Phys. B 10 (1996) 3293-3303.

[89] H. V. Ly, F. Reitich, M. R. Jolly, H. T. Banks and K. Ito, Simulations of Particle Dynamics in Magnetorheological Fluids, J. Comput. Phys. 155 (1999) 160-177.

[90] M. Mohebi, N. Jamasbi and J. Liu, Simulation of the formation of nonequilibrium structures in magnetorheological fluids subject to an external magnetic field, Phys. Rev. E 54 (1996) 5407.

[91] A. Satoh, Rheological properties and orientational distributions of dilute ferromagnetic spherocylinder particle dispersions: Approximate solutions by means of Galerkin's method, J. Colloid Interface Sci., 234 (2001) 425-433.

[92] R. C. Bell, E. D. Miller, J. O. Karli, A. N. Vavreck and D. T. Zimmerman, Influence of particle shape on the properties of magnetorheological fluids, Int. J. Mod. Phys. B 21 (2007) 5018-5025.

[93] D. J. Vicente, J. P. Segovia-Gutiérrez, E. Andablo-Reyes, F. Vereda and R. Hidalgo-Álvarez, Dynamic rheology of sphere- and rod-based magnetorheological fluids, J. Chem. Phys. 131

(2009) 194902.
[94] D. J. Vicente, F. Vereda, J. P. Segovia-Gutiérrez and R. Hidalgo-Álvarez, Effect of particle shape in magnetorheology, J. Rheol. 54 (2010) 1337-1343.
[95] K. Okada and A. Satoh, Regime of aggregate structures and magneto-rheological characteristics of a magnetic rod-like particle suspension: Monte Carlo and Brownian dynamics simulations, J. Magn. Magn. Mater. 437 (2017) 29-41.
[96] Y. Sakuda, M. Aoshima and A. Satoh, Negative magneto-rheological effect of a dispersion composed of spindle-like hematite particles, Mol. Phys. 110 (2012) 1429-1435.
[97] R. Cuadra and A. Satoh, Experimental verification of negative magnetorheological characteristics in spindle-like hematite particle suspensions, J. Magn. Magn. Mater. 469 (2019) 606-612.
[98] A. Satoh and Y. Sakuda, Theoretical analysis on the orientational characteristics and rheological properties of a rod-like hematite particle suspension in a simple shear flow, Colloids Surf., A 460 (2014) 473-482.
[99] A.Satoh, Influence of the spin Brownian motion on the negative magneto-rheological effect in a rod-like haematite particle suspension, Mol. Phys. 111 (2013) 1042-1052.

Chapter 2 Phase change phenomena of a cubic hematite particle suspension in a two-dimensional system from 2D Monte Carlo simulations

2.1 Introduction

Surface modification technology plays an important role for the development and synthesis of magnetic composite particles. Furthermore, depending on the synthesis method, effects such as particle diffusion and sedimentation phenomena in the gravitational field may affect the final quality of these functional particles. It is therefore required to develop a technology for controlling self-assembled layers, aggregate structures and the orientational characteristics of the magnetic particles deposited on a material surface after sedimentation by means of an external magnetic field. A variety of studies based on cubic hematite particles [1-6] have previously been conducted in order to develop a surface modification technology by evaluating the aggregate structures and order characteristics of particles on a material surface. It has been experimentally clarified that cubic hematite particles form large aggregate structures on the material surface in a face-to-face contact configuration that may transform due to the influence of an external magnetic field into chain-like clusters aligned in the field direction [1]. Simulation studies have also been conducted to investigate a phase change in the aggregate structures and the internal structure of the aggregates. Donaldson et al. [7] have investigated the most preferred particle configuration for clusters formed in a quasi-two-dimensional (quasi-2D) system. Linse [8] treated a dispersion composed of cubic hematite particles which have a full three-dimensional rotational ability in a quasi-2D system and clarified the relationship between cubic particle models with magnetic moments in three different directions and the aggregate structures. In these studies, they also investigated the dependence of the cluster formation on the geometrical shape of the magnetic particle by using a shape parameter whereby the particle shape can be described from a sphere into a cube.

In the present study, we consider a quasi-2D suspension composed of hematite cubic particles in thermodynamic equilibrium. Our particle model is a geometric cube under the assumption of a dominant gravitational force, therefore the particles are restricted to perform a translational motion with one face in contact with the material surface and a rotational motion about a line normal to the material surface. 2D Monte Carlo simulations have been performed in order to investigate the dependence of the aggregate structures on a variety of factors such as the magnetic particle-particle interaction strength, the magnetic particle-field interaction strength and the volumetric fraction of the particles.

2.2 Particle model

As shown in Fig.2.1, the particle is modeled as a cube with a side length *d* and a magnetic dipole moment ***m*** at the center of the cube laying along a diagonal. This particle model may be regarded as a first approximation to the cubic hematite particles that are experimentally synthesized [1]. It is noted that the red-colored part of the cube indicates the positive direction of the magnetic moment and the blue-colored part indicates the negative direction of the magnetic moment.

In the present study, we consider the motion of cubic hematite particles in thermodynamic equilibrium at a material surface. The particles are assumed to move with the lower surface of each cubic particle in contact with the plane of the material surface. Therefore, we treat the two types of cubic particle that have the magnetic moment pointing either in an upward diagonal direction or in a downward diagonal direction relative to the material surface. In this Chapter, we focus on a particular situation where half the number of particles have the magnetic moment pointing in the upward direction and the other half point in the downward direction. In this situation, the arbitrary motion of a particle can be expressed as a combination of a translational motion parallel to the material surface and a rotational motion about a line normal to the material surface. Therefore, we do not consider a full three-dimensional rotational ability for the cubic particles. In Linse's simulations noted above [8], it was assumed that the orientation of the cube has a full three-dimensional rotational ability. In contrast, we here consider the situation of a sufficiently strong gravitational field and therefore the cubic particles are not able to perform the most general three-dimensional rotational motion.

In practice, in order to obtain a stable particle suspension, particles dispersed in a base liquid are generally covered by a repulsive layer such as a steric or an electric double layer. However, we here employ a solid particle model without a repulsive layer because the inte raction energy due to the overlap of the repulsive layers has not currently been derived in mathematical terms for the case of two cubic particles.

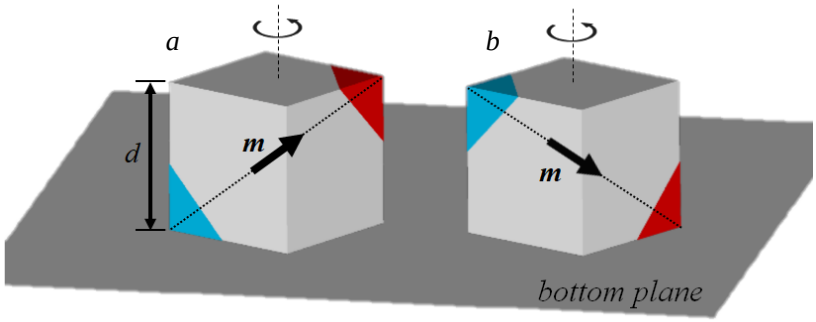

Fig. 2.1 Cubic particle model with two types of magnetic moment direction:(a) an upward diagonal direction and (b) a downward diagonal direction relative to the bottom or material plane.

In our Monte Carlo simulation, an external magnetic field is applied along the material surface in the y-axis direction as $\boldsymbol{H}=H\boldsymbol{h}$, where $\boldsymbol{h}=(0, 1, 0)$ is the unit vector denoting the field direction. If the position vector of particle i is denoted by $\boldsymbol{r}_i$ and the magnetic moment of particle i is denoted by $\boldsymbol{m}_i=m\boldsymbol{n}_i$, where $\boldsymbol{n}_i$ is the unit vector describing the magnetic moment direction, then the magnetic particle-particle interaction $u_{ij}^{(m)}$ and particle-field interaction $u_i^{(H)}$ are expressed as

$$u_{ij}^{(m)}= kT\lambda\frac{1}{(r_{ij}/d)^3}\left\{\boldsymbol{n}_i\cdot\boldsymbol{n}_j-3(\boldsymbol{n}_i\cdot\boldsymbol{t}_{ij})(\boldsymbol{n}_j\cdot\boldsymbol{t}_{ij})\right\} \tag{2.1}$$

$$u_i^{(H)}= -kT\xi\,\boldsymbol{n}_i\cdot\boldsymbol{H}/H \tag{2.2}$$

in which, $\boldsymbol{t}_{ij}$ is the unit vector denoting the direction of particle i relative to particle j, expressed as $\boldsymbol{t}_{ij} = \boldsymbol{r}_{ij} / r_{ij}$, where $\boldsymbol{r}_{ij} =\boldsymbol{r}_i - \boldsymbol{r}_j$ and $r_{ij}=|\boldsymbol{r}_{ij}|$. Moreover, λ and ξ are non-dimensional parameters and they are expressed as $\lambda=\mu_0 m^2/(4\pi d^3 kT)$ and $\xi=\mu_0 mH/(kT)$, where k is the Boltzmann's constant, T is the absolute temperature of the liquid and μ_0 is the permeability of free space. Two non-dimensional parameters λ and ξ represent the strengths of magnetic particle-particle and particle-field interactions relative to the thermal energy, respectively.

The cubic particle has a characteristic geometry in that it is composed of six plane surfaces and, in the situation of the magnetic particle-particle interaction strength being a dominant effect, this feature makes two cubes more likely to be in face-to-face contact. Hence, we now discuss the characteristics of the magnetic interaction potential with consideration of this preferred face-to-face configuration. Figure 2.2 shows a set of eleven typical configurations representing the location and orientation for two cubic particles. Figure 2.3 shows the potential energy for each case of the above eleven configurations, where the values of $\tilde{U}^m =u_{ij}^{(m)}/(kT\lambda)$ are shown as the ordinate. It is seen from Figs. 2.2 and 2.3 that the case $e2$ gives rise to the minimum energy value −1.3333 and the case $e1$ and $d1$ yield second and third minimum energy values. In the case of no applied magnetic field, configuration $e2$, $e1$ and $d1$ are the first, second and third preferred low energy configuration, respectively. In the situation of an applied magnetic field, the configuration $e1$ and $d1$ are expected to be the first and second preferred, respectively, since the magnetic moments of particles are restricted in the magnetic field y-axis direction.

For a 4-particle system, we may presume from the above results regarding the interaction energies that the configurations shown in Figs. 2.4(a) and 2.4(b) are the most preferred configuration for the cases of a strong external magnetic field and no external magnetic field, respectively. Large clusters in a multi-particle suspension may be formed by the combination and expansion of these basic cluster units.

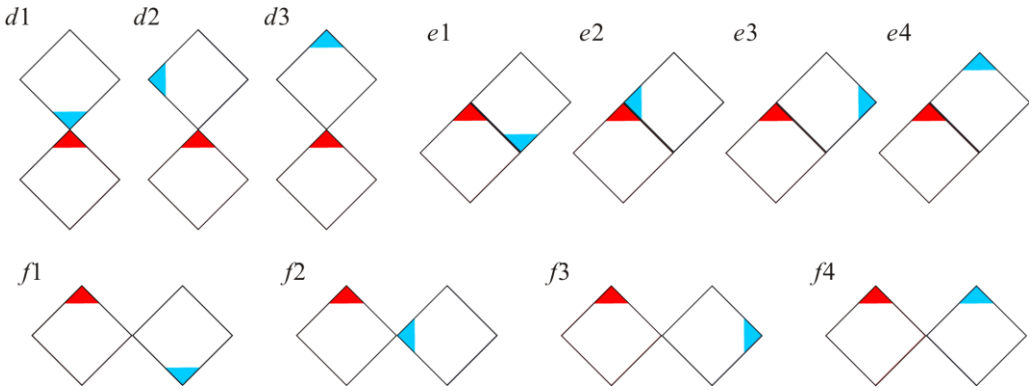

Fig. 2.2 Typical configuration of location and orientation for two cubic particles.

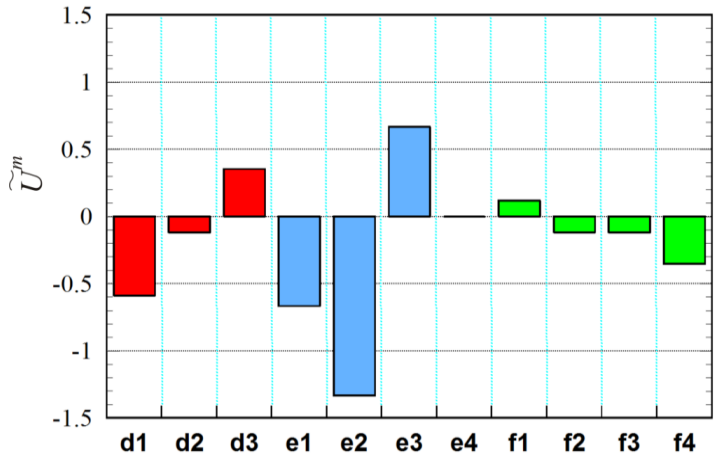

Fig. 2.3 Interaction energies for different particle configurations.

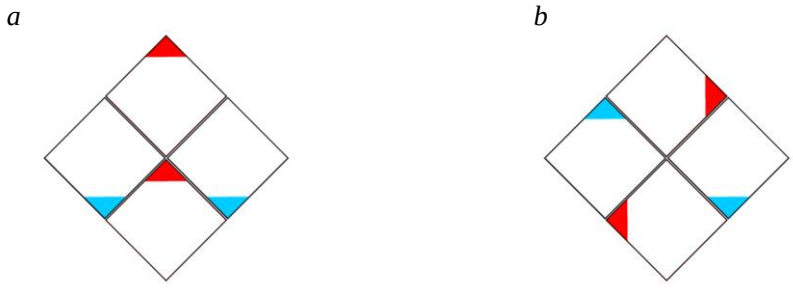

Fig. 2.4 The most preferred configuration for a 4-particle system: (a) in the case of a strong external magnetic field case and (b) in the case of no external magnetic field case.

2.3 Monte Carlo simulation

We employ the Monte Carlo simulation method in order to investigate the aggregate structures of cubic hematite particles in thermodynamic equilibrium. In the present system, the number of cubic particles N, the volume of the system V, and the system temperature T are prescribed and constant in the simulation. Therefore, we adopt the *NVT* Monte Carlo method or the canonical ensemble Monte Carlo method [9], for which we evaluate the total system potential energy U which is the sum of the particle-particle $u_{ij}^{(m)}$ and the particle-field $u_i^{(H)}$ interaction energies.

$$U = \sum_{i=1}^{N} u_{ij}^{(H)} + \sum_{i=1}^{N} \sum_{\substack{j=1 \\ (j>i)}}^{N} u_{ij}^{(m)} \tag{2.3}$$

This total potential energy U is used in the assessment procedure regarding the acceptance or rejection of a new position or a new orientation of a particle.

In a strongly-interacting system where particle aggregation is to be expected, we cannot capture physically reasonable aggregate structures from employing the ordinary Monte Carlo method. This is because, due to the energy considerations of the Monte Carlo methodology, a single constituent particle cannot dissociate from a cluster and thus be free to join a growing cluster. This implies that the convergence to an equilibrium state is prohibitively slow with ordinary MC simulations. From this background, the cluster-moving Monte Carlo method [10, 11] is seen to be a powerful technique in order to overcome this difficulty and obtain physically reasonable aggregate structures. In this method, clusters formed during the process of the simulation are regarded as a unitary particle and they are moved according to the usual Metropolis assessment procedure. Referring to Satoh's study [11], we have attempted to analyze the cluster formation in the system and then to move these clusters every 20 MC steps. In the present study, the constituent particles that make up clusters are only able to perform translational and rotational motion in a two-dimensional plane. However, clusters are only able to perform translational motion because the rotational movement of clusters is likely to cause particle overlap that is not physically reasonable.

2.4 Quantitative evaluation

2.4.1 Radial distribution function

The radial distribution function $g(r)$ is used to quantitatively describe the internal structure of aggregates. If a finite small area at distance r from an arbitrary particle is denoted by $\Delta S(r)=2\pi r\Delta r$ and the number of particles existing in this area is denoted by $\Delta N_i(r)$, then the radial distribution function $g(r)$ is expressed as [10]

$$g(r)=\frac{1}{n_0 N}\left\langle \sum_{i=1}^{N}\frac{\Delta N_i(r)}{2\pi r\Delta r}\right\rangle \tag{2.4}$$

in which n_0 is the particle number density and N is the number of particles.

2.4.2 Order parameters

In order to obtain quantitative characteristics for the configurations of cubic particle aggregates, we address the following order parameters. We first address the order parameter of the magnetic moment, $S_1^{(m)}$:

$$S_1^{(m)}=\frac{1}{N_{pair}}\left\langle \sum_{i=1}^{N}\sum_{\substack{j=1\\(>i)}}^{N}P_2(\cos\psi_{ij}^{(p)})\right\rangle \tag{2.5}$$

in which $P_2(-)$ is the second Legendre polynomial, expressed as $P_2(\cos\psi_{ij}^{(p)}) = (3\cos^2\psi_{ij}^{(p)}-1)/2$, $\psi_{ij}^{(p)}$ is the angle between the magnetic moment directions $\boldsymbol{n}_i$ and $\boldsymbol{n}_j$ of particles i and j, $\langle-\rangle$ is the ensemble average, the summation with respect to particles i and j treats all the pairs of particles, and $N_{pair}=N(N-1)/2$ is the number of these pairs of particles.

If the magnetic particle-particle interaction strength λ is sufficiently large, the cluster units shown in Fig. 2.4 are expected to be formed in the system, as already discussed. In order to characterize this type of cluster unit in an appropriate manner, we consider the projection of the magnetic moments on the bottom or material surface. The notation $\hat{\boldsymbol{n}}_i$ and $\hat{\boldsymbol{n}}_j$ are employed for the unit projection vectors of particles i and j, respectively, and $\theta_{ij}^{(n)}$ is used for the angle between them. If the cluster units shown in Fig. 2.4 are predominantly formed in the system, then the value of $\cos(4\theta_{ij}^{(n)})$ should give rise to unity. Hence, we address the second-order parameter $S_2^{(m)}$.

$$S_2^{(m)}=\frac{1}{N_{pair}}\left\langle \sum_{i=1}^{N}\sum_{\substack{j=1\\(>i)}}^{N}\cos(4\theta_{ij}^{(n)})\right\rangle \tag{2.6}$$

Moreover, we also focus on a third-order parameter in order to evaluate the alignment of the magnetic moments to an external magnetic field direction. This order parameter S_{ny} is defined as

$$S_{ny}=\frac{1}{N}\left\langle \sum_{i=1}^{N}P_2(\hat{\boldsymbol{n}}_i\cdot\boldsymbol{h})\right\rangle=\frac{1}{N}\left\langle \sum_{i=1}^{N}\frac{3\cos^2(\hat{\boldsymbol{n}}_i\cdot\boldsymbol{h})-1}{2}\right\rangle \tag{2.7}$$

in which $P_2(\hat{\boldsymbol{n}}_i\cdot\boldsymbol{h})$ is the second Legendre polynomial, expressed as $P_2(\hat{\boldsymbol{n}}_i\cdot\boldsymbol{h})=(3\cos^2(\hat{\boldsymbol{n}}_i\cdot\boldsymbol{h})-1)/2$.

2.5 Parameters for simulations

Unless specifically mentioned, the present simulation results were obtained by employing the following parameter values in performing the simulations. The volumetric fraction of particles ϕ_V, is set as ϕ_V=0.1, and the number of particles N is N=400. The non-dimensional parameters for the strength of the magnetic particle-particle interaction λ and particle-field interaction ξ are addressed in the wide range of values of λ=0~10 and ξ=0~20. Since we here treat a non-dense suspension, the phenomena of the crystallization and the multi-layers of cubic particles [3, 5, 12, 13] are not addressed. We focus on a particular situation where half of the total number of particles has a magnetic moment in the upward diagonal direction whilst the remainder has a magnetic moment in the downward diagonal direction. The cubic particles with up and down magnetic moment directions were initially located at random sites in the system and the external magnetic field is applied along the material surface in the y-axis direction. Moreover, in order to treat the boundary surfaces of the simulation area we employ periodic boundary conditions in the x-axis and y-axis directions. The cutoff distance r_{coff} for the evaluation of interaction energies is set as $r_{coff}^{*} = r_{coff}/d$=10, and the surface-to-surface criterion distance r_{clstr} for the assessment of the cluster formation is set at $r_{clstr}^{*} = r_{clstr}/d$=0.1. As previously mentioned in section 2.3, the cluster-moving procedure was carried out every 20 MC steps [10, 11]. The maximum random translational distance Δr_{MC} and rotation angle $\Delta\theta_{MC}$ for Monte Carlo procedures are adopted as Δr_{MC}=0.1d and $\Delta\theta_{MC}$=(2°/180°)π, respectively. The total MC steps N_{smplmx} are taken as N_{smplmx}=5,000,000 and the final 80% of the generated data were used for the date averaging procedure.

2.6 Results and discussion

2.6.1 Influence of the magnetic particle-particle interaction strength

First, we discuss the dependence of the aggregate regime of cubic particles on the magnetic particle-particle interaction strength λ for the case of no applied magnetic field ξ=0. The snapshots shown in Figure 2.5 show a qualitative difference between the internal structure of the particle aggregates for the three cases of magnetic particle-particle interaction strength λ=4, λ=7 and λ=10. In the case of a small magnetic particle-particle interaction λ=4, shown in Fig. 2.5(a), the particles do not aggregate to form specific clusters and magnetic moments of each particle do not tend to incline in a specific direction because the effect of thermal motion is more dominant. In the case of a relatively large magnetic particle-particle interaction strength λ=7, shown in Fig. 2.5(b), it is seen that small clusters are formed in the system and the basic configuration *e*2 shown in Fig. 2.2 and the cluster unit shown in Fig. 2.4(b) are clearly observed. As the magnetic particle-particle interaction strength is further increased to λ＝10, shown in Fig. 2.5(c), large aggregate structures are formed in the system and as already mentioned in Section 2.2, it is evident that these large aggregates are formed from a combination of the basic cluster unit shown in Fig. 2.4(b). These aggregates, being different from the chain-like clusters, are designated as closely-packed clusters. The internal structure of these closely-packed clusters is in good agreement with those in an 8-particle system that were obtained by molecular dynamics simulation [7]. Although the formation of loop-like clusters is mentioned for a round-edged cubic system in no applied magnetic field [8], the present sharp-edged cubic system does not exhibit such clear loop-like or necklace-like clusters that are usually observed in a suspension of magnetic spherical particles [14-17].

The internal structure of the above-mentioned clusters can be quantitatively evaluated by the radial distribution function. Figure 2.6 shows results of the radial distribution function for the three cases of the magnetic particle-particle interaction strength λ=4, λ=7 and λ=10. For the case of λ=4, the curve exhibits a gas-like distribution because specific clusters are not formed in the system. That is, it shows a value of almost unity except for the region where neighboring particles contact in a face-to-face manner. For the case of the intermediary magnetic particle-particle interaction strength λ=7, the first peak is more pronounced and a second lower peak can be seen. This characteristic implies that small clusters are formed in the system while the second peak dispersed around the distance $r^* \simeq 2$ implies that the third particle in these clusters is not attached in a perfect face-to-face contact. For the case of a strong magnetic particle-particle interaction strength λ=10, the curve shows a liquid-like distribution with a complex tail exhibiting an oscillatory nature. The reason why there are several high peaks in the radial distribution function for the case of λ=10 may be explained by using the diagram shown in Fig. 2.7. The first peak corresponds to the configuration r_1 shown in Fig. 2.7, where the second particle is located at the shorter distance of $r^* \simeq 1$ in a perfect face-to-face configuration. The second peak corresponds to the configuration r_2 in Fig. 2.7, where the second

particle is located at a distance of $r^*\simeq1.4$ diagonally from the first particle. Similarly, the third and fourth peaks of the radial distribution function correspond to the configurations r_3 and r_4 in Fig. 2.7, and are located respectively at distances $r^*\simeq2.0$ and $r^*\simeq2.2$. From these characteristics, we may understand the second peak at $r^*\simeq1.4$ and forth peak at $r^*\simeq2.2$ suggest the expansion of closely-packed structures. However, it is seen from Fig.2.6 that these peaks do not appear at their exact position shown in Fig. 2.8. This is because the random motion of the cubic particles induces an instability in the regular face-to-face configuration.

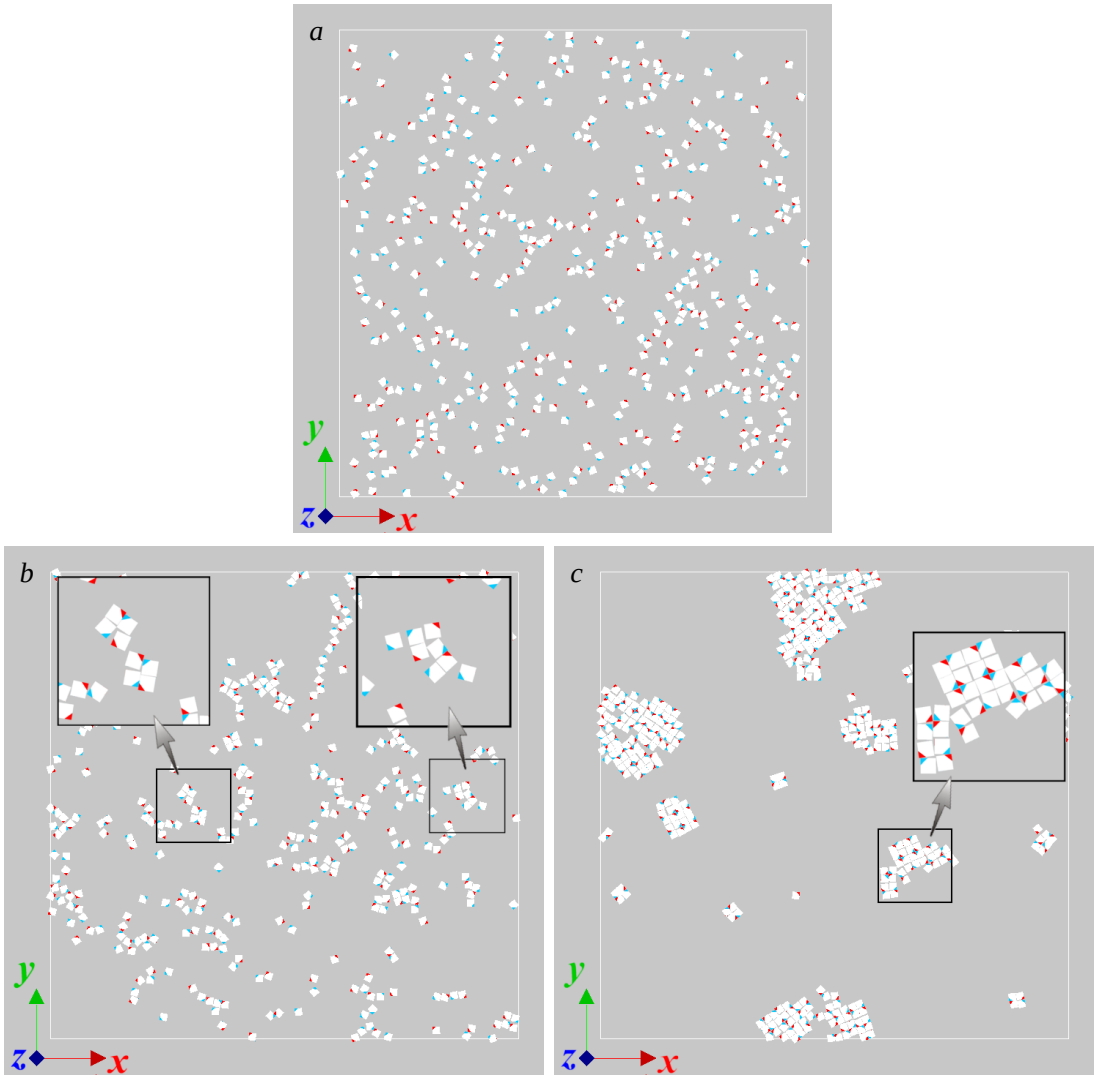

Fig. 2.5 Dependence of the aggregate structures on the magnetic particle-particle interaction strengths λ (a) λ=4, (b) λ=7 and (c) λ=10 in the absence of an applied magnetic field ξ=0.

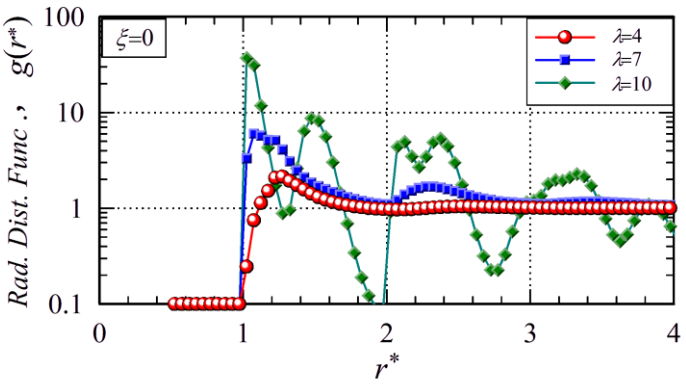

Fig. 2.6 Radial distribution function $g(r^*)$ for the three cases of the magnetic particle-particle interaction strength, λ=4, λ=7 and λ=10 in the absence of an applied magnetic field ξ=0.

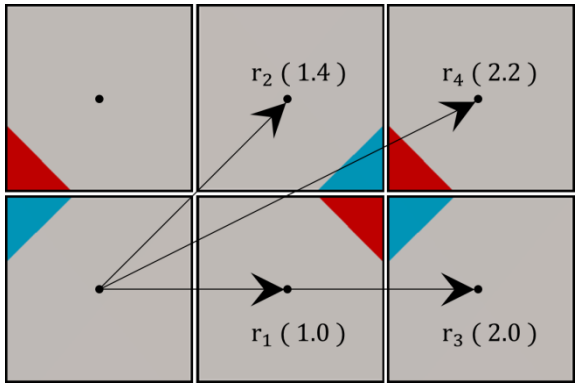

Fig. 2.7 The relationship between each peak in the radial distribution function and the configuration of cubic particles in a cluster.

We now employ the order parameter $S_2^{(m)}$,defined in Eq.(2.6), in order to discuss the regime change whereby an internal structure with no cluster formation is transformed into clusters with a closely-packed structure. Figure 2.8 shows the dependence of the order parameter $S_2^{(m)}$ on the magnetic particle-particle interaction strength λ for no applied magnetic field ξ=0. In the range of relatively low interaction strength $\lambda \lesssim 5$, the value of the order parameter tends to almost zero and clearly implies, as already discussed, that the particles do not aggregate to form clusters. The curve slowly starts to increase from $\lambda \simeq 6$ and further steeply increases between $\lambda \simeq 7.5$ and $\lambda \simeq 8.5$. This implies the occurrence of a regime change in internal structure during the increase in the value of the order parameter $S_2^{(m)}$, from a situation with no cluster formation to the formation of the large closely-packed structures shown in Fig. 2.5(b).

From the above discussion, we understand that an increase in the magnetic particle-particle interaction strength λ induces the formation of large closely-packed clusters in the situation of no applied magnetic field.

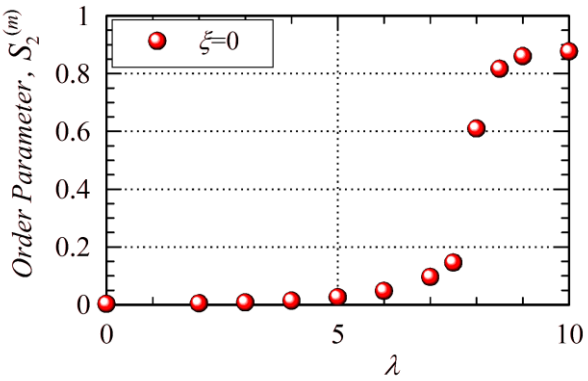

Fig. 2.8 Dependence of the order parameter of the magnetic moment $S_2^{(m)}$ on the magnetic particle-particle interaction strength λ for no applied magnetic field ξ=0.

2.6.2 Influence of the magnetic particle-field interaction strength

We now discuss the dependence of the internal structure of the particle aggregates on the external magnetic particle-field interaction strength ξ. Figure 2.9 shows results from snapshots for ξ=5 shown in Fig. 2.9(a) and ξ=20 shown in Fig. 2.9(b) for the relatively weak magnetic particle-particle interaction strength λ=7. For the case of relatively weak magnetic field ξ=5, it is seen that thin chain-like clusters are formed in the system along the magnetic field direction. As the magnetic particle-field interaction strength is increased to ξ=20, these thin chain-like clusters grow thicker along the field direction and as expected from section 2.2, the internal structure of these thick clusters is composed of the basic structure unit shown in Fig. 2.4(a). However, it is seen from the magnified pictures in Fig. 2.9(b) that the internal structure is relatively loose because the magnetic particle-particle interaction strength λ=7 is not sufficiently large for stable cluster formation. In the situation of a larger magnetic particle-field interaction strength, the magnetic moments of each particle are strongly restricted to the magnetic field direction, and therefore the particle configuration *e*1 shown in Fig. 2.2 is expected to appear more frequently in the case of a sufficiently large magnetic particle-particle interaction strength. Hence, we may presume that the insufficient magnetic particle-particle interaction of λ=7 induces the looser internal structure in the thick chain-like clusters shown in Fig. 2.9(b) and that was also predicted for a system of the round-edge cubes [8]. Figure 2.10 shows the dependence of the radial distribution function on the magnetic particle-field interaction strength. It is seen from Fig. 2.10 that the distribution exhibits clearer and higher second and third peaks with increasing value of the magnetic particle-field interaction strength. This quantitatively implies that thicker chain-like clusters are formed in the system with increasing magnetic particle-field interaction strength.

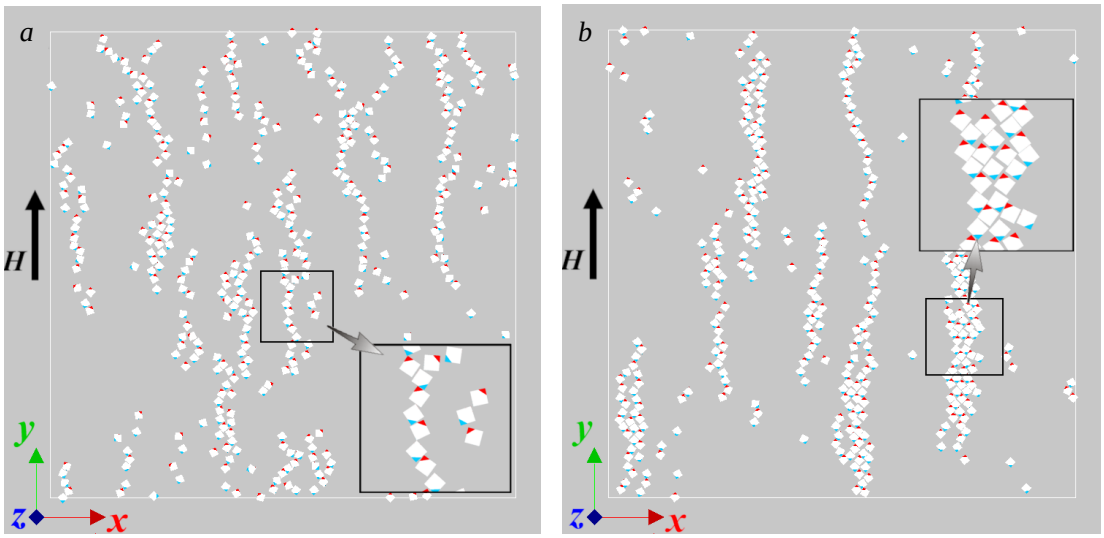

Fig. 2.9 Enhancement of thick chain-like clusters along the field direction by the external field strengths (a)ξ=5 and (b)ξ=20 for the magnetic particle-particle interaction strength λ=7.

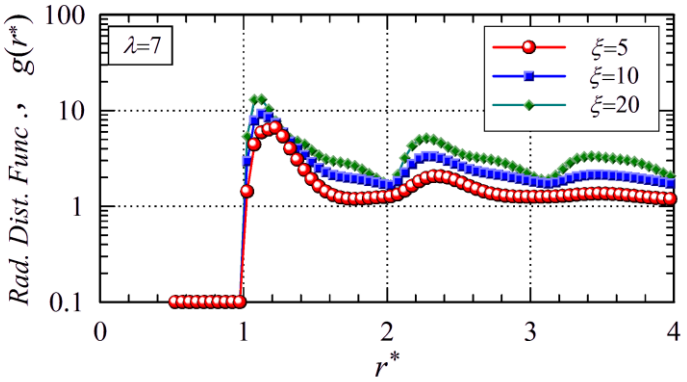

Fig. 2.10 Dependence of the radial distribution function $g(r^*)$ on the magnetic particle-field interaction strength for the three cases of ξ=5, ξ=10 and ξ=20 for the magnetic particle-particle interaction strength λ=7.

Figure 2.11 shows results from snapshots for the magnetic particle-field interaction strength ξ=3 shown in Fig. 2.11(a) and ξ=5 shown in Fig. 2.11(b) for the larger magnetic particle-particle interaction strength λ=10. It is clearly seen from Fig. 2.11 that the closely-packed structures shown in Fig. 2.5(c) are transformed into elongated thick chain-like clusters with increasing magnetic particle-field interaction strength. That is, an increase in the magnetic particle-field interaction strength induces a regime change from closely-packed clusters based on the cluster unit shown in Fig. 2.4(b) into a regime of thick chain-like clusters based on the cluster unit

shown in Fig. 2.4(a). The difference in the internal structure of particle aggregates can be recognized by addressing the radial distribution function $g(r^*)$ shown in Fig. 2.12. Figure 2.12 shows the dependence of the radial distribution function on the particle distance r^* for the magnetic particle-particle interaction strength λ=10. The curves for external particle-field interaction strengths ξ=5 and ξ=7 show characteristics slightly different from that for the case of ξ=3 in that the second, third and fourth peaks are smoother, suggesting that the regime change of the internal structure arises in a small range between ξ=3 and ξ=7. It is seen that the curve for ξ=3 in Fig. 2.12 is good agreement with that for λ=10 and ξ=0 in Fig. 2.6, although the peaks tend to be higher because of the enhancement of the longer clusters due to the influence of an external magnetic field. Similar to the case with no applied magnetic field ξ=0, there is a peak at $r^* \simeq 1.5$ in the curves of the radial distribution function $g(r^*)$ in Fig. 2.12, which implies that the internal structure of thick chain-like clusters is a combination of the basic structure shown in Fig. 2.4(a), and this internal structure may be relatively stable.

From the above results regarding the snapshot and radial distribution function, we conclude that an applied magnetic field functions to significantly enhance the formation of elongated closely-packed clusters along the magnetic field direction if the magnetic particle-particle interaction λ is sufficiently large, but does not strongly regularize the internal structure of these clusters. An increase in the magnetic particle-field interaction strength ξ induces the formation of elongated clusters along the magnetic field direction even if the magnetic particle-particle interaction strength is not that strong, i.e. λ=7.

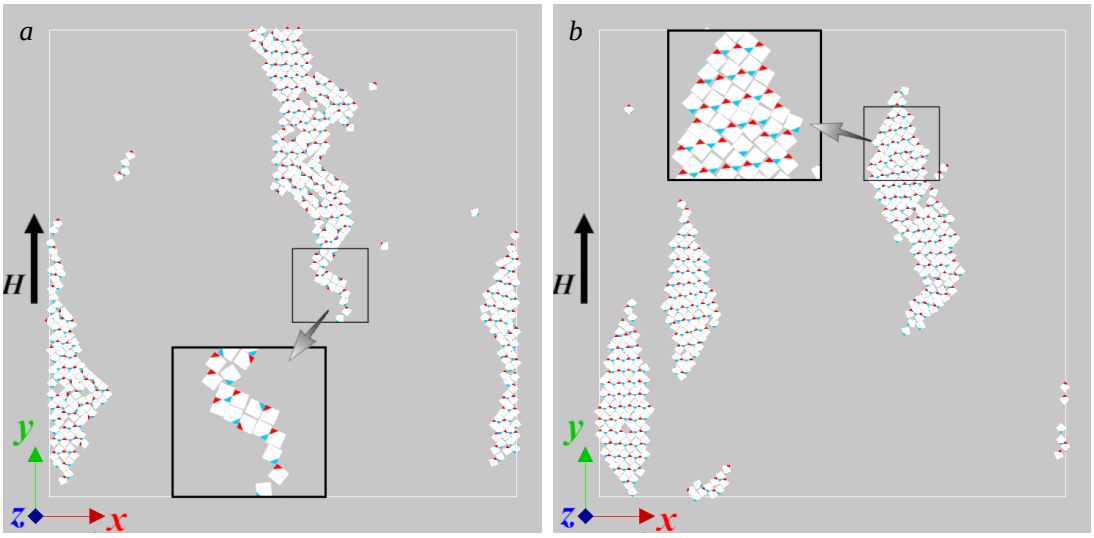

Fig. 2.11 Enhancement of thick chain-like clusters along the field direction by the external field interaction strengths (a) ξ=3 and (b) ξ=5 for the magnetic particle-particle interaction strength λ=10.

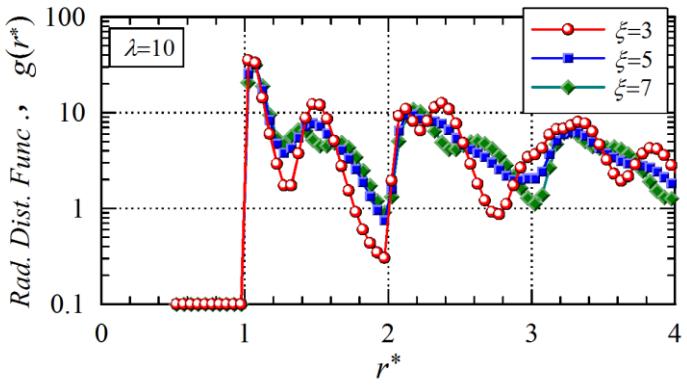

Fig. 2.12 Dependence of the radial distribution function $g(r^*)$ on the magnetic particle-field interaction strength for the three cases of ξ=3, ξ=5 and ξ=7 for the magnetic particle-particle interaction strength λ=10.

Figure 2.13 shows the dependence of the order parameter of the magnetic moment $S_1^{(m)}$ on the magnetic particle-field interaction strength ξ for the cases of magnetic particle-particle interaction strengths λ=0, λ=7 and λ=10. It is noted that the order parameter $S_1^{(m)}$ describes the degree of order regarding the correlation of the direction $\boldsymbol{n}_i$ and $\boldsymbol{n}_j$ of the magnetic moments. Hence, the value of $S_1^{(m)}$ approaches the theoretical value $S_1^{(m)}$ =0.33 when all the projection vectors of the magnetic moments incline in the field direction. For the case of λ=0, the value of the order parameter monotonically increases with increasing magnetic field because the magnetic moments of each particle are free to incline in the field direction. For the case of a relatively large magnetic particle-particle interaction strength λ=7, the curve significantly increases in comparison with the case λ=0, and this deviation becomes larger with increased magnetic particle-field interaction strength ξ. This is because an increase in the magnetic particle-field interaction strength induces the formation of elongated clusters, as already addressed. For the case of a strong magnetic particle-particle interaction strength λ=10, it is seen that the curve exhibits a significantly different characteristic than that shown by the previous cases. That is, in the range of smaller magnetic particle-field interaction strength $\xi \lesssim 3$, the order parameter shows almost zero value until there is a significant increase between $\xi \simeq 4$ and $\xi \simeq 7$ that tends to converge to a saturated value of $S_1^{(m)} \simeq 0.33$ around $\xi \simeq 10$. This steep increase clearly suggests the occurrence of the structural regime change in the particle aggregates from closely-packed clusters into elongated thick chain-like clusters along the magnetic field direction. The almost zero value of $S_1^{(m)}$ in the range of lower magnetic particle-field interaction strengths results from a cancellation effect arising from the basic structure in Fig. 4(b).

In the case of a larger magnetic particle-field interaction strength $\xi \gtrsim 7$, elongated chain-like

clusters are formed in the system and the magnetic particle-particle interaction in the clusters induces an enhancement of the alignment of the magnetic moments to the magnetic field direction that leads to the larger value of $S_1^{(m)}$.

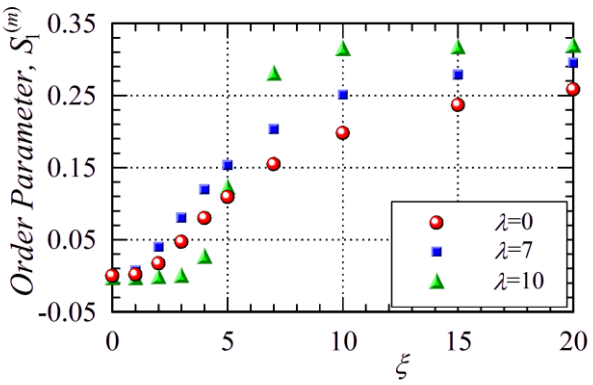

Fig. 2.13 Dependence of the order parameter of the magnetic moment $S_1^{(m)}$ on the magnetic particle-field interaction strength for three cases of the magnetic particle-particle interaction strength, λ=0, λ=7 and λ=10.

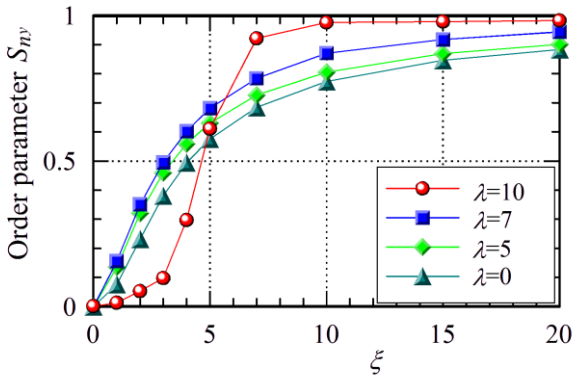

Fig. 2.14 Dependence of the order parameter S_{ny}, regarding the alignment of the magnetic moments with the applied magnetic field direction, on the magnetic particle-field interaction strength ξ for the four cases of the magnetic particle-particle interaction strength, λ=0, λ=5, λ=7 and λ=10.

The occurrence of a regime change is also supported by the results from the order parameter S_{ny} regarding the alignment of the magnetic moments with the applied magnetic field direction shown in Figure 2.14. The non-dimensional parameter ξ denotes the magnetic particle-field interaction strength relative to the effect of the thermal energy and the value of ξ=10 implies that the effect of the magnetic particle-field interaction is significantly more dominant than the influence of the random thermal motion. In a manner similar to the previous case, the curve for λ=10 exhibits completely different characteristics in a quantitative manner from those for the case of λ=0, λ=5 and λ=7. That is, the curve for λ=10 steeply increases and converges to almost unity at ξ=10, but the curves for λ=0, 5 and 7 continue to gradually increase with increasing magnetic particle-field interaction strength. These characteristics quantitatively also suggest a difference in the features of the internal structure of the aggregates. In the case of λ=10 shown in Fig. 2.11, long and stable thick chain-like clusters are formed in contrast to the single-moving particles for λ=0 and short clusters with a loose internal structure that are formed for the case λ=5. From the characteristics of the order parameter S_{ny} in Fig. 2.14, it is seen that the magnetic particle-particle interaction significantly enhances the alignment of the magnetic moments toward the magnetic field direction. Relative to other order parameters, we understand that the order parameter S_{ny} can reflect both the difference in the characteristics of the alignment of the magnetic moments and the difference in the internal structure of particle aggregates more sensitively and clearly.

2.6.3 Influence of the volumetric fraction of particles

Finally, we discuss the influence of the volumetric fraction ϕ_V of cubic particles on the cluster formation. Figure 2.15 shows snapshots for only a small part of the whole system for the case of a large magnetic particle-particle interaction strength λ=10 and no applied magnetic field ξ=0. In the case of ϕ_V=0.01 shown in Fig. 2.15(a), there is a small closely-packed cluster composed of approximately only 16 particles. In contrast, for the case of ϕ_V=0.2 shown in Fig. 2.15(b), larger closely-packed clusters are formed throughout the system and they are clearly seen to be composed of the basic cluster unit shown in Fig. 2.4(b). It is understood from these snapshots that larger closely-packed clusters are formed with increasing volumetric fraction and this is because a small volumetric fraction scarcely provides an opportunity for the smaller cluster units to approach each other.

Lastly, we discuss the dependence of the internal structure of the clusters on the volumetric fraction of particles, using the radial distribution function $g(r^*)$ where Figure 2.16 shows results for the case of a large magnetic particle-particle interaction strength λ=10 and no applied magnetic field ξ=0. It is seen from Fig. 2.16 that the position of each peak does not significantly change although the height of each peak slightly decreases with increasing volumetric fraction. This clearly implies that the essence of the internal cluster structure is not significantly dependent on the volumetric

fraction of particles. That is, a regime change in the internal structure of aggregates does not occur due to the influence of the volumetric fraction of particles. The reason why there is a decrease in the height of the peaks with increasing volumetric fraction may be explained as follows. In the situation of a relatively large volumetric fraction ϕ_V=0.2, a large main cluster is formed from a combination of medium-sized clusters that incline in slightly different directions to each other. This combination of the different directional characteristics of the medium-size clusters induces a decrease in the regularity of the larger cluster configuration and leads to a decrease in the height of the peaks of the radial distribution function.

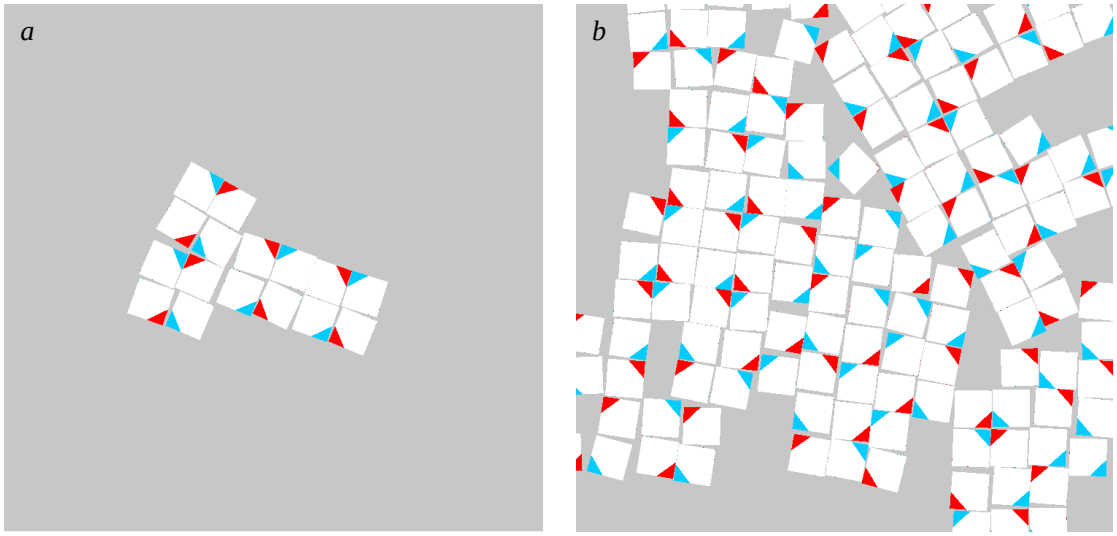

Fig. 2.15 Dependence of the aggregate structures on the particle volumetric fraction (a) ϕ_V=0.01 and (b) ϕ_V=0.2 for the case of a large magnetic particle-particle interaction strength λ=10 and no applied magnetic field ξ=0.

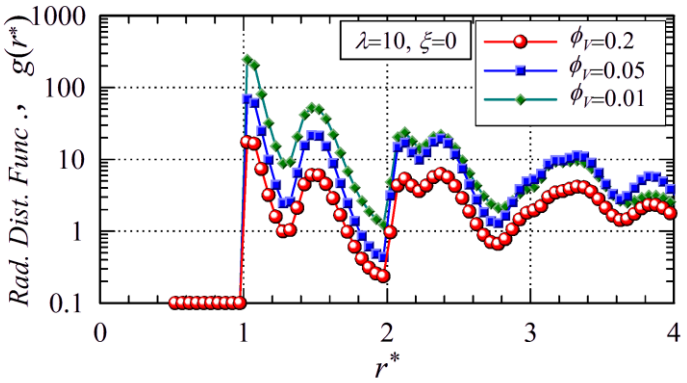

Fig. 2.16 Dependence of the radial distribution function $g(r^*)$ on the particle volumetric fraction for the three cases of ϕ_V=0.01, ϕ_V=0.05 and ϕ_V=0.2.

From the above characteristics exhibited by the aggregate structures, we may conclude that a large volumetric fraction of particles will significantly enhance the size of the clusters although it does not significantly influence the internal structure of the larger closely-packed clusters.

2.7 Conclusion

We have addressed a suspension composed of magnetic cubic particles in thermodynamic equilibrium by means of Monte Carlo simulations in order to investigate particle aggregate structures. From the viewpoint of developing a surface modification technology, we have focused on a quasi-2D system in thermodynamic equilibrium where an external magnetic field is applied in the plane of the material surface. In order to qualitatively and quantitatively discuss the characterization of the internal structure of the aggregates, we have addressed the simulation snapshots, a radial distribution function and system order parameters. We have considered the effects of the magnetic particle-particle interaction strength, the magnetic particle-field interaction strength and the volumetric fraction of particles for clarifying the characteristics of the regime changes that are dependent on these factors. If the magnetic particle-particle interaction strength is sufficiently large, the particles aggregate to form closely-packed clusters where the constituent particles are located with an almost perfect face-to-face contact. The regime change in the internal structure from a no cluster to a significant cluster formation is quantitatively evaluated by an order parameter, where the value of this order parameter steeply increases within a small range of the magnetic particle-particle interaction strength. As the magnetic particle-field interaction strength is increased, the closely-packed clusters are transformed into the chain-like clusters laying along the magnetic field direction. The chain-like clusters are formed in the system even if the magnetic particle-particle interaction strength is not relatively large and the effect of an external magnetic field functions to enhance a chain-like formation. This clearly implies that an applied magnetic field induces a transition in the aggregate structures of a magnetic cubic particle suspension. Larger closely-packed clusters are formed with increasing volumetric fraction because a larger volumetric fraction is able to provide a greater probability for the particles to approach each other. However, the internal structure of the closely-packed clusters is not significantly influenced by a change in the volumetric fraction.

References

[1] M. Aoshima, M. Ozaki and A. Satoh, Structural analysis of self-assembled lattice structures composed of cubic hematite particles, J. Phys. Chem. C 116 (2012) 17862-17871.

[2] S. I. R. Castillo, C.E. Pompe, J. Van Mourik, D. M. A. Verbart, D. M. E. Thies-Weesie, P.E. De Jongh and A.P. Philipse, Colloidal cubes for the enhanced degradation of organic dyes, J. Mater. Chem. A 2 (2014) 0193-10201.

[3] J. M. Meijer, D. Byelov, L. Rossi, A. Snigirev, I. Snigireva, A. P. Philipse and A. V. Petukhov, Self-assembly of colloidal hematite cubes: a microradian X-ray diffraction of exploration of sedimentary crystals, Soft matter 9 (2013) 10729-10738.

[4] M. V. Kovalenko, M. I. Bodnarchuk, R. T. Lechner, G. Hesser, F. Schäffler and W. Heiss, Fatty acid salts as stabilizers in size- and shape-controlled nanocrystal synthesis: The case of inverse spinel iron oxide, J. Am. Chem. Soc. 129 (2007) 6352-6353.

[5] J. M. Meijer, F. Hagemans, L. Rossi, D. Byelov, S. I. R. Castillo, I. Snigireva, A. P. Philipse and A. V. Petukhov, Self-assembly of colloidal cubes via vertical deposition, Langmuir 28 (2012) 7631-7638.

[6] L. Rossi, S. Sacanna, W. T. M. Irvine, P. M. Chaikin, D. J. Pine and A. P. Philipse, Cubic crystals from cubic colloids, Soft Matter 7 (2011) 4139-4142.

[7] J. G. Donaldson and S. S. Kantorovich, Directional self-assembly of permanently magnetised nanocubes in quasi two dimensional layers, Nanoscale 7 (2015) 3217-3228.

[8] P. Linse, Quasi-2D fluids of dipolar superballs in an external field, Soft Matter 11 (2015) 3900-3912.

[9] M. P. Allen and D. J. Tildesley, *Computer Simulation of Liquids* (Clarendon Press, Oxford, 1987).

[10] A. Satoh, *Introduction to Molecular-Microsimulation of Colloidal Dispersions* (Elsevier, Amsterdam, 2003).

[11] A. Satoh, A new technique for metropolis Monte Carlo simulation to capture aggregate structures of fine particles: Cluster-moving Monte Carlo algorithm, J. Colloid Interface Sci. 150 (1992) 461-472.

[12] L. Rossi, V. Soni, D. J. Ashton, D. J. Pine, A. P. Philipse, P. M. Chaikin, M. Dijkstra, S. Sacanna and W. T. M. Irvine, Shape- sensitive crystallization in colloidal superball fluids, Proc. Natl. Acad. Sci. U. S. A. (edited by D. A. Weitz) 112 (2015) 5286-5290.

[13] H. W. Hatch, W. P. Krekelberg, S. D. Hudson, and V. K. Shen, Depletion-driven crystallization of cubic colloids sedimented on a surface, J. Chem. Phys. 144 (2016) 194902.

[14] M. Aoshima, A. Satoh and R. W. Chantrell, Influence of perpendicular external magnetic field on microstructures of monolayer composed of ferromagnetic particles: Analysis by means of quasi-two-dimensional Monte Carlo simulation, J. Colloid Interface Sci. 323 (2008) 158-168.

[15] M. Aoshima and A. Satoh, Two-dimensional Monte Carlo simulations of a polydisperse colloidal dispersion composed of ferromagnetic particles for the case of no external magnetic field, J. Colloid Interface Sci. 280 (2004) 83-90.

[16] J. M. Tavares, J. J. Weis and M. M. T. Da Gama, Quasi-two-dimensional dipolar fluid at low densities: Monte Carlo simulations and theory, Phys. Rev. E. 65 (2002) 061201.

[17] P. D. Duncan and P. J. Camp, Structure and dynamics in a monolayer of dipolar spheres, J. Chem. Phys. 121 (2004) 11322-11331.

Chapter 3 Dependence of a regime change on the composition ratio of cubic particles with different magnetic moment directions via 2D Monte Carlo simulations

3.1 Introduction

From the viewpoint of the development of a surface modification technology [1-3], in Chapter 2 we discussed the phase change in the aggregate structure of a suspension composed of cubic hematite particles on a material surface by means of 2D Monte Carlo simulations. We focused on a situation where half the number of particles have a magnetic moment pointing in the upward direction and the remainder have a magnetic moment pointing in the downward diagonal direction relative to the material surface. This assumption of half upward and half downward seems to be quite reasonable in the situation where the effect of the gravitational field is more dominant than thermal motion and an external magnetic field is applied in the plane of the material surface. If the external magnetic field is applied in the direction of the gravitational field, normal to the material surface, this assumption may not be acceptable. If we treat a suspension composed of cubic particles with a limited rotational ability as in Chapter 2, we should take into account of the ratio of the number of particles with upward and downward magnetic moments. In contrast, if the cubic particles have the full three-dimensional rotational ability, as in Linse's study [4], it is not necessary to consider the composition ratio. In Linse's study [4], the dependence of the cluster formation on the variation of geometrical shape of the magnetic particle, from a spherical to a cube-like shape, was investigated with a full three-dimensional rotational ability. Similarly, the effect of the geometrical shape on the aggregate structures has been investigated for dipolar superballs [5, 6].

From this background, we here expand the previous study of Chapter 2 to a variety of composition ratios for the number of cubic particles with the two different magnetic moment directions. As will be seen from the following results and discussion, the composition of the moment ratio of these cubic particles has a significant effect on the structural regime of the aggregates. As in the previous study, the particle model is a geometric cube and under the assumption of a dominant gravitational force whereby the particles perform a translational motion with one face in contact with the material surface and the rotational motion is restricted about a line normal to the plane of the material surface.

In Chapter 3, we consider a quasi-two dimensional system composed of cubic hematite particles in thermodynamic equilibrium. Monte Carlo simulations have been performed in order to elucidate the dependence of particle aggregates on the magnetic moment composition ratio, magnetic particle-particle interaction strength and magnetic particle-field interaction strength.

3.2 Model of magnetic cubic particles

As in the previous study of Chapter 2, we treat the two types of cubic particles with the magnetic moment pointing in the upward or downward diagonal direction relative to the bottom or material surface. As shown in Fig. 3.1, the particles are idealized with the geometry of a cube of side length d and with a magnetic dipole moment $\boldsymbol{m}=m\boldsymbol{n}$ at the center of the cube pointing in a diagonal direction which is a typical characteristic of cube-like hematite particles [7, 8]. In contrast to our study in Chapter 2, we here consider a variety of situations of ensemble ratios for the number of particles with different magnetic moment directions relative to the material surface. The composition ratio of the system regarding the number of the two types of particles is denoted by $R_{updwn}=N_{up}/N_{dwn}$, where N_{up} is the number of upward and N_{dwn} is the number of downward pointing magnetic moments relative to the material surface. From our results we will discuss the dependence of the internal structure of particle aggregates on the composition ratio R_{updwn}. In order to visually discern the difference of the composition ratio R_{updwn} in the figures and the snapshots shown below, the cubes with a magnetic moment in the upward diagonal direction are shown red whilst cubes with a magnetic moment in the downward diagonal direction are shown blue.

The absolute orthogonal coordinate system xyz is set with the z-axis in the positive direction normal to the bottom or material surface. Employing this coordinate system, an external magnetic field $\boldsymbol{H}$ is expressed as $\boldsymbol{H}=H\boldsymbol{h}=(0, H, 0)$, where $\boldsymbol{h}$ is the unit vector denoting the field direction. If the position vector and the magnetic moment of particle i are denoted by $\boldsymbol{r}_i$ and $\boldsymbol{m}_i$, respectively, then the magnetic particle-particle interaction energy $u_{ij}^{(m)}$ and magnetic particle-field interaction energy $u_i^{(H)}$ are expressed as

$$u_{ij}^{(m)}=kT\lambda\frac{1}{(r_{ij}/d)^3}\left\{\boldsymbol{n}_i\cdot\boldsymbol{n}_j-3(\boldsymbol{n}_i\cdot\boldsymbol{t}_{ij})(\boldsymbol{n}_j\cdot\boldsymbol{t}_{ij})\right\} \tag{3.1}$$

$$u_i^{(H)}=-kT\xi\,\boldsymbol{n}_i\cdot\boldsymbol{H}/H \tag{3.2}$$

in which, $\boldsymbol{n}_i$ is the unit vector of the magnetic moment direction, $\boldsymbol{t}_{ij}$ is the unit vector denoting the direction of particle i relative to particle j, expressed as $\boldsymbol{t}_{ij}=\boldsymbol{r}_{ij}/r_{ij}$, where $\boldsymbol{r}_{ij}=\boldsymbol{r}_i-\boldsymbol{r}_j$ is the relative position of particle i to particle j, and $r_{ij}=|\boldsymbol{r}_{ij}|$.

From the non-dimensionalization procedure, it is seen that the present phenomenon is governed by two non-dimensional parameters, $\lambda=\mu_0 m^2/(4\pi d^3 kT)$ and $\xi=\mu_0 mH/(kT)$, which imply the strengths relative to the thermal energy of the magnetic particle-particle interaction and magnetic particle-field interaction, respectively. In these parameters, μ_0 is the permeability of free space, k is Boltzmann's constant, and T is the absolute temperature of a suspension.

From the perspective of a surface modification technology, it may be desirable to take into account surface forces. However, in the present study, we concentrate on the magnetic

particle-particle interaction λ and the magnetic particle-field interaction ξ, since we regard this approach as a reasonable first step to elucidate the behavior of the cubic hematite particles on a material surface.

Figure 3.2 shows part of the results from the analysis of the interaction energy $\tilde{u}_{ij}^{(m)} = u_{ij}^{(m)} / (\mu_0 m^2 / 4\pi d^3)$ which has already been discussed in Chapter 2. The Figs. 3.2(a) and 3.2(c) are for the case of two particles with the magnetic moment of one pointing in the upward and the other in the downward diagonal direction relative to the material surface, referred to as the upward and the downward particle from now on and the Figs. 3.2(b) and 3.2 (d) are for the case of two downward particles. The Figs. 3.2(a) and 3.2(b) show a difference in the interaction energy between two typical particle configurations which give rise to a minimum interaction energy for a two-particle system. The particle configuration shown in Fig. 3.2(a), gives rise to a relatively low interaction energy $\tilde{u}_{ij}^{(m)} = -1.333$ compared to the value $\tilde{u}_{ij}^{(m)} = -0.666$ shown for the case of configuration Fig. 3.2(b). Similarly, the configurations Fig. 3.2(c) yield the interaction energies $\tilde{u}_{ij}^{(m)} = -0.666$ or -0.5892, whereas the configuration in Fig. 2(d) leads to the larger energy $\tilde{u}_{ij}^{(m)} = -0.3535$.

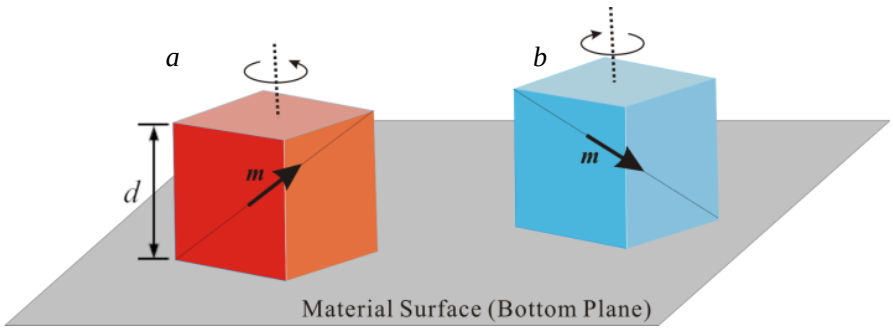

Fig. 3.1 Particle model with two types of magnetic moment direction: (a) upward diagonal direction and (b) downward diagonal direction relative to the bottom plane or material surface.

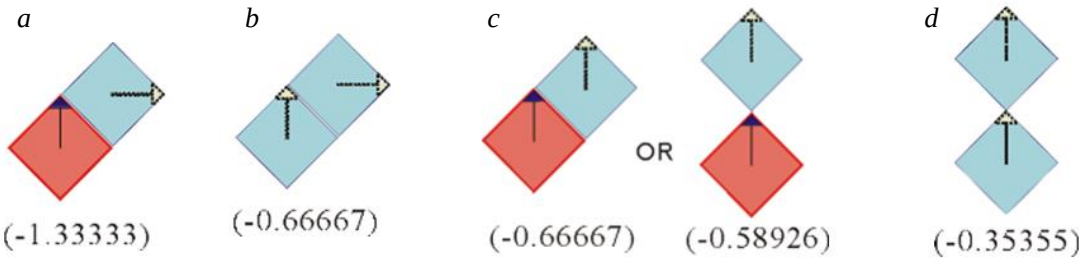

Fig.3.2 Preferred configuration in (a) main clusters and (b) sub-clusters for no external magnetic field, and (c) main clusters and (d) sub-clusters for a strong magnetic field.

3.3 Order parameters

As in Chapter 2, we focus on the following order parameter in order to quantitatively discuss the configuration features of the aggregates.

$$S_2^{(m)} = \frac{1}{N_{pair}} \left\langle \sum_{i=1}^{N} \sum_{\substack{j=1 \\ (>i)}}^{N} \cos(4\theta_{ij}^{(n)}) \right\rangle \tag{3.3}$$

where $N_{pair} = N(N-1)/2$ is the number of pairs of particles, $\hat{\boldsymbol{n}}_i$ and $\hat{\boldsymbol{n}}_j$ are the unit projection vectors of the magnetic moment of particle i and j, respectively and $\theta_{ij}^{(n)}$ is the angle between the unit vectors $\hat{\boldsymbol{n}}_i$ and $\hat{\boldsymbol{n}}_j$. It is noted that the value of order parameter $S_2{}^{(m)}$ approaches unity as closely-packed aggregates are formed in the system.

Moreover, we also employ an order parameter S_{ny} regarding the alignment of the magnetic moments with the applied magnetic field direction.

$$S_{ny} = \frac{1}{N} \left\langle \sum_{i=1}^{N} P_2(\hat{\boldsymbol{n}}_i \cdot \boldsymbol{h}) \right\rangle = \frac{1}{N} \left\langle \sum_{i=1}^{N} \frac{3\cos^2(\hat{\boldsymbol{n}}_i \cdot \boldsymbol{h}) - 1}{2} \right\rangle \tag{3.4}$$

in which $P_2(\hat{\boldsymbol{n}}_i \cdot \boldsymbol{h})$ is the second Legendre polynomial, expressed as $P_2(\hat{\boldsymbol{n}}_i \cdot \boldsymbol{h}) = (3\cos^2(\hat{\boldsymbol{n}}_i \cdot \boldsymbol{h}) - 1)/2$. We have already understood from Chapter 2 that the order parameter S_{ny} can reflect the difference in the features of the alignment of the magnetic moments sensitively and clearly.

3.4 Parameters for simulations

Unless specifically noted, the present results were obtained by adopting the following parameter values. The volumetric fraction of magnetic cubic particles is set to $\phi_V = 0.1$, and the number of particles N=400. The non-dimensional parameters for the magnetic particle-particle interaction strength λ and the magnetic particle-field interaction strength ξ are addressed in a wide range of values with λ=0~10 and ξ=0~20. In Chapter 2, we focused on a particular case where half of the total number of particle moments were in the upward whilst the remainder were in the downward diagonal direction. In the present study we wish to discuss the effect of the composition ratio $R_{updwn}(=N_{up}/N_{dwn})$ on the aggregate structures therefore we treat several more general cases where the ensemble is characterized by the composition ratio taken over the wide range of values R_{updwn}=1/4, 1/3, 1/2 and 1. We employed a periodic boundary condition for treatment at the boundary surfaces of the simulation box both in the x-direction and y-direction. The cubic particles are initially located randomly in the system. The cutoff distance r_{coff} is set as $r_{coff} = 10d$ and the surface-to-surface criterion distance r_{clstr} is set as $r_{clstr} = 0.1d$. The total MC steps is taken as N_{timemx} = 1,000,000 and the

final 80% of the data were used for the data averaging procedures. The cluster-moving procedure was carried out every 20 Monte Carlo steps [9, 10]. In order to clarify the behavior of the cubic particles on a material surface in a variety of situations, we have employed a wide range of values for the non-dimensional parameters. In order to compare experimental results with results obtained from the present simulations, it is necessary to evaluate several non-dimensional parameters that relate to the experimental situations, for example, the liquid temperature and the dimensions of cubic particles.

3.5 Results and discussion

3.5.1 Dependence of the aggregate structures on the magnetic particle-particle interaction strength for no external magnetic field

We discuss the influence of the composition ratio R_{updwn} on the aggregate structures in the absence of an external magnetic field. The Fig. 3.3 and Fig. 3.4 show the aggregate structures for the cases of R_{updwn}=1/2 and R_{updwn}=1/4, respectively, where each figure has two snapshots for the magnetic particle-particle interaction strengths of (a) λ=7 and (b) λ=10.

For the case of an insufficient magnetic particle-particle interaction strength λ=7, shown in Fig. 3.3(a), many small clusters are formed in the system although single particles still remain without aggregating to form specific clusters. This feature is not significantly different from that for the case of a smaller composition ratio R_{updwn} = 1/4, shown in Fig. 3.4(a). The formation of small clusters shown in Figs. 3.3(a) and 3.4(a) is clearly due to the relatively weak magnetic particle-particle interaction strength of λ=7. These small clusters are made up of upward and downward particles, and the small clusters seen in the case of R_{updwn} =1/2, shown in Fig. 3.3(a), are relatively larger than those seen in the case of R_{updwn} =1/4, shown in Fig. 3.4(a).

For the case of a large magnetic particle-particle interaction strength λ=10, it is seen from Figs. 3.3(b) and 3.4(b) that closely-packed clusters are formed in the system, although many single particles and several small clusters remain independent of the large closely-packed clusters. From a comparison between the snapshots of Figs. 3.3(b) and 3.4(b), the size of closely-packed clusters is seen to become smaller with a decreasing value of the composition ratio R_{updwn}. As already discussed in Chapter 2, the closely-packed clusters shown in Figs. 3.3(b) and 3.4(b) are formed from the combination and expansion of the basic cluster unit shown in Fig. 3.2(a). Under conditions where the number of upward particles, N_{up}, is much smaller than the number of downward particles, N_{dwn}, there are almost no single upward particles remaining after the formation of a large closely-packed cluster that may further contribute to their growth. That is, in the vicinity around a closely-packed cluster it is mainly downward particles that remain and may possibly aggregate to form clusters. However, even for the case of λ=10, the interaction energy between downward particles is not sufficiently lower than thermal energy, therefore only short clusters are formed and they do not tend to grow into

larger clusters. The reason why a smaller closely-packed cluster is formed in the system with a decreasing composition ratio is that, after the reduction in the number of the single upward particles, the growth of a closely-packed cluster will finish much earlier. This may also explain why the number of single downward particles around a closely-packed cluster becomes much larger as the composition ratio is decreased.

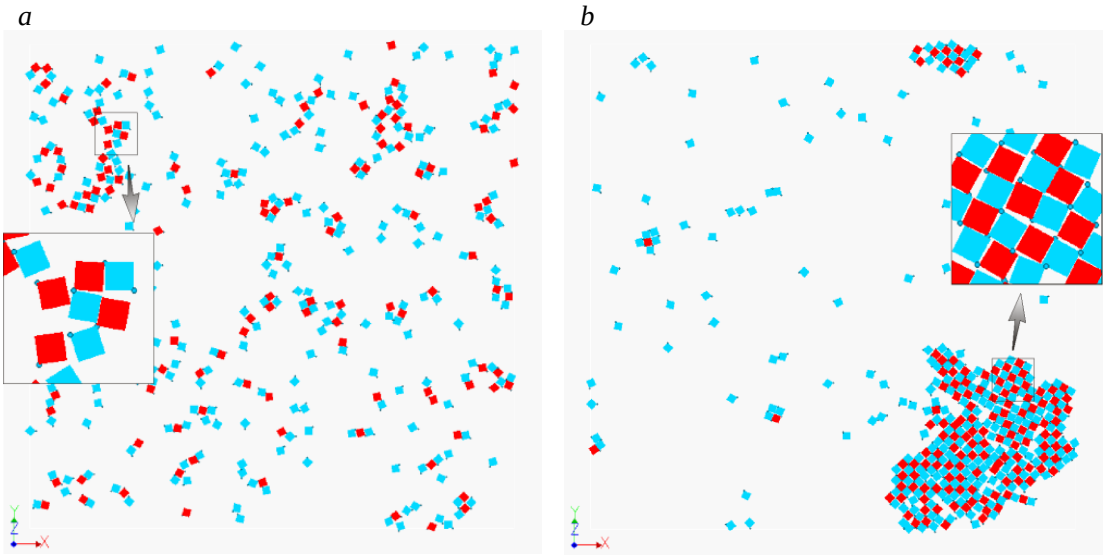

Fig. 3.3 Dependence of the aggregate structures on the magnetic particle-particle interaction strength (a) λ=7 and (b) λ=10 for the composition rate of R_{updwn}=1/2.

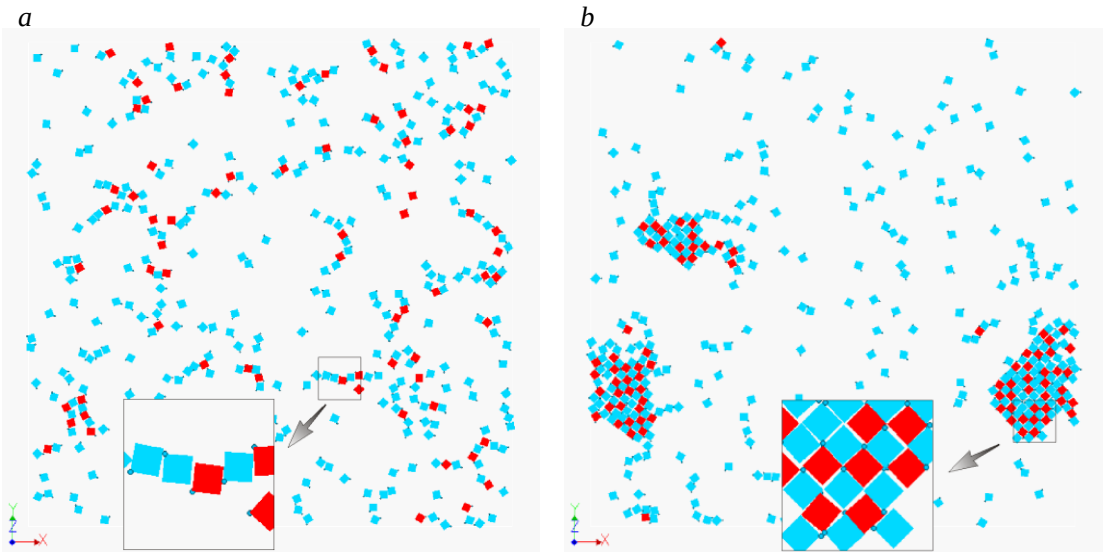

Fig. 3.4 Dependence of the aggregate structures on the magnetic particle-particle interaction strength (a) λ=7 and (b) λ=10 for the composition rate of R_{updwn}=1/4.

These characteristics are supported by results of the following cluster size distribution function. Figures 3.5(a) and 3.5(b) show results of the cluster size distribution for the magnetic particle-particle interaction strengths λ=7 and λ=10, respectively, for various cases of the composition ratio, R_{updwn}= 1, 1/2, 1/3 and 1/4, where the parameter s implies the number of particles that make up each cluster. In the case of λ=7, it is seen from Fig. 3.5(a) that each curve shows large values in the region of low values of s/N, which quantitatively implies that the particle system is composed of single particles and small clusters, as shown in Figs. 3.3(a) and 3.4(a). Since large aggregate structures are not formed in the situation of the relatively weak magnetic particle-particle interaction strength of λ=7, the curves are independent of the moment composition ratio. In contrast, the curves shown in Fig. 3.5(b) for the case of λ=10 exhibit different characteristics that imply they are dependent on the value of the composition ratio R_{updwn}. As the value of the composition ratio is increases, the peaks become higher and shift toward the larger values of s/N. This characteristic clearly implies that a larger composition ratio leads to the formation of larger closely-packed clusters as is seen from Figs. 3.3(b) and 3.4(b). From these results, we conclude that a decrease in the composition ratio leads to the suppression of the growth of large closely-packed clusters. This suggests that the composition ratio may be used as a technique for controlling the cluster formation and the size of closely-packed clusters of cubic hematite particles on the material surface.

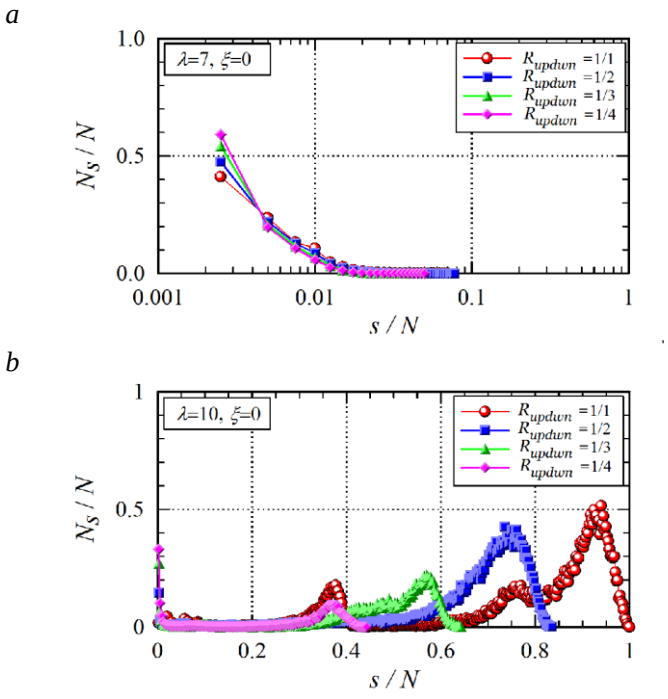

Fig.3.5 Dependence of the cluster size distribution on the composition ratio in the absence of external magnetic field, ξ=0, for the magnetic particle-particle interaction strengths (a) λ=7 and (b) λ=10.

3.5.2 Dependence of the aggregate structures on the magnetic particle-field interaction strength

In this section, we discuss the dependence of the internal structure of particle aggregates on the applied magnetic particle-field interaction strength ξ for several cases of the composition ratio. We here focus on the case of a low composition ratio R_{updwn} = 1/4, which is expected to have a different characteristic from that for the case of a large composition ratio R_{updwn} = 1, that was discussed in Chapter 2. Figure 3.6 shows the snapshots of particle aggregates for the relatively weak magnetic particle-particle interaction strength λ=7 and the low composition ratio R_{updwn} = 1/4. The snapshot for external magnetic particle-field interaction strength ξ=5 is shown in Fig. 3.6(a) and for strength ξ=20 is shown in Fig. 3.6(b).

For the case of R_{updwn} = 1, shown in Fig. 2.9 in Chapter 2, a significant regime change in the internal structure from linear chain-like clusters into thick chain-like clusters arises due to the influence of the magnetic particle-field interaction. However, for the case of R_{updwn} = 1/4, shown in Fig. 3.6, such a significant regime change does not appear and linear chain-like clusters and single particles still remain in the system. This is because there are not a sufficient number of the basic cluster units shown in Fig. 3.2(c) formed in the system for the case of a small composition ratio R_{updwn} = 1/4.

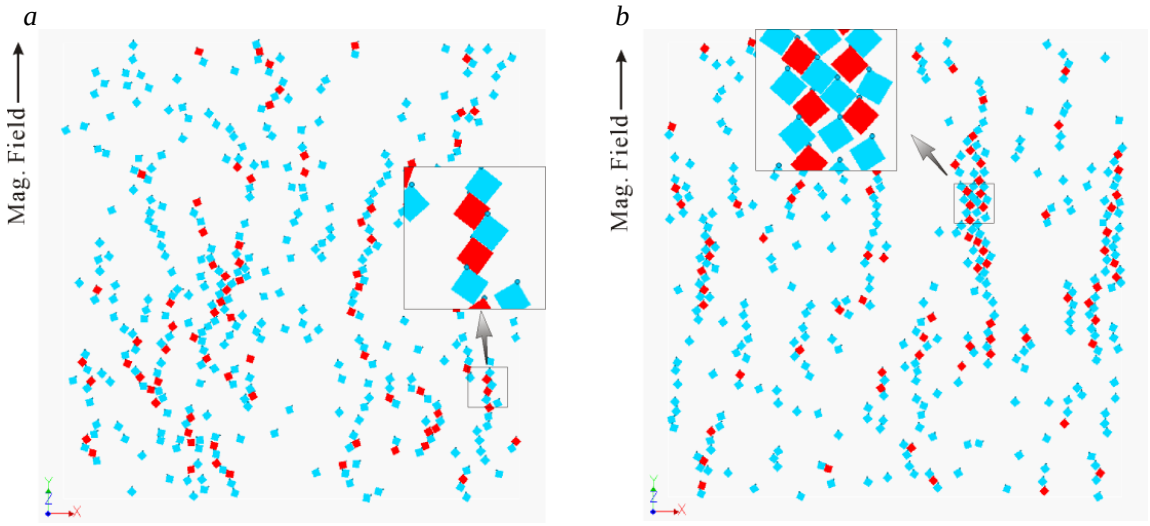

Fig. 3.6 Dependence of the aggregate structures on the magnetic particle-field interaction strength (a) ξ=5 and (b) ξ=20 for the composition rate of R_{updwn}=1/4 and magnetic particle-particle interaction strength λ=7.

These characteristics are supported by the features of the radial distribution function, shown in Fig.3.7 for the magnetic particle-particle interaction strength λ=7 for the magnetic particle-field interaction strengths (a) ξ=5 and (b) ξ=20. It is seen from Fig. 3.7(a) for ξ=5 that each curve shows similar characteristics and is almost independent of the value of the composition ratio. That is, in the situation of the weak applied magnetic particle-field interaction ξ=5, small linear chain-like clusters are formed in the system, independent of the composition ratio. In contrast, from Fig. 3.7(b) for ξ=20 it is seen that several peaks come to appear more significantly with increasing composition ratio. This quantitatively implies that the particles aggregate to form thick chain-like clusters as the value of composition ratio is increased.

From these results, we understand that an external magnetic field does not induce the regime change whereby linear chain-like clusters are transformed into thick chain-like clusters in the case of the smaller composition ratio. Hence, the composition ratio may be used for controlling the aggregate formation even in a strong magnetic field situation.

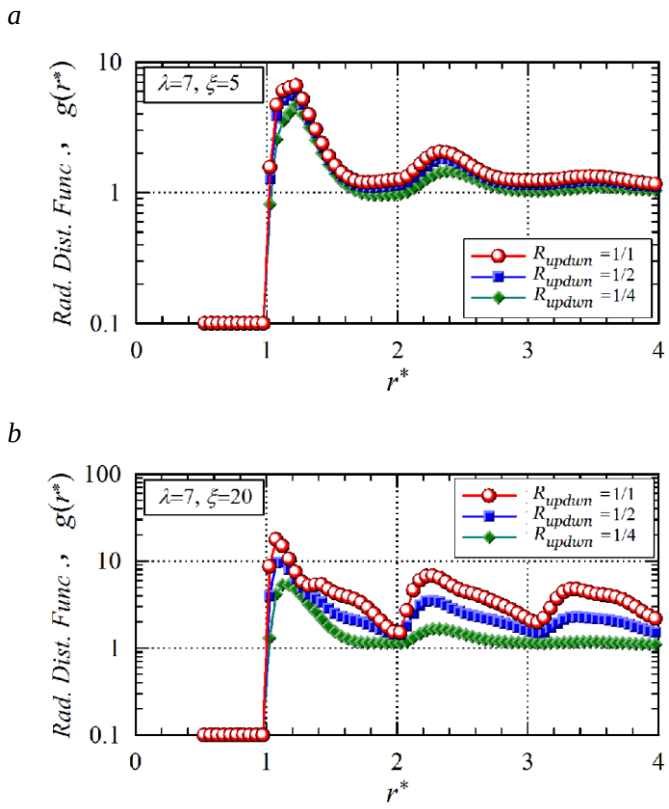

Fig. 3.7 Dependence of the radial distribution function on the composition ratio R_{updwn} for the magnetic particle-particle interaction strength λ=7 for the magnetic particle-field interaction strengths (a) ξ=5 and (b) ξ=20.

Figure 3.8 shows results of the snapshots of particle aggregates for values of the external magnetic particle-field interaction strength ξ=5 shown in Figs. 3.8(a) and ξ=20 shown in Figs. 3.8(b) for the strong magnetic particle-particle interaction strength λ=10 and the small composition ratio R_{updwn} = 1/4. From a comparison with the snapshot for ξ=0 and λ=10, shown in Fig. 3.4(b), it is seen from Fig. 3.8 that the large closely-packed clusters are transformed into elongated thick chain-like structures along the magnetic field direction due to the influence of an external magnetic field. Moreover, as the magnetic particle-field interaction strength is increased from ξ=5 to ξ=20, it is seen that the two relatively small closely-packed clusters combine with each other to form the larger closely-packed cluster which is clearly shown in Fig. 3.8(b). After the combination, this closely-packed cluster cannot further grow since there are only downward particles remaining in the neighboring region. That is, the size of this closely-packed cluster does not change because there are almost no upward particles that would be required to contribute to the growth. In the case of R_{updwn} =1, as already discussed in Chapter 2, many basic cluster units of the type shown in Fig. 3.2(c) are formed around the growing clusters and therefore thicker and larger chain-like clusters tend to be formed more strongly with increasing magnetic particle-field interaction strength.

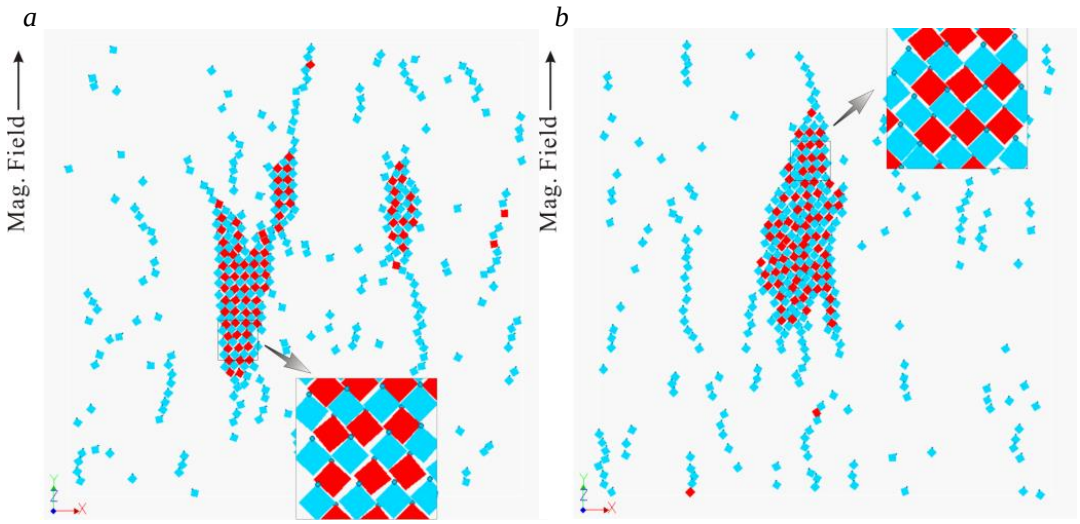

Fig. 3.8 Dependence of the aggregate structures on the magnetic particle-field interaction strengths (a) ξ=5 and (b) ξ=20 for the composition rate of R_{updwn}=1/4 and for the magnetic particle-particle interaction strength λ=10.

Figure 3.9 results the radial distribution function for the case of λ=10 and ξ=5. It is seen that there are high peaks at the positions of integer times the particle size, which implies the formation of stable and large clusters. Moreover, peaks at an intermediate position such as $r^* \simeq 1.4$ suggest the internal structure of the closely-packed clusters which are based on the combination of the basic cluster unit shown in Fig.3.2(c). As the value of the composition ratio is decreased, these peaks become lower, which implies that the size of elongated closely-packed clusters becomes smaller. From these characteristics, we understand that the composition ratio may control the size of elongated closely-packed clusters even in the situation of a strong magnetic field.

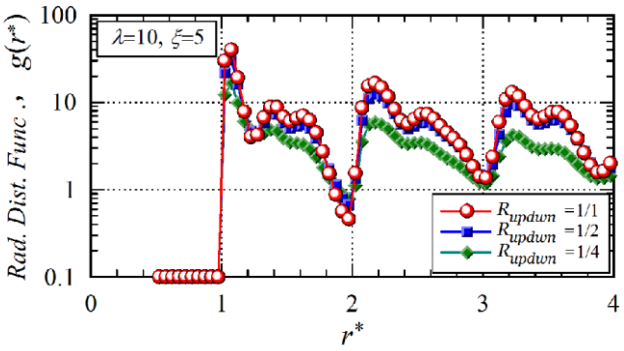

Fig. 3.9 Dependence of the radial distribution function on the composition ratio R_{updwn} for the magnetic particle-particle interaction strength λ=10 and the magnetic particle-field interaction strength ξ=5.

3.5.3 Main and sub-clusters in the aggregate structures

In this section, we discuss the internal structure of the elongated closely-packed clusters (referred to as main clusters) and the other types of clusters (referred to as sub-clusters) in more detail. Figures 3.10(a) and 3.10(b) show a main cluster and a sub-cluster that may be observed in the snapshot shown in Fig. 3.8(a). It is clearly seen from Fig. 3.10(a) that the main cluster is composed of both upward and downward particles and the internal structure is based on the basic cluster unit shown in Fig. 3.2(c). In contrast, the sub-cluster shown in Fig. 3.10(b) is made up of only downward particles as shown in Fig. 3.2(d). Figure 3.11 shows results of the radial distribution function where Fig. 3.11(a) is for the main clusters and Fig. 3.11(b) is for the sub-clusters for the case of magnetic particle-particle interaction strength λ=10 and magnetic particle-field interaction strength ξ=5. It is seen from these figures that there is a significant difference between the main clusters and the sub-clusters. For the case of the main clusters, shown in Fig. 3.11(a), the curves exhibit several peaks that imply the formation of thick chain-like clusters, as already discussed in Chapter 2, and the height of each peak tends to become lower with decreasing moment composition ratio. This characteristic quantitatively suggests that for the case of a smaller composition ratio the elongated thick chain-like clusters do not tend to grow larger. For the case of the sub-clusters, shown in Fig. 3.11(b), there is no high peak at $r^* \simeq 1.4$, and these curves exhibit features that are quite similar to those for a spherical particle system [10]. These characteristics clearly imply that the internal structure of sub-clusters is not based on the basic cluster unit shown in Fig.3.2(c).

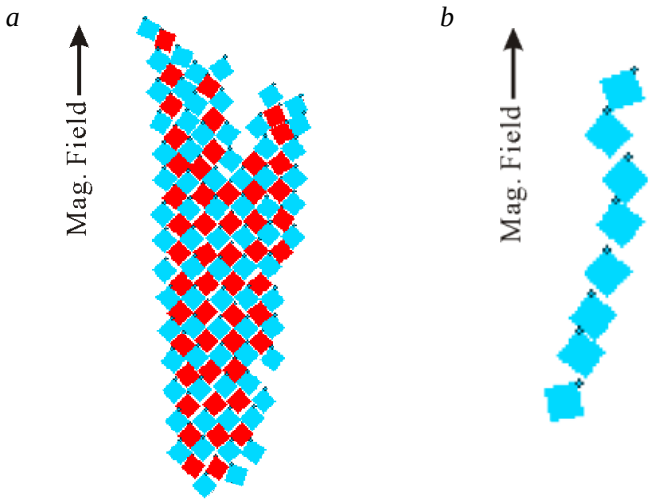

Fig. 3.10 Difference in the internal structure between (a) a main cluster and (b) a sub-cluster for the case of R_{updwn}=1/4, for the magnetic particle-particle interaction strength λ=10 and the magnetic particle-field interaction strength ξ=5.

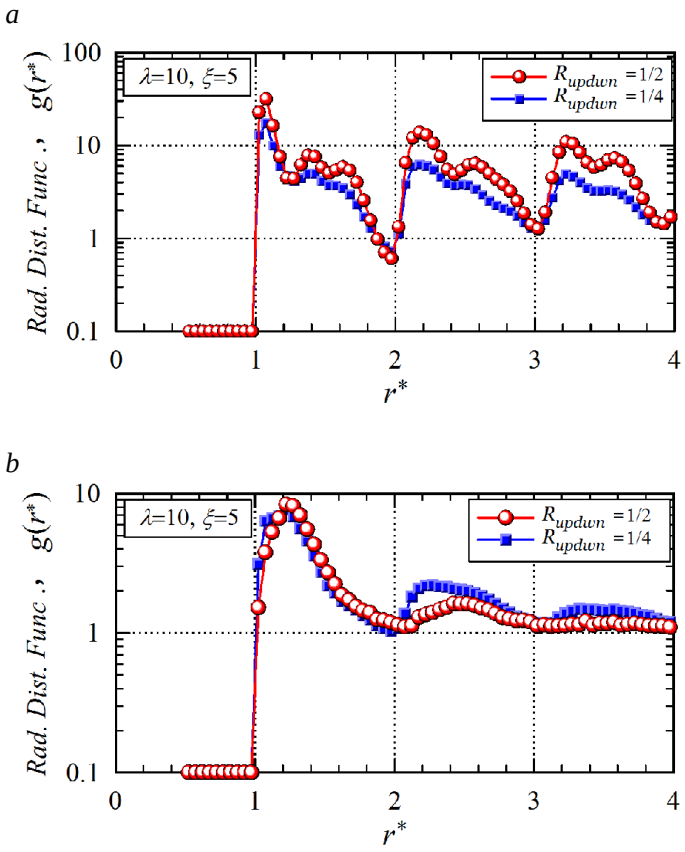

Fig. 3.11 Difference in the radial distribution function between (a) main clusters and (b) sub-clusters for the case of the magnetic particle-particle interaction strength λ=10 and the particle-field interaction strength ξ=5.

3.5.4 Order parameters for expression of a regime change in the internal structure of particle aggregates

Finally, we discuss the regime change in the internal structure of particle aggregates in terms of the order parameters $S_2^{(m)}$ and S_{ny}. Figure 3.12 shows the dependence of the order parameter $S_2^{(m)}$ on the magnetic particle-particle interaction strength λ for no applied magnetic field ξ=0. For the case of R_{updwn}=1, the order parameter steeply increases from λ=7 and approaches a large value $S_2^{(m)}\simeq$0.6 at λ=10. This characteristic is dulled with decreasing composition ratio R_{updwn} whereby the saturated value at λ=10 tends to a lower value. This feature, which has already been discussed in previous sections, clearly implies that smaller clusters are formed in the system for the case of a smaller moment composition ratio. On the other hand, the starting point for an increase in the order parameter is not significantly dependent of the value of the composition ratio R_{updwn}. This may be reasonably understood because the magnetic particle-particle interaction strength between a pair of upward and downward particles is a main factor in the formation of specific clusters.

Figure 3.13 shows the dependence of the order parameter S_{ny} on the magnetic particle-field interaction strength ξ for the magnetic particle-particle interaction strength λ=10. It is seen that the order parameter S_{ny} monotonically increases with increasing values of magnetic particle-field interaction strength, and this feature is common among the three cases of the moment composition ratio. The reason why the curve for R_{updwn} =1 increases more slowly than the curves for the other cases in the region between $\xi \simeq 1$ and $\xi \simeq 3$ is that the closely-packed clusters are more stable against a dissociation as the magnetic moments can align with the magnetic field direction.

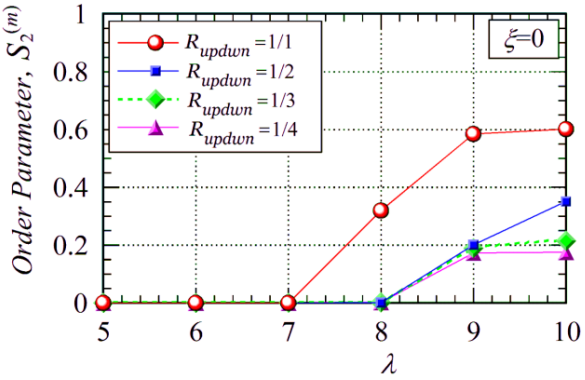

Fig. 3.12 Dependence of the magnetic moment order parameter $S_2^{(m)}$ on the magnetic particle-particle interaction strength λ for various cases of the moment composition ratio R_{updwn}.

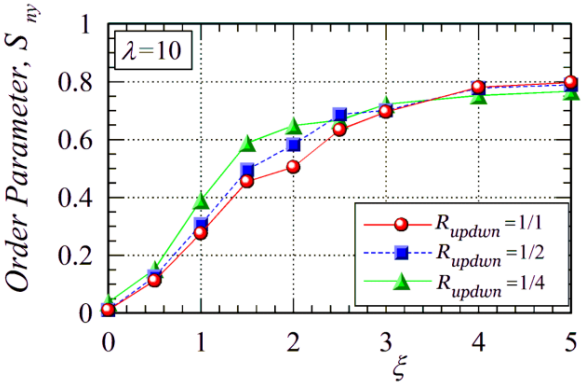

Fig. 3.13 Dependence of the order parameter S_{ny}, regarding the alignment of the magnetic moments with the applied magnetic field direction, on the magnetic particle-field interaction strength ξ for the various cases of the moment composition ratio R_{updwn}.

3.6 Conclusion

We have investigated the behavior of a suspension composed of magnetic cubic particles on a material surface in order to apply the characteristics of a cubic magnetic particle dispersion to the development of the surface modification technology. We have expanded the study in Chapter 2 to consider a variety of ratios of the number of particles with the magnetic moments aligning in the upward and downward directions. The simulations are conducted in the situation of a magnetic field applied parallel to the material surface and a strong gravitational field acting normal to the material surface. We have treated a quasi-2D suspension composed of cubic hematite particles in the situation of thermodynamic equilibrium. Monte Carlo simulations have been performed in order to elucidate the dependence of particle aggregation on the moment composition ratio, the magnetic particle-particle interaction strength and the magnetic particle-field interaction strength. From the Monte Carlo simulations, it is seen that the moment composition ratio has a significant effect on the regime of particle aggregates. As the value of the moment composition ratio is decreased in the situation of no applied magnetic field the size of closely-packed clusters becomes smaller and in the situation of a strong magnetic field thin linear clusters are formed. Therefore we understand that a decrease in the moment composition ratio leads to a suppression of the growth of large closely-packed clusters. This suggests that the composition ratio may be used as a technique for controlling the size of closely-packed clusters of cubic hematite particles on the material surface, even in the situation of a strong magnetic field.

References

[1] S. I. R. Castillo, C.E. Pompe, J. Van Mourik, D. M. A. Verbart, D. M. E. Thies-Weesie, P.E. De Jongh and A.P. Philipse, Colloidal cubes for the enhanced degradation of organic dyes, J. Mater. Chem. A 2 (2014) 10193-10201.

[2] J. M. Meijer, D. Byelov, L. Rossi, A. Snigirev, I. Snigireva, A. P. Philipse and A. V. Petukhov, Self-assembly of colloidal hematite cubes: a microradian X-ray diffraction of exploration of sedimentary crystals, Soft matter 9 (2013) 10729-10738.

[3] M. V. Kovalenko, M. I. Bodnarchuk, R. T. Lechner, G. Hesser, F. Schäffler and W. Heiss, Fatty acid salts as stabilizers in size- and shape-controlled nanocrystal synthesis: The case of inverse spinel iron oxide, J. Am. Chem. Soc. 129 (2007) 6352-6353.

[4] P. Linse, Quasi-2D fluids of dipolar superballs in an external field, Soft Matter 11 (2015) 3900-3912.

[5] J. G. Donaldson, P. Linse, S. S. Kantorovich, How cube-like must magnetic nanoparticles be to modify their self-assembly?, Nanoscale 19 (2017) 6448-6462.

[6] E. S. Pyanzina, A. V. Gudkova, J. G. Donaldson, S. S. Kantorovich, Cluster analysis in systems of magnetic spheres and cubes, J. Magn. Magn. Mater. 431 (2017) 201-204.

[7] M. Aoshima, A. Satoh and R. W. Chantrell, Influence of perpendicular external magnetic field on microstructures of monolayer composed of ferromagnetic particles: Analysis by means of quasi-two-dimensional Monte Carlo simulation, J. Colloid Interface Sci. 323 (2008) 158-168.

[8] M. Ozakia, H. Suzukia, K. Takahashia and E. Matijević, Reversible ordered agglomeration of hematite particles due to weak magnetic interactions, J. Colloid Interface Sci. 113 (1986) 76-80.

[9] A. Satoh, *Introduction to Molecular-Microsimulation of Colloidal Dispersions* (Elsevier, Amsterdam, 2003).

[10] A. Satoh, A new technique for metropolis Monte Carlo simulation to capture aggregate structures of fine particles: Cluster-moving Monte Carlo algorithm, J. Colloid Interface Sci. 150 (1992) 461-472.

Chapter 4 Internal structures of the particle aggregates of a suspension composed of cubic hematite particles from 3D Monte Carlo simulations

4.1 Introduction

In Chapters 2 and 3, from the viewpoint of application to a surface modification technology, we have considered a quasi-2D suspension composed of cubic hematite particles in thermodynamic equilibrium in order to investigate the regime of phase change in the aggregate structures. In the quasi-2D system, we have treated a limited motion, where the cubic particles do not perform a full three dimensional (3D) rotational motion. In contrast to the implementation of a 2D system, it is significantly more difficult to treat the translational and rotational motion of cubic particles in a 3D simulation because the assessment of a particle-particle overlap is more complex.

There have been several simulation studies a 3D system regarding a suspension composed of magnetic and non-magnetic cubic particles [1-6]. Pyanzina, et al. have compared the self-assembly in the systems of both magnetic spherical particles and magnetic cubic particles by means of molecular dynamics simulations [1]. Donaldson, et al. have investigated the self-assembly processes of magnetic superball particles for which the particle geometry is changed from sphere to a perfect cube by employing a shape parameter [2, 3]. Vutukuri, et al. have discussed the phase behavior of cubic colloidal particles in an electric field by means of Monte Carlo simulations [4]. John et al. have investigated the lyotropic phase behavior of hard cubic particles by means of Monte Carlo simulations [5, 6]. In these studies, several cases of cubic particle models have been addressed with the magnetic dipole moment pointing a direction toward the face (1, 0, 0), the edge (1, 1, 0) and the corner (1, 1, 1) of the cube.

As was mentioned in Chapter 1, a magnetic particle suspension has a potential for application to both mechanical dampers and magnetic hyperthermia treatments. The cluster formation of cubic particles is expected to have a significant effect on the physical characteristics of the suspension such as the magnetorheological properties and the particle orientational properties that are important factors in these applications. For the successful application of a cubic magnetic particle suspension, it is necessary to further investigate the aggregate structures of magnetic cubic particles both in thermodynamic equilibrium and in a flow field.

From this background, we treat a 3D suspension composed of cubic hematite particles in thermodynamic equilibrium and investigate, by means of 3D Monte Carlo simulations, the dependence of the aggregate structures on a variety of factors such as the magnetic particle-particle interaction strength, the magnetic particle-field interaction strength and the particle volumetric fraction. In order to quantitatively and qualitatively discuss the aggregate structures, we use snapshots of particle aggregates, a radial distribution function, an order parameter and an orientational distribution function.

4.2 Model of magnetic cubic particles

In the present study, we employ the simplified model of a cubic hematite particle that is shown in the Fig. 4.1. A cube with side length d is assumed to be magnetized in a diagonal direction with a magnetic dipole moment $\boldsymbol{m}=m\boldsymbol{n}$ situated at the particle center. In the present Monte Carlo simulation, a uniform magnetic field $\boldsymbol{H}$ is applied in the z-axis direction as $\boldsymbol{H}=H\boldsymbol{h}=(0, 0, H)$.

In Chapters 2 and 3, we treated a quasi-2D system with the rotational motion restricted about a line normal to the plane of the material surface under the assumption of a relatively strong gravitational field. In contrast the present study employs a 3D Monte Carlo simulation where the cubic particles are free to perform a full rotational and translational motion. The magnetic particle-particle interaction energy $u_{ij}^{(m)}$ and the magnetic particle-field interaction energy $u_i^{(H)}$ employed in Chapter 2 and Chapter 3 remain applicable and the present phenomenon is governed by the non-dimensional parameters λ which represent the strengths of magnetic particle-particle interaction $\lambda=\mu_0 m^2/(4\pi d^3 kT)$ and ξ which represent the strengths of the magnetic particle-field interactions $\xi=\mu_0 mH/(kT)$ relative to the thermal energy. In these non-dimensional parameters, μ_0 is the permeability of free space, k is Boltzmann's constant, and T is the absolute temperature of a suspension.

In the case of a 2D system, the cluster unit composed of 4 particles, shown in Fig. 4.2 (a) is the preferred configuration in the situation of no applied magnetic field, as already discussed in Chapter 2. On the other hand, in the case of a 3D system, these 4 particle cluster units tend to combine with each other to grow a cluster unit composed of 8 particles, shown in Fig. 4.2(b). From the energy analysis of cluster units, we understand that these cluster units shown in Fig. 4.2(b) provide the lowest magnetic interaction energy for an 8-particle system. Therefore, in the absence of an external magnetic field, a large closely-packed cluster is expected to be formed by means of the combination and expansion of these cluster units.

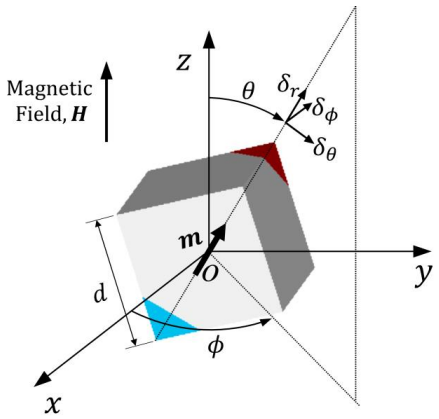

Fig. 4.1 Particle model showing the coordinate system and the z-direction of the applied magnetic field.

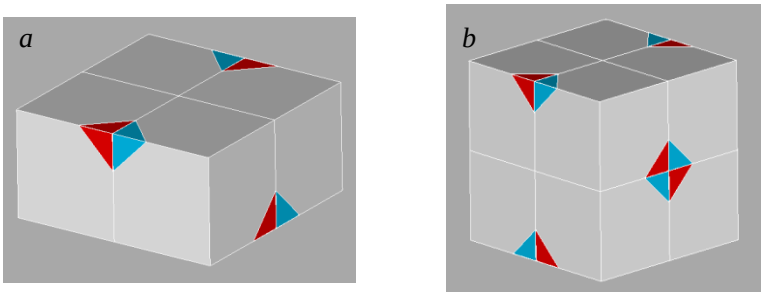

Fig. 4.2 Preferred configurations for clusters in the absence of an applied magnetic field. (a) a cluster unit composed of 4 particles and (b) a cluster unit composed of 8 particles.

4.3 Description of the characteristics of the system

In Chapter 2, we employed two order parameters $S_1^{(m)}$ and $S_2^{(m)}$ for the quantitative discussion of the characteristics of the aggregate structures of cubic hematite particles for a 2D system. In the present study, we discuss the aggregate structures in a 3D system and address a related order parameter $S_3^{(m)}$ expressed below as,

$$S_3^{(m)} = \frac{1}{N_{pair}} \left\langle \sum_{i=1}^{N} \sum_{\substack{j=1 \\ (j>i)}}^{N} (6\cos 5\psi_{ij}^{(n)} - 1)/5 \right\rangle \tag{4.1}$$

in which $\psi_{ij}^{(n)}$ is the angle between the magnetic moment direction $\boldsymbol{n}_i$ and $\boldsymbol{n}_j$ of particle i and j, $N_{pair}=N(N-1)/2$ is the number of pairs of particles and $\langle - \rangle$ is the ensemble average. It is noted that the order parameter $S_3^{(m)}$ approaches unity as large closely-packed clusters are formed in the system.

4.4 Parameters for simulations

Unless specifically noted, the present results were obtained by adopting the following parameter values. The volumetric fraction of cubic hematite particles is ϕ_V=0.1, the number of particles N=490, and the cutoff radius $r_{coff}^{*}=r_{coff}/d$=10 for calculating particle-particle interactions. The previously defined non-dimensional parameters λ and ξ that characterize the present phenomenon are set in the wide range of values λ=0~13.5 and ξ=0~20. We employed the usual periodic boundary condition in all the axis directions. The external magnetic field is applied in the z-axis direction and in the situation of a strong magnetic field it is expected that long chain-like clusters are formed in the magnetic field direction. We therefore employ a rectangular-parallelepiped simulation box aligned in the magnetic field direction. The size of the simulation region in each axis direction L_x, L_y, L_z is set with the ratio L_x: L_y: L_z=1:1:1.5. In the case of volumetric fraction ϕ_V=0.1, the lengths of the simulation region are L_x=14.8, L_y=14.8 and L_z=22.3. The total number of Monte Carlo steps per simulation run, N_{smplmx} is taken as N_{smplmx}=5,000,000 and the final 80% of the simulation data were used for the data averaging procedure.

4.5 Results and discussion

4.5.1 Influence of the magnetic particle-particle interaction strength

First, we discuss the dependence of the aggregate structures on the magnetic particle-particle interaction strength λ in the absence of an applied magnetic field. Figure 4.3 shows the snapshots of aggregate structures for the case of no applied magnetic field ξ=0 for the cases of λ=5 shown in Fig. 4.3(a), λ=13 shown in Fig. 4.3(b) and λ=13.5 shown in Fig. 4.3(c). Fig. 4.4 shows the order parameter $S_3^{(m)}$ defined in Eq. (4.1). It is noted that the value of the order parameter $S_3^{(m)}$ will increase as larger closely-packed clusters are formed in the system.

In the case of the relatively low particle-particle interaction strength λ=5, shown in Fig. 4.3(a), the particles do not aggregate to form specific clusters and the magnetic moments of the particles tend to incline in random directions. In the case of the relatively strong magnetic particle-particle interaction strength λ=13, shown in Fig. 4.3(b), it is seen that particles tend to form large loosely-packed clusters where there are a few constituent particles in face-to-face contact although specific clusters are not observed. Since the neighboring particles in the loosely-packed aggregate do not contact each other in a perfect face-to-face manner, the magnetic moments of particles tend not to be restricted to a specific direction. In the case of λ=13.5, shown in Fig. 4.3(c), closely-packed aggregate structures have been formed by the combination and expansion of the cluster unit shown in Fig. 4.2. A regime change in the internal structures of aggregates has occurred in the narrow range of λ=13~13.5.

These characteristics are clearly exhibited by the order parameter $S_3^{(m)}$ shown in Fig. 4.4. Since initially there are no specific clusters initially formed in the system, the order parameter exhibits a value almost zero until around λ=13. However, the value of the order parameter then steeply increases from $S_3^{(m)}$=0 at λ=13 to the value of $S_3^{(m)}$ =0.79 at λ=13.5, which clearly implies a regime change on the formation of the closely-packed clusters. The reason why the order parameter steeply increases within a narrow range can be explained in the following. In the case of cubic particles, the growth of the clusters is expected to be significantly influenced by the onset of the face-to-face particle configuration. For the case of λ=13, the particles weakly aggregate to form loosely-packed clusters where there are few neighboring particles in stable face-to-face contact, which leads to an almost zero value of the order parameter. On the other hand, for the case of λ=13.5, the particles aggregate to form the cluster unit composed of 4 particles in stable face-to-face contact, as observed in Fig. 4.3(c), which may be a necessary step in forming large closely-packed clusters. Therefore, the stable face-to-face contact configuration significantly contributes to the growth of closely-packed clusters, whereupon the order parameter shows a large value of $S_3^{(m)}$ =0.79.

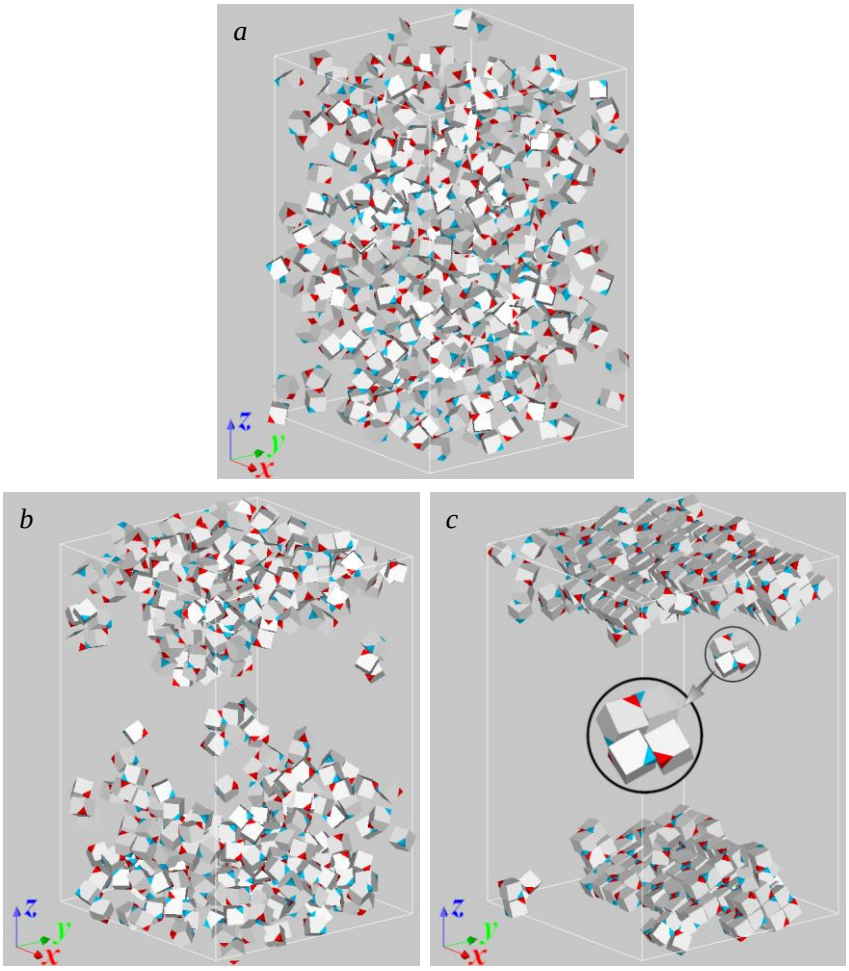

Fig. 4.3 Aggregate structures for the magnetic particle-particle interaction strength of (a) λ=5, (b) λ=13 and (c) λ=13.5 for the case of no applied magnetic field ξ=0.

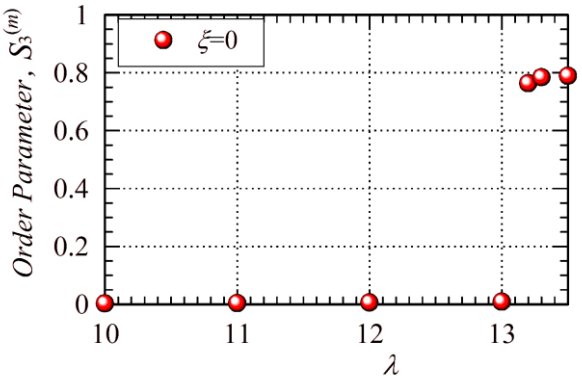

Fig. 4.4 Order parameter of the magnetic moment direction as a function of the magnetic particle-particle interaction strength λ.

We here discuss the internal structure of the above-mentioned clusters in terms of the orientational distribution function. Figure 4.5 shows the orientational distribution function $\Psi_{\theta\phi}$ for the case of no applied magnetic field ξ=0, where Fig. 4.5(a) is for the magnetic particle-particle interaction strength of λ=13 and Fig. 4.5(b) is for λ=13.5. It is noted that the results in Fig. 4.5 show the orientational characteristics of the magnetic moments of the cubic particles where, as shown in Fig. 4.1, θ is the polar angle from the z-axis and ϕ is the azimuthal angle from the x-axis. In the case of λ=13, shown in Fig. 4.5(a), the uniform distribution lacks a specific peak and quantitatively implies that the magnetic moments incline in random directions and that specific clusters are not formed in the system. In the case of λ=13.5, shown in Fig. 4.5(b), there are 8 relatively high peaks in the orientational space that quantitatively imply large closely-packed clusters are formed in the system. The reason why there are 8 high peaks may be explained because, in our cubic model, the magnetic moment may point in the direction towards any one of the 8 corners of the cube. If the closely-packed clusters are formed with particle alignment in a perfect face-to-face contact, as shown in Fig. 4.2(b), then the direction of the magnetic moment of each constituent particle is strongly restricted to one of the possible 8 corner directions. The large closely-packed clusters, as shown in Fig. 4.3(c), are formed from the combination of this basic cluster unit, hence, the orientational characteristics of this cluster unit appear in the orientational space as shown in Fig. 4.5(b). From the above discussion, we conclude that in the situation of no applied magnetic field, an increase in the magnetic particle-particle interaction strength induces the formation of closely-packed clusters. Moreover, we understand that these closely-packed clusters are a characteristic cluster formation for a suspension of magnetic cubic particles.

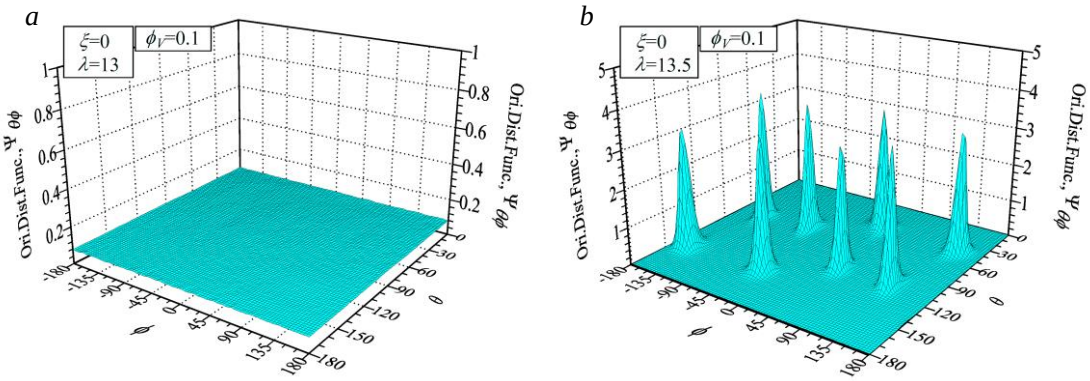

Fig. 4.5 The orientational distribution function for the magnetic particle-particle interaction strengths of (a) λ=13 and (b) λ=13.5 for the case of no applied magnetic field ξ=0.

4.5.2 Influence of the magnetic particle-field interaction strength

Next, we discuss the effect of an external magnetic field on the regime change in the closely-packed clusters, shown in Fig. 4.3(c). Figure 4.6 shows snapshots of aggregate structures in the case of a strong magnetic particle-particle interaction strength λ=13.5 where Fig. 4.6(a) is for the case of the magnetic particle-field strength ξ=4 and Fig. 4.6(b) is for the case of ξ=7. In the case of a relatively weak applied magnetic particle-field interaction ξ=4, shown in Fig. 4.6(a), it is seen that the closely-packed aggregate structures observed in Fig. 4.3(c) have collapsed due to the influence of the external magnetic field. As the magnetic particle-field strength is further increased to ξ=7, shown in Fig. 4.6(b), it is seen that the closely-packed clusters are transformed into wall-like clusters aligned in the magnetic field direction. The configuration of neighboring particles in the wall-like structures is very distinctive whereby they combine with each other in an offset face-to-face configuration. From the analysis of the potential curves [7], it is clearly indicated that the configuration based on an offset face-to-face contact is preferred in the situation of a strong magnetic field. From these results, we understand that a magnetic field induces a regime change from the closely-packed clusters in Fig. 4.3(c) into the wall-like clusters in Fig. 4.6(c).

The characteristic of the order parameter $S_{nz}^{(m)}$ of the magnetic moment direction evidently implies that there is a regime change in the internal structure. Figure 4.7 shows the dependence of the order parameters $S_{nz}^{(m)}$ on the magnetic particle-field strength ξ for the two cases of magnetic particle-particle interaction strength λ=5 and λ=13.5. For the case of a small magnetic particle-particle interaction strength λ=5, the order parameter gradually increases relatively smoothly with increasing value of the magnetic particle-field strength as the magnetic moment of each single particle inclines toward the magnetic field direction. In contrast, in the case of λ=13.5, where the closely-packed clusters are formed without an applied magnetic field, the values of the order parameter exhibit lower values than for the case of λ=5 until around $\xi \simeq 5$. This is because the magnetic particle-particle interactions function to prevent the magnetic moments from inclining toward the magnetic field direction. That is, if the closely-packed clusters shown in Fig. 4.3(c) are formed in the system, the magnetic moments of constituent particles do not tend to incline in the magnetic field direction which leads to a nearly zero value of the order parameter $S_{nz}^{(m)}$. As the magnetic particle-field strength is increased to $\xi \simeq 6$, the value of the order parameter significantly increases, which quantitatively implies that there is a regime change in the internal structure from the closely-packed structures in Fig. 4.3(c) into the wall-like structures in Fig. 4.6(b). That is, due to the influence of the magnetic field, the magnetic moments of constituent particles in closely-packed clusters incline in the magnetic field direction. In the situation of a strong magnetic field, the orientations of the magnetic moments of the constituent particles of the wall-like aggregates are strongly restricted due to the influence of the magnetic interactions between neighboring particles, which leads to larger values of the order parameter in the region of $\xi \gtrsim 5$.

Figure 4.8 shows results of the orientational distribution function $\Psi_{\theta\phi}$ for the case of a weak applied magnetic particle-field ξ=4 where Figs. 4.7(a) and 4.7(b) are for the two cases of magnetic particle-particle interaction strength λ=0 and λ=13.5. For both cases, only a single peak appears at the zenithal angle of θ =0°. This characteristic is in contrast to that for the case of ξ=0 and λ=0 shown in Fig. 4.5(b). The reason why the height of the peak in the case for λ=13.5 is lower than that for the case λ=0 is that the magnetic particle-particle interaction plays a role to prevent the magnetic moments from inclining in the field direction, as already mentioned above.

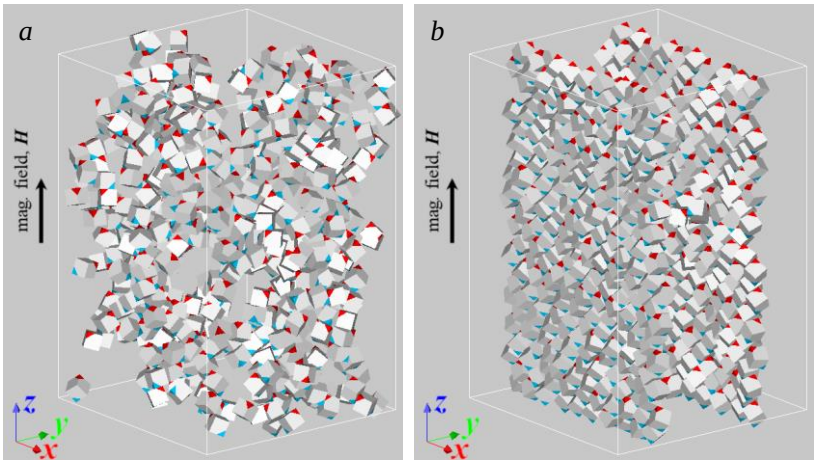

Fig. 4.6 Aggregate structures for the magnetic particle-field strength (a) ξ=4 and (b) ξ=7 for the magnetic particle-particle interaction strength λ=13.5.

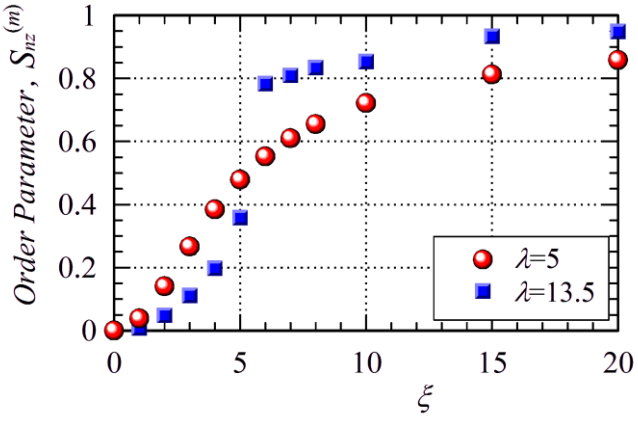

Fig. 4.7 Order parameter $S_{nz}^{(m)}$ of the magnetic moment direction for the magnetic particle-particle interaction strength of (a) λ=5 and (b) λ=13.5 as a function of the magnetic particle-field strength ξ.

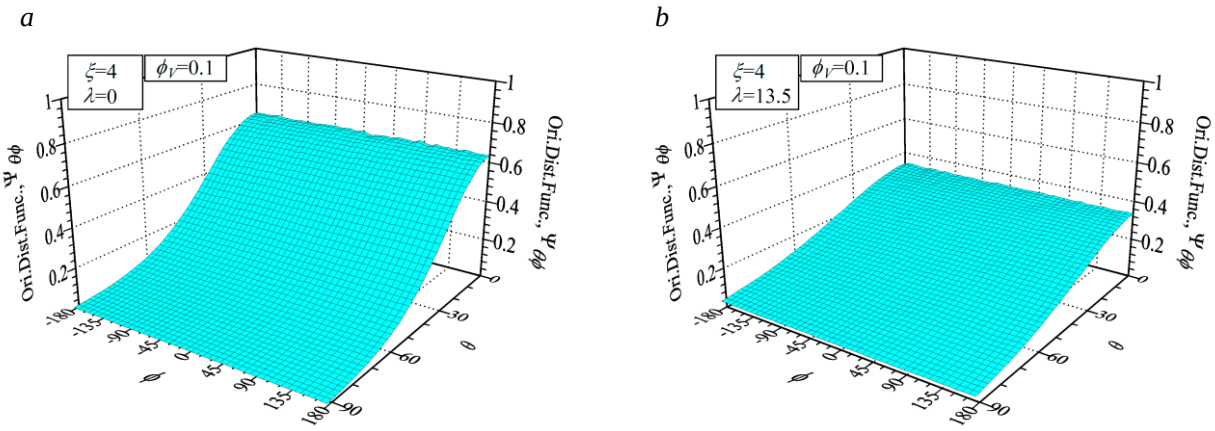

Fig. 4.8 Dependence of the orientational distribution function $\Psi_{\theta\phi}$ on the magnetic particle-particle interaction strength (a) λ=0 and (b) λ=13.5 for the magnetic particle-field strength ξ=4 and volumetric fraction ϕ_V=0.1.

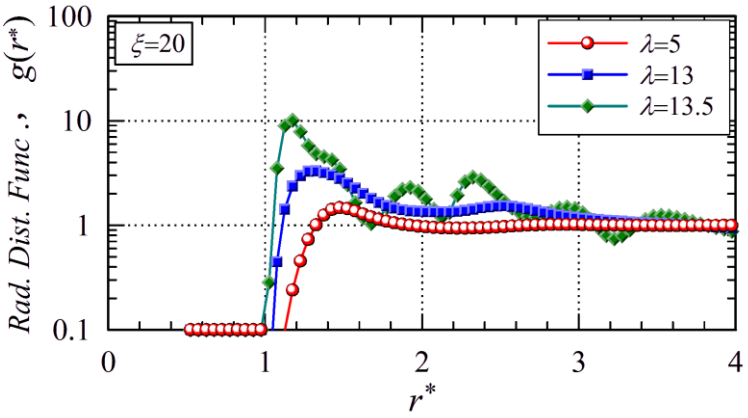

Fig. 4.9 Dependence of the radial distribution function on the magnetic particle-particle interaction strengths λ=5, λ=13 and λ=13.5 for a strong magnetic particle-field strength ξ=20.

Figure 4.9 shows the radial distribution function for the strong external magnetic particle-field ξ=20, where three cases of the magnetic particle-particle interaction strength are shown for λ=5, λ=13 and λ=13.5. In the case of a relatively weak interaction strength λ=5, the curve shows a gas-like distribution, which implies there is no cluster formation. As the magnetic particle-particle interaction strength is increased to λ=13, it shows a slight liquid-like characteristic with a first peak at $r^* \simeq 1.2$ and a lower second peak at $r^* \simeq 2.5$. As the magnetic particle-particle interaction strength is further increased to λ=13.5, several relatively high peaks appear at distances $r^* \simeq 1.1$, 1.9, 2.3, 2.9, 3.5, etc. The first and third peaks evidently correlate to the characteristics of a linear chain-like cluster. If

the wall-like structures are formed, as shown in Fig. 4.6(b), then neighboring particles contact each other in a face-to-face configuration with an offset distance of r^*=0.5. Therefore, the first peak in the radial distribution function appears at $r^*=(0.5^2+1^2)^{1/2}$ ≃1.12, and the third peak occurs at $r^*=((0.5^2+0.5^2)^2+(1^2+1^2)^2)^{1/2}$ ≃1.12 and implies the next neighboring pair of cubes. The second peak appearing at $r^*=(0.5+1.0)^2+(0.5+0.5)^2)^{1/2}$ ≃1.80 implies a twisted configuration formed from the first, second and third cubes [7]. The other peaks arise due to a similar configuration of wall-like clusters that are formed from the combination of the above-mentioned chain-like clusters.

4.5.3 Influence of the volumetric fraction of particles

Finally, we discuss the influence of the volumetric fraction of particles ϕ_V on the cluster formation. Figure 4.10 shows snapshots of the aggregate structures for a strong magnetic particle-particle interaction strength λ=13.5 and a small volumetric fraction ϕ_V =0.01 where Fig. 4.10(a) is for the magnetic particle-field strength ξ=0 and Fig. 4.10(b) is for ξ=15. It is noted that Figure 4.10 shows only a small part of the whole system in order to discern the internal structure more clearly. For the case of no applied magnetic field ξ=0 several cluster units of the type shown in Fig. 4.2(b) are formed in the system. However, the larger closely-packed clusters shown in Fig. 4.3(c) are not formed. This is because a small volumetric fraction provides little opportunity for the cluster units to contact with each other. In contrast, in the situation of a high volumetric fraction ϕ_V =0.1, such an opportunity frequently appears, and therefore cluster units may grow to form the large closely-packed clusters shown in Fig. 4.3(c). It is evident from the formation of the cluster units observed in Fig. 4.10(a), that large closely-packed clusters are formed by the combination and expansion of these basic cluster units. On the other hand, in the case of a strong magnetic particle-field strength ξ=15 shown in Fig. 4.10(b), long chain-like clusters are formed in the z-axis direction of the magnetic field. From a comparison with the wall-like structures shown in Fig. 4.6(b), it is seen that for a strong magnetic particle-field strength, an increase in the volumetric fraction of particles induces a regime change from the thick chain-like clusters into the wall-like clusters. This is because a large volumetric fraction can provide an opportunity for chain-like clusters to contact with each other. That is, we may understand that the wall-like clusters in Fig. 4.6(b) are formed by the process of the chain-like clusters combining with each other.

Finally, we discuss the influence of the magnetic particle-field interaction strength on the aggregate structures in a dilute system that is implied from the order parameter $S_{nz}^{(m)}$. Figure 4.11 shows the dependence of the order parameter $S_{nz}^{(m)}$ on the magnetic particle-field strength ξ for a volumetric fraction ϕ_V =0.01 and magnetic particle-particle interaction strength λ=13.5. In this figure, the result already shown in Fig. 4.11 for ϕ_V =0.1 has been replotted for reference. In the case of a small volumetric fraction ϕ_V =0.01, the order parameter gradually increases with increasing values of the magnetic particle-field strength. This is quite different from the curve for ϕ_V =0.1 and clearly

implies that small cluster units are easily transformed into chain-like clusters with increasing magnetic particle-field strength. Moreover, it is reasonably presumed that the lower values of the order parameter in the range of $\xi \lesssim 5$ for the case ϕ_V =0.1 is due to the magnetic particle-particle interactions of the large closely-packed clusters shown in Fig. 4.3 (c).

From these characteristics, we can conclude that in the case of a lager volumetric fraction of particles a larger magnetic particle-field strength is necessary in order to induce a regime change from the closely-packed structures into the chain-like or wall-like structures.

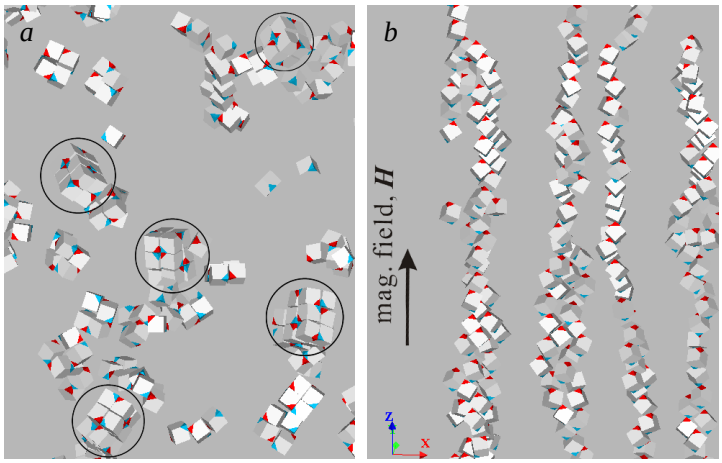

Fig. 4.10 Aggregate structures for the magnetic particle-field strength (a) ξ=0 and (b) ξ=15 for the magnetic particle-particle interaction strength λ=13.5 and the volumetric fraction ϕ_V =0.01.

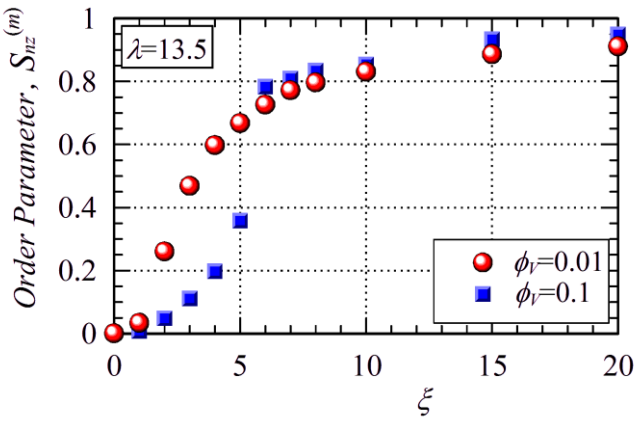

Fig. 4.11 Order parameter of the magnetic moments for the volumetric fraction ϕ_V =0.01 and ϕ_V =0.1 and the magnetic particle-particle interaction strength λ=13.5 as a function of the magnetic particle-field strength ξ.

4.6 Conclusion

We have investigated the aggregate structures for a dispersion in thermodynamic equilibrium composed of magnetic cubic particles by means of 3D Monte Carlo simulations. From the Monte Carlo simulations, we attempt to elucidate the dependence of a regime change in the aggregate structures on various physical parameters such as the magnetic particle-particle interaction strength, the magnetic particle-field interaction strength and the volumetric fraction of particles. We use the snapshots of aggregate structures for a qualitative discussion, and the radial distribution function, the order parameters and the orientational distribution function for a quantitative discussion. We summarize the main results obtained here in the following. In the situation of no applied magnetic field, as the magnetic particle-particle interaction strength is increased, closely-packed aggregate structures are formed by the combination and expansion of a basic cluster unit composed of 8 particles. A regime change from the situation of no cluster formation to the formation of closely-packed clusters was found to occur in a narrow range of the magnetic particle-particle interaction strength. This is because closely-packed clusters tend to growth on the occurrence of a perfect face-to-face configuration. As the magnetic particle-field strength is increased, the magnetic moments of particles tend to incline in the magnetic field direction and wall-like clusters are formed in the system. That is, the magnetic field induces a regime change in the internal aggregate structure from the closely-packed clusters into the wall-like clusters. Moreover, in the case of no applied magnetic field, larger closely-packed clusters are formed in the system with an increasing volumetric fraction of particles. This is because a high volumetric fraction tends to enhance the opportunity for the particles to contact with each other. Similarly, in a strong external magnetic field, an increase in the volumetric fraction of particles induces a regime change from the thick chain-like clusters into the wall-like clusters.

References

[1] E. S. Pyanzina, A. V. Gudkova, J. D. Donaldson and S. S. Kantorovich, Cluster analysis in systems of magnetic spheres and cubes. J. Magn. Magn. Mater. 431 (2017) 201-204.

[2] J. G. Donaldson, E. S. Pyanzina and S. S. Kantorovich, Nanoparticle shape influences the magnetic response of ferro-colloids. ACS nano. 11 (2017) 8153-8166.

[3] J. G. Donaldson, P. Linse and S. S. Kantorovich, How cube-like must magnetic nanoparticles be to modify their self-assembly?, Nanoscale. 19 (2017) 6448-6462.

[4] H. R. Vutukuri, F. Smallenburg, S. Badaire, A. Imhof, M. Dijkstra and A. van Blaaderen, An experimental and simulation study on the self-assembly of colloidal cubes in external electric fields. Soft Matter. 10 (2014) 9110-9119.

[5] B. S. John, A. Stroock and F. A. Escobedo, Cubatic liquid-crystalline behavior in a system of hard cuboids, J. Chem. Phys. 120 (2004) 9383-9389.

[6] B. S. John and F. A. Escobedo, Phase Behavior of Colloidal Hard Tetragonal Parallelepipeds (Cuboids): A Monte Carlo Simulation Study, J. Phys. Chem. B 109 (2005) 23008-23015.

[7] A. Satoh, Modeling of Magnetic Particle Suspensions for Simulations, (CRC Press, Boca Laton, FL, 2017).

Chapter 5 The translational and rotational friction coefficients of a cubic particle

5.1 Introduction

In Chapter 4, we investigated the aggregate structure in thermodynamic equilibrium by means of 3D Monte Carlo simulations, and we have understood that cubic particles aggregate in a face-to-face configuration. In the field of fluid engineering, typical applications for a magnetic particle suspension are mechanical dampers and actuators [1, 2] where a magnetorheological characteristic is controlled by means of an external magnetic field. A suspension composed of cubic hematite particles is expected to exhibit complex magnetorheological properties because the cubic particles tend to aggregate with an atypical face-to-face contact configuration.

In order to elucidate the magnetorheological properties of a particle suspension, there are a variety of micro-analysis simulation methods such as molecular dynamics, Brownian dynamics, lattice Boltzmann, dissipative particle dynamics and multi-particle collision dynamics [3, 4]. Among these simulation methods, perhaps the most straightforward is Brownian dynamics, although in this method the multi-body hydrodynamic interactions among the particles are not taken into account. However, Brownian dynamics is not directly applicable to a suspension composed of particles with a non-axisymmetric geometry, i.e cubic particles, because many of the translational and rotational friction coefficients or diffusion coefficients have not fully been clarified at the present. Hence, for a cubic particle suspension, we are required to develop a simulation technique with appropriate friction or diffusion coefficients which, in turn, may lead to the development of new applications for mechanical dampers and actuators.

The surface modification technology is one area of application for magnetic cubic particles, and consequently many researchers have investigated the phenomenon of the deposition of magnetic cubic particles on a material plane surface [5-8]. In many of these studies, an external magnetic field is used for controlling physical characteristics in regard to orientational properties and attachment properties. However, we understand that an applied magnetic field by itself cannot completely control the above-mentioned physical characteristics. If the magnetic particles are also charged, these characteristics are expected to be controlled more accurately by means of both an electric field and a magnetic field. From these considerations, it is evident that the development of a particle-based simulation method which is able to treat particle Brownian motion is important for the analysis of the dynamic characteristics of a dispersion composed of magnetic cubic particles.

From this background, in the following we estimate the translational and rotational diffusion coefficients of a cubic particle that are required for performing the Brownian dynamics simulations of a cubic particle suspension. In addition, we discuss the characteristic of a coupling between the translational motion and rotational motion. In concrete, we have analyzed the flow field around a cube via the commercial software ANSYS CFX in order to evaluate the force and torque

acting on a cube. The results of a numerical analysis are used for estimating the diffusion coefficients of a cubic particle and for discussing the coupling relationship between the translational and the rotational motion.

5.2 Evaluation procedure for the friction coefficients

The force $\boldsymbol{F}$ and the torque $\boldsymbol{T}$ acting on the ambient fluid by a particle are related to the fluid velocity $\boldsymbol{v}$ and the angular velocity $\boldsymbol{\omega}$ as

$$\begin{pmatrix} \boldsymbol{F} \\ \boldsymbol{T} \end{pmatrix} = \boldsymbol{R} \cdot \begin{pmatrix} \boldsymbol{v} \\ \boldsymbol{\omega} \end{pmatrix} \tag{5.1}$$

in which $\boldsymbol{R}$ is the resistance matrix, expressed as

$$\boldsymbol{R} = \begin{pmatrix} \boldsymbol{R}_a & \boldsymbol{R}_c \\ \boldsymbol{R}_b & \boldsymbol{R}_d \end{pmatrix} \tag{5.2}$$

Equation (1) is rewritten using Eq. (2) as

$$\begin{cases} \boldsymbol{F} = \boldsymbol{R}_a \cdot \boldsymbol{v} + \boldsymbol{R}_c \cdot \boldsymbol{\omega} \\ \boldsymbol{T} = \boldsymbol{R}_b \cdot \boldsymbol{v} + \boldsymbol{R}_d \cdot \boldsymbol{\omega} \end{cases} \tag{5.3}$$

We here describe the physical meaning of each component of the resistance matrix $\boldsymbol{R}$. The matrix $\boldsymbol{R}_a$ relates the force acting on the ambient fluid to the translational velocity, and the matrix $\boldsymbol{R}_d$ relates the torque acting on the ambient fluid to the angular velocity. The matrices $\boldsymbol{R}_b$ and $\boldsymbol{R}_c$ imply the rate of the coupling between the translational motion and the rotational motion. That is, the situation of $\boldsymbol{R}_b=\boldsymbol{0}$ suggests that the translational motion is not influenced by the rotational motion, and similarly the situation of $\boldsymbol{R}_c=\boldsymbol{0}$ implies that the translational motion does not induce a rotational motion. If the relationship of $\boldsymbol{R}_b=\boldsymbol{R}_b=\boldsymbol{0}$ is satisfied, then there is no coupling between the translational motion and the rotational motion. Hence, if the components of the resistance matrices are known, the force and the torque acting on the cube may be evaluated. In the situation of low Reynolds numbers that are much smaller than unity, it is known that the matrices $\boldsymbol{R}_a$ and $\boldsymbol{R}_d$ are diagonal with a common component ξ_{cube}^{T} and ξ_{cube}^{R} which are respectively the translational and the rotational friction coefficient of a cube, as discussed by Brenner [9]. However, the coupling characteristics of the translational and the rotational motion of a cube and the correct values of the friction coefficients ξ_{cube}^{T} and ξ_{cube}^{R} were not addressed in Brenner's paper [9].

In the present study, we analyze a flow field past a cube fixed in the system via the commercial software ANSYS CFX in order to elucidate the features of the resistance component

matrices. The flow field was obtained by numerically solving the Navier-Stokes equation with the continuity equation. In the following, we address a flow past a sphere and explain the evaluation procedure for deriving the friction or diffusion coefficients from the flow field analysis. We employ a similar derivation procedure in order to estimate the friction coefficients of a cube.

If we concentrate on a sufficiently slow flow problem past a sphere with the Reynolds number being much smaller than unity $Re<<1$, then the force $\boldsymbol{F}$ and the torque $\boldsymbol{T}$ acting on the ambient fluid are related to the translational velocity $\boldsymbol{v}$ and the angular velocity $\boldsymbol{\omega}$ of the particle as

$$\boldsymbol{F} = \xi_{sphere}^{T} \boldsymbol{v} \tag{5.4}$$

$$\boldsymbol{T} = \xi_{sphere}^{R} \boldsymbol{\omega} \tag{5.5}$$

where ξ_{sphere}^{T} and ξ_{sphere}^{R} are the translational and the rotational friction coefficient, respectively. In the case of a sphere, these friction coefficients are known and may be expressed as

$$\xi_{sphere}^{T} = 6\pi\eta a \tag{5.6}$$

$$\xi_{sphere}^{R} = 8\pi\eta a^{3} \tag{5.7}$$

in which η is the liquid viscosity and a is the radius of the sphere, whereby the translational and the rotational diffusion coefficients D_{sphere}^{T} and D_{sphere}^{R} may then be expressed

$$D_{sphere}^{T} = \frac{kT}{\xi_{sphere}^{T}} \tag{5.8}$$

$$D_{sphere}^{R} = \frac{kT}{\xi_{sphere}^{R}} \tag{5.9}$$

in which k is Boltzmann's constant and T is the liquid temperature. For the case of a sphere, it is known that there is no coupling between the translational and the rotational motion, and therefore the resistance component matrices $\boldsymbol{R}_b$ and $\boldsymbol{R}_c$ in Eq. (5.3) yield to the relationship $\boldsymbol{R}_b=\boldsymbol{R}_c=\boldsymbol{0}$. In contrast, the resistance component matrices $\boldsymbol{R}_a$ and $\boldsymbol{R}_d$ are diagonal matrices with a common component ξ_{sphere}^{T} and ξ_{sphere}^{R}, respectively.

As in the case of a cube, where the friction or diffusion coefficients are not known in the form of analytical expressions, they may be evaluated by a numerical analysis method in the following manner. A sphere is fixed at a certain position in a uniform flow field $\boldsymbol{U}$ and the flow field is solved and the force $\boldsymbol{F}^{P}=(F_x^{P}, F_y^{P}, F_z^{P})$ acting on the sphere may be evaluated from numerical analysis. If the uniform flow field is applied in the x-axis direction as $\boldsymbol{U}=(U_x, 0, 0)$, then the translational friction coefficient ξ_{sphere}^{T} may be obtained from Eq. (5.3) using F_x^{P} and U_x as

$$\xi^{T}_{sphere} = \frac{F_x^{\ P}}{U_x} \tag{5.10}$$

In a similar procedure, if the rotational flow field $\boldsymbol{\Omega}=(\Omega_x, 0, 0)$ is applied about the x-axis direction, the rotational friction coefficient ξ^{R}_{sphere} is expressed as

$$\xi^{R}_{sphere} = \frac{T_x^{\ P}}{\Omega_x} \tag{5.11}$$

In the case of a cube, the relationship of $\boldsymbol{R}_b=\boldsymbol{R}_c=\boldsymbol{0}$ is not necessarily satisfied but rather the resistance component matrices are expected to be dependent on the orientational configuration relative to a uniform flow and also on the Reynolds number Re, defined as

$$Re = \frac{U_0 d}{\nu} \tag{5.12}$$

in which U_0 is the representative velocity, d is the side length of the cube and ν is the kinematic viscosity.

5.3 Assignment of the simulation parameters

We employed the following values of the system parameters in performing the numerical simulations both for a uniform flow past a cube and for a rotational flow about the x-axis direction. We treat a slow problem for water with physical properties of viscosity η=889.9×10^{-6} Pa·s, density ρ=997 kg/m^3 and kinematic viscosity ν =8.926×10^{-7} m^2/s relating to a temperature of 25 ℃. The side length of a cube is set as d=0.01 m and the cube is fixed at the origin of the xyz-coordinate system. It is required that the unit mesh size is taken sufficiently smaller than the side length of the cube, and therefore the side of a cube may be taken as any value provided the lattice system can be taken sufficiently fine. For the case of a uniform flow in the x-axis direction, the simulation box is rectangular, for the case of a rotational flow about the x-axis direction, it is cylindrical. We employ a no-slip boundary condition at the surface of the cube, and a zero-gradient condition at the outer boundary surface. In order to ensure the independence of the simulation results, the size of the simulation region, (L_x, L_y, L_z)=(1m, 0.5m, 0.5m), , is taken to be sufficiently large relative to the particle size. It is noted that we have confirmed that a simulation region taken double the size yields at most only a 1% deviation in the results. The inflowing uniform velocity is set as U_x=1×10^{-6} m/s and the angular velocity is taken as Ω_x=1×10^{-6} rad/s. A uniform flow with U_x=1×10^{-6} m/s gives rise to Re=1.12×10^{-2} that is evaluated from Eq.(5.12) with $U_0=U_x$ and similarly, the rotational flow with

Ω_x=1×10^{-6} rad/s leads to Re=1.12× 10^{-4} with $U_0=\Omega_x d$. Both these cases satisfy the condition of a sufficiently slow flow with $Re<<1$.

Table 1 shows the validity of the present numerical analysis for a spherical particle, where the numerical results are compared with the corresponding theory for the case of a slow uniform flow with U_x=1×10^{-6} m/s and a slow rotational flow with Ω_x=1×10^{-6} rad/s. It is clearly seen from Table 1 that the numerical results of the force and the torque acting on the sphere are in good agreement with the theory.

Table 5.1 The force and torque acting on the spherical particle.

	The force acting on the spherical particle	The torque acting on the spherical particle
The theoretical values	$F_x^{Theory}=6\pi\eta a U_x=8.387\times10^{-11}$[N]	$T_x^{Theory}=8\pi\eta a^3\Omega_x\approx2.796\times10^{-15}$[N·m]
The calculated values by ANSYS	$F_x^{ANSYS}=8.392\times10^{-11}$[N]	$T_x^{ANSYS}=2.770\times10^{-15}$[N·m]

5.4 Results and discussion

5.4.1 For the case of a uniform flow with a sufficiently low Reynolds number of $Re=1.12\times10^{-2}$

We first consider the problem of a uniform flow past a cube in the x-direction in order to clarify the characteristics of the resistances matrices $\boldsymbol{R}_a$ and $\boldsymbol{R}_b$. It is noted that θ is the angle between the direction of the z-axis and a representative direction of the cube that is normal to a criterion face and ϕ is the rotation angle of a representative vertex about the z-axis measured from the x-axis toward the y-axis. The following results were obtained for a uniform flow with a sufficiently low Reynolds number of $Re=1.12\times10^{-2}$.

Figure 5.1 shows results of the flow field around a cube for the three different cases of configuration ϕ =0° 5.1(a), ϕ =30° 5.1(b) and ϕ =45° 5.1(c), at the fixed value of θ=0°. Since a slow uniform flow is addressed, the fluid tends to flow along the faces of the cube and into the region behind the cube without flow separation for all cases of the slant angle ϕ. From the flow shown in Figs. 5.1(a) and 5.1(c), it is recognized that the flow lines are approximately symmetric about the y-axis line. This characteristic is well known for the case of a slow uniform flow past a circular cylinder. Figure 5.2 shows the components of the force Fig. 5.2(a) and the components of torque Fig. 5.2(b) acting on the cube in the uniform flow field. It is seen from Fig. 5.2(a) that the force component F_x in the x-direction is independent of the slant angle ϕ and exhibits a constant value $F_x\simeq1.161\times10^{-10}$ N. In contrast, the face components F_y and F_z are almost zero and thus negligible in comparison to the force component F_x along the uniform flow direction. Moreover, considering the torque F_x (d/2)≃0.58×10^{-12} Nm evaluated with $F_x\simeq1.161\times10^{-10}$ N as a criterion value for comparison, it is seen from Fig. 5.2(b) that all the torque components T_x, T_y and T_z may be regarded as approximately zero. From these characteristics, we understand that a uniform flow gives rise to a force acting on the cube only in the uniform flow direction and does not induce a torque for any orientational configuration relative to the uniform flow.

We next consider the components of the force and torque for the case of a more general orientational configuration, i.e. (θ, ϕ)=(54.74°, 15°), of the cube in a uniform flow as shown in Fig.5.3. Table 5.2 shows the components of force and torque acting on the cube, where also shown for reference, $\langle F_x\rangle$, is the mean value of F_x for different ϕ from the previous case shown in Fig. 5.2(a). As in the previous case, the fluid flows along the faces of the cube and leaves the cube without flow separation. It is seen from Table 5.2 that the force components F_y and F_z are sufficiently negligible and the force component F_x is equivalent to the value from the previous case shown in Fig. 5.2. Moreover, the torque components have negligible values that may be considered meaningless in comparison to the previous criterion value of F_x (d/2)≃0.58×10^{-12} Nm.

From these results, we conclude that the uniform flow with a sufficiently low Reynolds number gives rise to a force acting on the cube only in the uniform flow direction, and does not

induce a torque for any orientational configuration relative to the uniform flow direction.

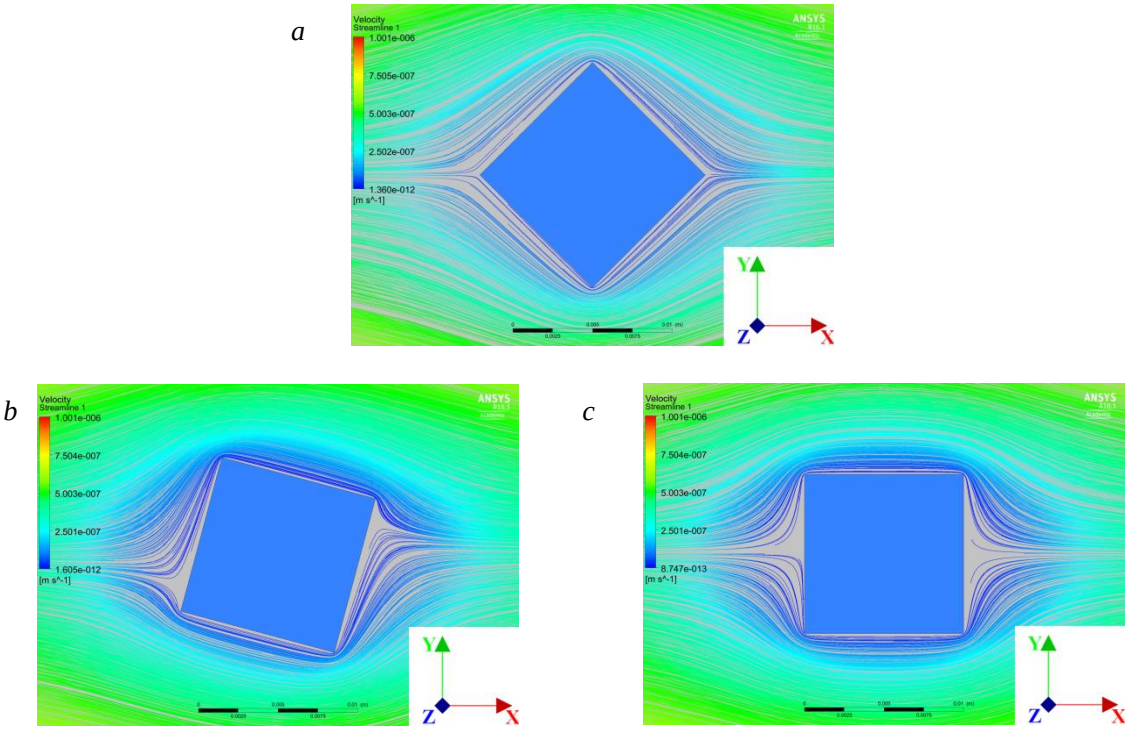

Fig. 5.1 The flow field past a cube for the three different cases of configuration angle (a) ϕ =0°, (b) ϕ =30° and (c) ϕ =45° at the fixed value of θ=0° in the situation of a uniform flow field with a sufficiently low Reynolds number of Re=1.12×10^{-2}.

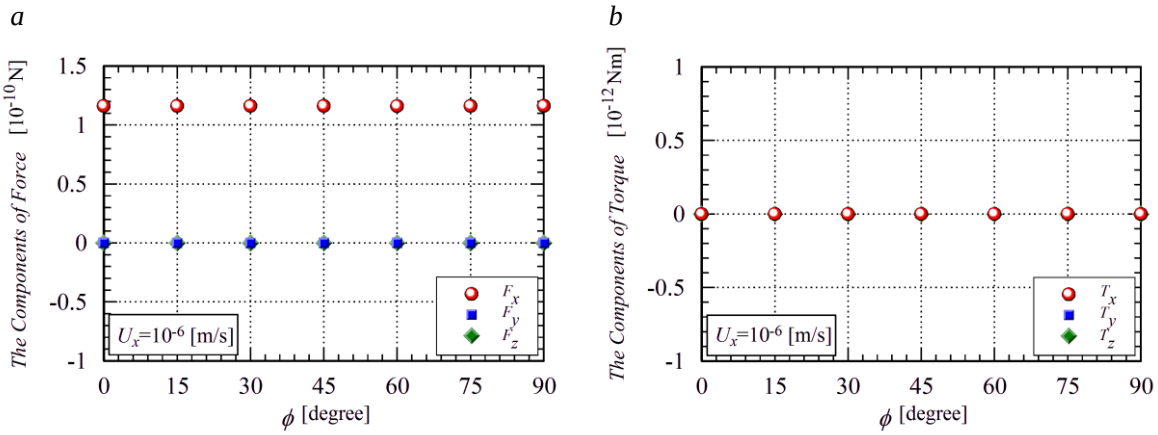

Fig. 5.2 The components of force (a) and the components of torque (b) acting on the cube in a uniform flow field with a sufficiently low Reynolds number Re=1.12×10^{-2}.

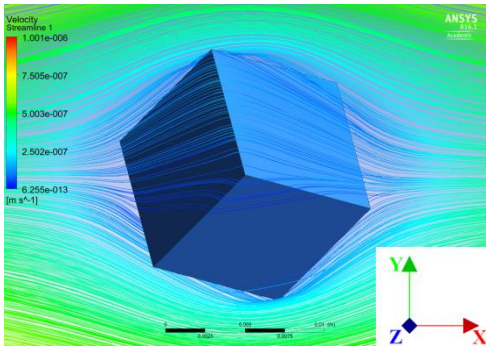

Fig. 5.3 The flow field past the cube in the more general orientational configuration of (θ, ϕ)=(54.74°, 15°) in a 3D system.

Table 5.2 The components of force and torque for the case of the more general orientational configuration (θ, ϕ)=(54.74°, 15°) in a uniform flow field.

F_x [N]	1.161×10^{-10}
F_y [N]	4.36×10^{-15}
F_z [N]	1.03×10^{-14}
T_x [Nm]	1.31×10^{-17}
T_y [Nm]	2.55×10^{-17}
T_z [Nm]	-2.94×10^{-18}
$\langle F_x \rangle$ [N]	1.161×10^{-10}

We now describe the friction coefficients for a cube that are valid for a flow field with a sufficiently low Reynolds number Re <<1, using the above-mentioned flow characteristics. Since a uniform flow gives rise to a force acting on the cube only in the uniform flow direction as in the case of a sphere, the resistance component matrix $\boldsymbol{R}_a$ is expressed as a diagonal matrix:

$$\boldsymbol{R}_a = \begin{pmatrix} \xi_{cube}^T & 0 & 0 \\ 0 & \xi_{cube}^T & 0 \\ 0 & 0 & \xi_{cube}^T \end{pmatrix} \tag{5.13}$$

in which ξ_{cube}^T is the translational friction coefficient of the cube and is evaluated from Eq. (5.10) with the values of $\langle F_x \rangle$ and U_x as

$$\xi_{cube}^T = \frac{\langle F_x \rangle}{U_x} = \frac{1.161\times10^{-10}}{1.0\times10^{-6}} = 1.161\times10^{-4} = 1.384\times(3\pi\eta d) \tag{5.14}$$

Since a torque is not induced by a slow uniform flow, the resistance component matrix $\boldsymbol{R}_b$ is

expressed as

$$\boldsymbol{R}_b = \begin{pmatrix} 0 & 0 & 0 \\ 0 & 0 & 0 \\ 0 & 0 & 0 \end{pmatrix} \tag{5.15}$$

This expression $\boldsymbol{R}_b=\boldsymbol{0}$ implies that a rotational motion is not induced by a uniform flow.

5.4.2 For the case of a rotational flow with a sufficiently low Reynolds number of $Re=1.12\times10^{-4}$

We consider the problem of a rotational flow about the x-axis direction in order to evaluate the components of the resistance matrices $\boldsymbol{R}_c$ and $\boldsymbol{R}_d$. The following results were obtained for a rotational flow with a sufficiently low Reynolds number of $Re=1.12\times10^{-4}$. Figure 5.4 shows the results of the components of the force Fig. 5.4(a) and the components of the torque Fig. 5.4(b) acting on the cube in the rotational flow field. It is noted that the results shown in Fig. 5.4 are for a variety of cases of the orientational angle ϕ with a fixed angle of $\theta=0°$.

It is seen from Fig. 5.4(b) that the torque component T_x has a meaningful value, independent of the orientational angle ϕ and exhibits a constant value $T_x\simeq7.14\times10^{-15}$ Nm. In contrast, the components T_y and T_z are negligible in comparison to the torque component T_x. Moreover, considering a criterion value of $T_x/(d/2)\simeq1.43\times10^{-12}$ N where evaluated with $T_x\simeq7.14\times10^{-15}$ Nm, it is seen from Fig. 5.4(a) that all the force components F_x, F_y and F_z may be regarded as negligibly small.

From these characteristics, we understand that a rotational flow induces only a torque about the direction of the rotational flow field and does not induce a resultant force acting on the cube in a specific direction.

We next consider the force and torque components for the case of the more general orientational configuration of $(\theta, \phi)=(54.74°,15°)$ in a rotational flow. Table 5.3 shows results of the components of force and torque acting on the cube, where the mean value $\langle T_x\rangle$ of the torque component T_x evaluated from the previous case is also shown for reference. It is seen from Table 5.3 that the torque component T_x may be regarded as being equivalent to the mean value $\langle T_x\rangle$ from the previous case. The torque components T_y and T_z are seen to be sufficiently small relative to the component T_x and they may be considered negligible in comparison to the value of T_x. This characteristic implies that the torque acting on the cube in a rotational flow field is determined only by the torque about the direction of the rotational flow. Moreover, as in the previous case, all the force components may be considered negligible in comparison to the criterion value of $T_x/(d/2)\simeq1.43\times10^{-12}$ N.

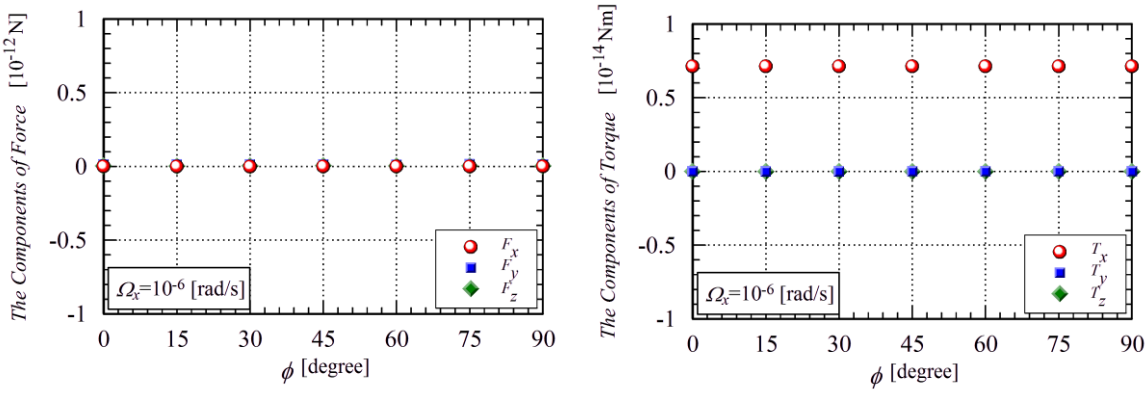

Fig. 5.4 The components of force (a) and the components of torque (b) acting on the cube in a rotational flow field with a sufficiently low Reynolds number Re=1.12×10^{-4}.

Table 5.3 The components of force and torque for the case of the more general orientational configuration (θ, ϕ)=(54.74°, 15°) in a rotational flow field.

F_x [N]	-2.23×10^{-16}
F_y [N]	1.19×10^{-14}
F_z [N]	3.94×10^{-15}
T_x [Nm]	7.140×10^{-15}
T_y [Nm]	1.95×10^{-18}
T_z [Nm]	1.43×10^{-18}
$\langle T_x \rangle$ [Nm]	7.134×10^{-15}

From these results, we understand that the rotational flow with a sufficiently low Reynolds number induces only a torque about the direction of the rotational flow field and does not induce a force acting on the cube for the case of any orientational configuration. That is, the rotational motion does not induce a translational motion of the cube for this rotational flow field.

We now describe the friction coefficients for a cube that are valid for a flow field with a sufficiently low Reynolds number Re <<1, derived from the above-mentioned flow characteristics. Since a rotational flow induces a torque only in the direction of the rotational flow field, the resistance component matrix $\boldsymbol{R}_d$ is expressed as a diagonal matrix as follows:

$$\boldsymbol{R}_d = \begin{pmatrix} \xi^R_{cube} & 0 & 0 \\ 0 & \xi^R_{cube} & 0 \\ 0 & 0 & \xi^R_{cube} \end{pmatrix} \tag{5.16}$$

in which ξ^R_{cube} is the rotational friction coefficient of a cube and is evaluated from Eq. (5.11) with the value $\langle T_x \rangle$ shown in Table 5.3 and the angular velocity Ω_x of the rotational flow field as

$$\xi^R_{cube} = \frac{\langle T_x \rangle}{\Omega_x} = \frac{7.134 \times 10^{-15}}{1.0 \times 10^{-6}} = 7.134 \times 10^{-9} = 2.552 \times (\pi \eta d^3) \tag{5.17}$$

Since a slow rotational flow does not induce a force acting on the cube, the resistance component $\boldsymbol{R}_c$ is expressed as

$$\boldsymbol{R}_c = \begin{pmatrix} 0 & 0 & 0 \\ 0 & 0 & 0 \\ 0 & 0 & 0 \end{pmatrix} \tag{5.18}$$

From the characteristics of the friction coefficients of a cube that have been obtained from both a uniform flow and a rotational flow, we conclude that there is no coupling between the translational motion and the rotational motion in the situation of a sufficiently low Reynolds number. Therefore, as in the case of the sphere, the motion of the cube may be characterized by the two friction coefficients, i.e. the translational friction coefficient shown in Eq. (5.14) and rotational friction coefficient shown in Eq. (5.17).

5.5 Application to the Brownian dynamics simulation method

5.5.1 The basic equations of the translational and rotational motion of cubic particles

Finally, we are able to describe the basic equations for the translational and rotational motion of cubic particles by taking into account the characteristics of the friction coefficients that were obtained in the previous sections. We have also concluded that there is no coupling between the translational motion and the rotational motion for a cube particle system as in the case of a spherical particle system. This characteristic implies that we are able to treat the translational motion and the rotational motion separately in a Brownian dynamics simulation.

If the position vector of the cubic particle is $\boldsymbol{r}$ and the unit vector of the magnetic moment $\boldsymbol{m}=m\boldsymbol{n}$ is $\boldsymbol{n}$, then the basic equations of the particle position and the magnetic moment direction employed in a Brownian dynamics simulation may be written as [10, 11]

$$\boldsymbol{r}(t+\Delta t) = \boldsymbol{r}(t) + \frac{1}{kT} D^T_{cube} \boldsymbol{F}^P(t) \Delta t + \Delta \boldsymbol{r}^B \tag{5.19}$$

$$\boldsymbol{n}(t+\Delta t) = \boldsymbol{n}(t) + \frac{1}{kT} D_{cube}^{R} \boldsymbol{T}^{P}(t) \times \boldsymbol{n}\Delta t + \Delta \boldsymbol{\phi}^{B} \tag{5.20}$$

in which Δt is the time interval, k is Boltzmann's constant, T is the liquid temperature. $\boldsymbol{F}^{P}$ and $\boldsymbol{T}^{P}$ are the total force and torque acting on the particle. $\Delta \boldsymbol{r}^{B}$ and $\Delta \boldsymbol{\phi}^{B}$ are respectively the random displacements inducing the translational and rotational Brownian motion. D_{cube}^{T} and D_{cube}^{R} are the diffusion coefficients of a cubic particle, and are expressed as

$$D_{cube}^{T} = \frac{kT}{\xi_{cube}^{T}} \tag{5.21}$$

$$D_{cube}^{R} = \frac{kT}{\xi_{cube}^{R}} \tag{5.22}$$

Although the friction coefficients ξ_{cube}^{T} and ξ_{cube}^{R} have been shown in Eqs. (5.14) and (5.17), they are rewritten here in a different form. The friction coefficients $\xi_{sphere}^{T(mean)}$ and $\xi_{sphere}^{R(mean)}$ of the sphere with the mean diameter of an inscribed and a circumscribed sphere are written as

$$\xi_{sphere}^{T(mean)} = \frac{1+\sqrt{3}}{2} \xi_{sphere}^{T} \tag{5.23}$$

$$\xi_{sphere}^{R(mean)} = (\frac{1+\sqrt{3}}{2})^{3} \xi_{sphere}^{R} \tag{5.24}$$

in which ξ_{sphere}^{T} and ξ_{sphere}^{R} are the friction coefficients of the inscribed sphere with diameter d. Using these mean friction coefficients, the translational and rotational friction coefficients ξ_{cube}^{T} and ξ_{cube}^{R} for the cube are written as

$$\xi_{cube}^{T} = \alpha_{cube}^{T} \xi_{sphere}^{T(mean)} \tag{5.25}$$

$$\xi_{cube}^{R} = \alpha_{cube}^{R} \xi_{sphere}^{R(mean)} \tag{5.26}$$

in which α_{cube}^{T} and α_{cube}^{R} are modification coefficients given as α_{cube}^{T}=1.013 and α_{cube}^{R}=1.001 from Eqs. (5.14) and (5.17). The values of α_{cube}^{T} and α_{cube}^{R} are approximately equivalent to unity and therefore, as a first approximation, the friction coefficients of the cube can be expressed by using those for a spherical particle with the mean diameter of an inscribed and a circumscribed sphere.

From the above discussion in regard to the friction coefficients, we may conclude that in

the case of a sufficiently low Reynolds number, the Brownian dynamics simulation method for a spherical particle system is straightforwardly applicable to a suspension composed of cubic particles by employing the above-mentioned friction coefficients of the cube in Eqs. (5.25) and (5.26).

5.5.2 The validity of the Brownian dynamics simulations for cubic particles

In order to verify the validity of the Brownian dynamics simulations employing the friction coefficients shown in Eqs. (5.25) and (5.26), we discuss the aggregate structure of magnetic cubic particles by focusing on simulation snapshots and the radial distribution function. It is noted that the distribution function is a reasonable index for a quantitative discussion on the internal structure of particle aggregates since it is significantly sensitive to the form of an aggregate structure. For performing the Brownian dynamics simulation, although it is necessary to consider a repulsive layer model, we will omit the description in this chapter and we will discuss the model in detail in Chapter 6. We employ the results obtained from Monte Carlo simulations as a criterion result since Monte Carlo is a fully developed simulation technique and may be regarded as corresponding to a theoretical solution for an equilibrium state. Since the Brownian dynamics method for the simulation of magnetic cubic particles will be discussed in Chapter 6, we here only described the non-dimensional parameters λ and ξ that characterize the aggregation phenomenon. Two non-dimensional parameters λ and ξ respectively imply the strengths of the magnetic particle-particle interaction and the magnetic particle-field interaction.

Figure 5.5 shows the snapshots for the large magnetic particle-particle interaction strength of λ=30 for the case of no applied magnetic field ξ=0. Figure 5.5 shows the results obtained from a Brownian dynamics simulation Fig. 5.5(a) and a Monte Carlo simulation Figs. 5.5(b). Figure 5.6 shows the radial distribution functions obtained from a Brownian dynamics simulation and a Monte Carlo simulation of a suspension with a magnetic particle-particle interaction strength λ=30 in the absence of an applied magnetic field ξ=0, with a volumetric fraction ϕ_V=0.05 and a particle number N=490.

It is seen from Fig. 5.5(a) that the particles aggregate to form closely-packed clusters in the absence of an applied magnetic field ξ=0. Similarly, it is seen from Fig. 5.5(b) that the closely-packed clusters are also observed by means of a Monte Carlo simulation. This closely-packed cluster is based on the cluster unit shown in Fig. 4.2(b) which leads to a minimum energy configuration as already discussed in Chapter 4. From a comparison of these two snapshots, it is qualitatively understood that a physically reasonable result may be obtained by the above Brownian dynamics method for cubic particles. This is quantitatively supported by results from the radial distribution function shown in Fig. 5.6 where it is evident that the result obtained by a Brownian dynamics simulation is in good agreement with the corresponding Monte Carlo simulation in regard to the shape of the curve, peak position and the height of each peak. This quantitatively

implies that the aggregate structure of the magnetic cubic particles is in good agreement with that obtained by a Monte Carlo simulation. This evidently verifies that the diffusion coefficients shown in Eqs. (5.14) and (5.17) are able to be used for the case of a cubic particle in Brownian dynamics simulations shown in Eqs. (5.25) and (5.26).

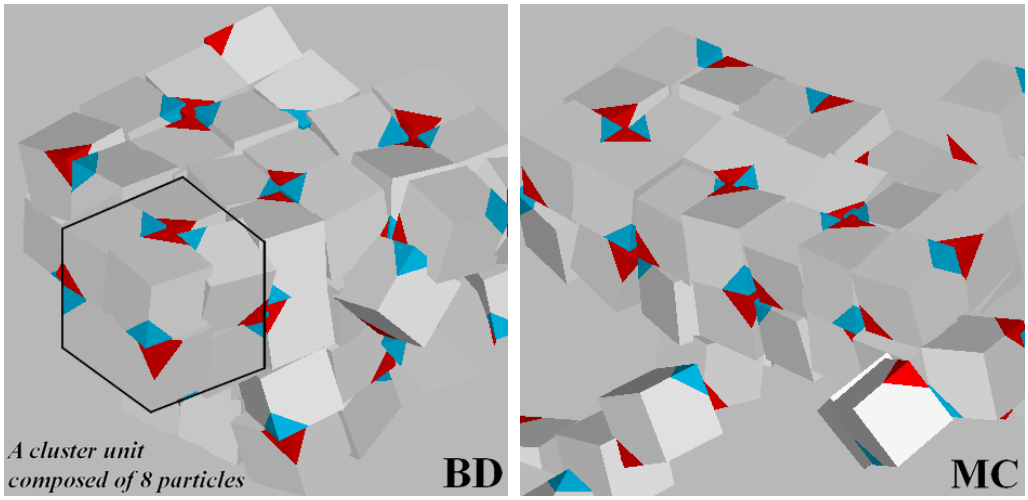

Fig. 5.5 The snapshots from (a) Brownian dynamics simulations and (b) Monte Carlo simulations for the large magnetic particle-particle interaction strength λ=30 and no applied magnetic field ξ=0.

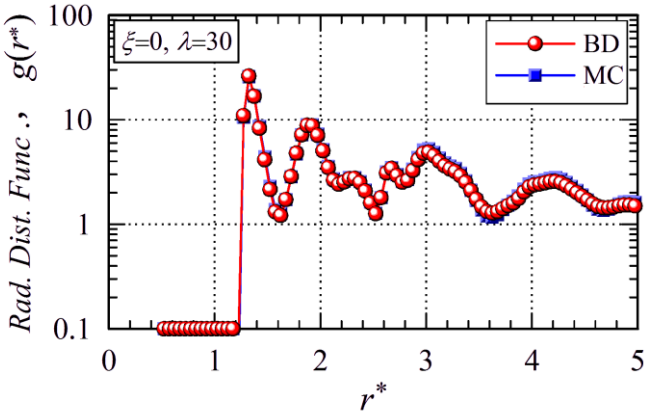

Fig. 5.6 Radial distribution functions for the magnetic particle-particle interaction strength λ=30 for no applied magnetic field ξ=0.

5.6 Conclusion

In the present study, we considered the problem of flow past a cube by means of numerical analysis in order to clarify the characteristics of the translational and rotational friction coefficients that are required to perform a Brownian dynamics simulation for a cubic particle system. In concrete, by estimating the force and torque acting on a cube in the case of a uniform flow field and a rotational flow field with Reynolds number being much smaller than unity, we have discussed whether or not the translational and the rotational motion have a coupling characteristic in the situation of a sufficiently slow flow field. From the characteristics of the friction coefficients of a cube that have been obtained from both a uniform flow and a rotational flow, we may understand that there is no coupling between the translational motion and the rotational motion. This characteristic is significantly similar to that for the case of a spherical particle. Hence, the motion of the cube can be expressed with only two friction coefficients, as in the case of a spherical particle, i.e. the translational friction coefficient and the rotational friction coefficient. Moreover, we have shown that the friction coefficients of a cubic particle may be expressed, as a first approximation, by the friction coefficients of a sphere with the mean diameter of an inscribed and a circumscribed sphere. Employment of these friction coefficients for a cube enables the implementation of a Brownian dynamics simulation for a suspension composed of cubic particles as in the same manner as for the case of a spherical particle suspension.

References

[1] W. A. Bullough, (ed.), *Electro-Rheological Fluids, Magneto-Rheological Suspensions and Associated Technology* (World Scientific, Singapore, 1996).

[2] N. M. Wereley, (ed.), *Magnetorheology*: *Advances and Applications* (Royal Society of Chemistry, London. 2013).

[3] M. P. Allen and D. J. Tildesley, *Computer Simulation of Liquids* (Clarendon Press, Oxford, 1987).

[4] A. Satoh, *Modeling of Magnetic Particle Suspensions for Simulations* (CRC Press, Boca Laton, 2017).

[5] S. I. R. Castillo, C. E. Pompe, J. Van Mourik, D. M. A. Verbart, D. M. E. Thies - Weesie, P. E. De Jongh and A. P. Philipse, Colloidal cubes for the enhanced degradation of organic dyes, J. Mater. Chem. A 2 (2014) 10193-10201.

[6] J. M. Meijer, D. Byelov, L. Rossi, A. Snigirev, I. Snigireva, A. P. Philipse and A. V. Petukhov, Self-assembly of colloidal hematite cubes: a microradian X-ray diffraction exploration of sedimentary crystals, Soft matter 9 (2013) 10729-10738.

[7] J. M. Meijer, F. Hagemans, L. Rossi, D. Byelov, S.I.R. Castillo, I. Snigireva, A.P. Philipse and A.V. Petukhov, Self-Assembly of Colloidal Cubes via Vertical Deposition, Langmuir 28 (2012) 7631-7638.

[8] L. Rossi, S. Sacanna, W.T.M. Irvine, P.M. Chaikin, D.J. Pine and A.P. Philipse, Cubic crystals from cubic colloids, Soft Matter 7 (2011) 4139-4142.

[9] H. Brenner, The Stokes resistance of an arbitrary particle, Chem. Eng. Sci. 18 (1963) 1-25.

[10] A. Satoh, *Introduction to Molecular-Microsimulation of Colloidal Dispersions* (Elsevier, Amsterdam, 2003).

[11] A. Satoh, *Introduction to Practice of Molecular Simulation: Molecular Dynamics, Monte Carlo, Brownian Dynamics, Lattice Boltzmann and Dissipative Particle Dynamics* (Elsevier, Amsterdam, 2010).

Chapter 6 Brownian dynamics simulations of a suspension composed of cubic hematite particles in the equilibrium situation

6.1 Introduction

In addition to the application of magnetic particle suspensions in the field of fluid engineering to mechanical fluid devices such as mechanical dampers and actuators, they also have a significant potential for application in the field of medical engineering. For example, a variety of studies regarding magnetic hyperthermia treatments have been addressed [1-3]. This is a treatment that kills tumor or cancer cells by employing the heating effect generated by the relaxation phenomenon of the magnetic moments of dispersed particles in an alternating magnetic field. Several simulation studies have been conducted in order to investigate the relationship between the characteristics of a heating effect and the behavior of the aggregate structures of magnetic particles in an alternating magnetic field [4-6]. However, these studies treated a suspension composed of spherical particles, and therefore it may be desirable to expand this kind of study to a suspension composed of non-spherical particles such as rod-like, disk-like and cube-like particles. The relationship between the aggregate structures and their heat generation characteristics in an alternating magnetic field may be elucidated by a particle-based simulation method such as Brownian dynamics. The Brownian dynamics simulation is considered to be a useful simulation tool for a suspension of axisymmetric particles such as spherical, rod-like and disk-like particles [7]. However, the Brownian dynamics method for non-axisymmetric cube-like particles has not been currently developed because the relationship between the components of the friction or diffusion tensor in the case of cubic particles has not fully been clarified. From this background, in order to develop a Brownian dynamics simulation for a cube-like particle suspension, in Chapter 5 we clarified there is no coupling between the translational motion and the rotational motion, as in the case of a spherical particle, in the situation of the Reynolds number being sufficiently smaller than unity.

The remaining difficulty in developing a Brownian dynamics simulation code is the treatment of particle-particle overlap and the treatment of the particle-particle repulsive interaction. Up to the present, various simulation models for a cubic particle have been employed by several researchers [8-12]. John et al. modeled cube-like particles as clusters of hard spheres within a cubic frame in order to investigate the lyotropic phase behavior of cube-like particles by means of Monte Carlo simulations [8, 9]. Donaldson et al. [10] employed a repulsive layer model based on an assembly of sub-unit spheres when they investigated the most preferred particle configuration for clusters formed in a quasi-two dimensional (quasi-2D) system by means of molecular dynamics simulations. In addition, they employed a similar model in order to investigate the aggregate structures of magnetic cube-like particles in a three dimensional (3D) system also by means of molecular dynamics simulations [11, 12]. Brownian dynamics simulations require relatively high

computation time, and therefore an efficient repulsive layer model is desirable in order to obtain a more accurate result with a much lower simulation cost.

From this background, in the present study, we first propose a new steric layer model for the steric particle-particle interactions and verify the validity of this interaction model by performing 3D Brownian dynamics simulations in order to make a comparison with the corresponding Monte Carlo simulation.

6.2 Particle model

As in previous Chapters, we employ a simplified model of a cubic hematite particle with a side length d, which has a magnetic dipole moment $\boldsymbol{m}=m\boldsymbol{n}$ pointing in a diagonal direction at the center of the cube as shown in Fig. 6.1(a). The cubic particle is assumed to be coated by a uniform steric layer with thickness δ. If the position vector of particle i is denoted by $\boldsymbol{r}_i$ and the magnetic moment of particle i is denoted by $\boldsymbol{m}_i=m\boldsymbol{n}_i$, then the expressions for the forces and torques acting on a particle i expressed as

$$\boldsymbol{F}_{ij}^{(m)*}=-\frac{3\lambda}{r_{ij}^{*4}}\left[-(\boldsymbol{n}_i\cdot\boldsymbol{n}_j)\boldsymbol{t}_{ij}+5(\boldsymbol{n}_i\cdot\boldsymbol{t}_{ij})(\boldsymbol{n}_j\cdot\boldsymbol{t}_{ij})-\left\{(\boldsymbol{n}_j\cdot\boldsymbol{t}_{ij})\boldsymbol{n}_i+(\boldsymbol{n}_i\cdot\boldsymbol{t}_{ij})\boldsymbol{n}_j\right\}\right] \tag{6.1}$$

$$\boldsymbol{T}_{ij}^{(m)*}=\frac{\lambda}{r_{ij}^{*3}}\left\{3(\boldsymbol{n}_j\cdot\boldsymbol{t}_{ij})\boldsymbol{n}_i\times\boldsymbol{t}_{ij}-\boldsymbol{n}_i\times\boldsymbol{n}_j\right\} \tag{6.2}$$

$$\boldsymbol{T}_i^{(H)*}=\xi\,\boldsymbol{n}_i\times\boldsymbol{H}/H \tag{6.3}$$

in which $\boldsymbol{F}_{ij}^{(m)*}$ and $\boldsymbol{T}_{ij}^{(m)*}$ are the magnetic force and torque acting on particle i by particle j due to the magnetic particle-particle interactions between the particles and $\boldsymbol{T}_i^{(H)*}$ is the magnetic torque acting on particle i due to an external magnetic field $\boldsymbol{H}$ ($H=|\boldsymbol{H}|$). Also, $\boldsymbol{n}_i$ is the unit vector of the magnetic moment $\boldsymbol{m}_i$ of particle i, $\boldsymbol{t}_{ij}$ is the unit vector denoting the direction of particle i relative to particle j, expressed as $\boldsymbol{t}_{ij}=\boldsymbol{r}_{ij}/r_{ij}$, where $\boldsymbol{r}_{ij}=\boldsymbol{r}_i-\boldsymbol{r}_j$ is the relative position of particle i to particle j, and $r_{ij}=|\boldsymbol{r}_{ij}|$. The non-dimensional parameters λ and ξ are expressed as $\lambda=\mu_0 m^2/(4\pi d^3 kT)$ and $\xi=\mu_0 mH/(kT)$, where k is the Boltzmann's constant, T is the absolute temperature of the liquid and μ_0 is the permeability of free space. These non-dimensional parameters λ and ξ implies the strength of the magnetic particle-particle interaction and the magnetic particle-field interaction, respectively.

The particles dispersed in the base liquid are generally coated with an electric double-layer or a steric layer in order to obtain a stable dispersion. In the previous Chapters 2, 3 and 4, we employed a solid particle model without a repulsive layer because the interaction energy due to the overlap of the repulsive layers for the case of two cubic particles has not, to date, been derived as a mathematical expression. In the Monte Carlo simulations, the solid particle model above is a reasonable first approximation, but in the Brownian dynamics simulations, the use of a solid particle

model may have fatal consequences. In order to consider the interaction due to the overlap of the repulsive layers, Donaldson et al. modeled the repulsive layer of a cubic particle by employing spherical particles with the same diameter. They concluded that the N_{sph}=5 model as shown in Fig. 6.1(b) is an appropriate model from the viewpoint of simulation time and simulation accuracy [10], where N_{sph} is the number of spherical particles per cube side. However, if we apply the Donaldson model shown in Fig. 6.1(b) to the dispersion treated in the present study, composed of some 500 particles, then the computation time would be prohibitively large. Therefore, in the present study, we propose the new steric layer model as shown in Fig. 6.1(c), which is expected to obtain results with a reasonably high degree of accuracy with less computation time.

The interaction energy ${u_{iajb}}^{(V)*}$ due to the overlap of the steric layers between two spheres i_a and j_b with different diameters d_{ia} and d_{jb} coated with the steric layer of thickness δ has already been proposed by Suzuki et al. [13], and the theoretical expression for ${u_{iajb}}^{(V)*}$ has been described in detail in their paper. The force ${\boldsymbol{F}_{iajb}}^{(V)*}$ and torque ${\boldsymbol{T}_{iajb}}^{(V)*}$ acting on the particles due to the overlap of steric layers may be obtained from vector analysis of the interaction energy ${u_{iajb}}^{(V)*}$ [13], and are expressed as

$$\boldsymbol{F}_{iajb}^{(V)*} = \lambda_V \boldsymbol{t}_{iajb}\left[2d_{ia}^{*}\left\{\frac{\partial s_{ia}^{*}}{\partial r_{iajb}^{*}}\ln\left(\frac{\delta^{*}}{s_{ia}^{*}}\right)\right\} + 2d_{jb}^{*}\left\{\frac{\partial s_{jb}^{*}}{\partial r_{iajb}^{*}}\ln\left(\frac{\delta^{*}}{s_{jb}^{*}}\right)\right\}\right] \tag{6.4}$$

$$\boldsymbol{T}_{iajb}^{(V)*} = \boldsymbol{r}_{ia}^{*} \times \boldsymbol{F}_{iajb}^{(V)*} \tag{6.5}$$

in which

$$\frac{\partial s_{ia}^{*}}{\partial r_{iajb}^{*}} = \frac{{r_{iajb}^{*}}^{2} - \left\{(d_{ia}^{*}/2+\delta^{*})^{2} - (d_{jb}^{*}/2+\delta^{*})^{2}\right\}}{2{r_{iajb}^{*}}^{2}} \tag{6.6}$$

$$\frac{\partial s_{jb}^{*}}{\partial r_{iajb}^{*}} = \frac{{r_{iajb}^{*}}^{2} - \left\{(d_{jb}^{*}/2+\delta^{*})^{2} - (d_{ib}^{*}/2+\delta^{*})^{2}\right\}}{2{r_{iajb}^{*}}^{2}} \tag{6.7}$$

That is, the repulsive force $|\boldsymbol{F}^{(V)*}|$ acting between cubic particles is expressed as

$$\left|\boldsymbol{F}^{(V)*}\right| = \left|\sum_{ia=1}^{Np}\sum_{jb=1}^{Np}\boldsymbol{F}_{iajb}^{(V)*}\right| \tag{6.8}$$

in which N_p is the number of constituent spherical particles for the model of one cubic particle with a steric layer. The non-dimensional parameter λ_V, arising from the non-dimensionalization procedure,

represents the strength of the repulsive interaction relative to the thermal energy and is expressed as $\lambda_V=\pi n_s d_0^2/2$, where n_s is the number of surfactant molecules per unit area on the surface of a spherical particle and d_0 is the diameter of a representative spherical particle, and in the case of the present study, the side length d of the cubic particle is employed.

Here, we describe our sphere-connected model, shown in Fig. 6.1(c), for treating the repulsive interaction due to the overlap between the steric layers that uniformly coat the cubic particles. In this model, a cubic particle with side length d employs three different size spherical particles with diameters denoted as d_{center}, d_{edge} and d_{corner}. An inscribed sphere of diameter $d_{center}=d$ is initially placed at the center of the cube and then 12 spheres of diameter d_{edge} are arranged so that each sphere is in contact with the inscribed sphere and also with the two faces which constitute the intersection line of the sides of the cube. Finally, in order to represent the corners of the cube, 8 spheres with diameter d_{corner} are then arranged in contact with the inscribed sphere and also with the three faces which constitute the corner of the cube. As it is assumed each spherical particle is coated by a steric layer of thickness δ, the steric layer model shown in Fig. 6.1(c) is employed for evaluating the repulsive interaction energy or force between the two cubic particles coated by a uniform steric layer in the manner shown in Fig. 6.1(a). Each diameter d_{center}, d_{edge} and d_{corner} can be straightforwardly evaluated from a geometric calculation.

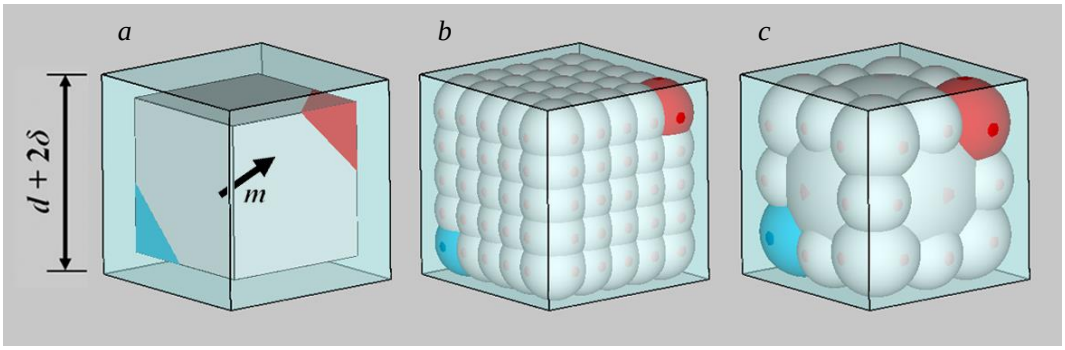

Fig. 6.1 Particle model: showing (a) the cubic particle coated by a steric layer, (b) the repulsive layer model of Donaldson et al. and (c) our model employed for the evaluation of the repulsive interaction between two cubic particles.

6.3 Brownian dynamics simulations

In Chapter 5, we clarified that there is no coupling between the translational motion and the rotational motion of a cubic particle; as in the case of a sphere, in the situation of a sufficiently slow flow field, and we have briefly described the basic equations of the translational and rotational motion of cubic particles. In this section, we describe in more detail the equations of motion of cubic particles. If the position vector of a cubic particle is $\boldsymbol{r}$ and the unit vector of the magnetic moment $\boldsymbol{m}=m\boldsymbol{n}$ is $\boldsymbol{n}$, then the Brownian dynamics simulations are performed with the following equations. It is noted that a component normal to the magnetic moment direction is denoted by the subscript $\perp$, and a component parallel the magnetic moment direction is denoted by the subscript $\parallel$.

$$\boldsymbol{r}(t+\Delta t)=\boldsymbol{r}(t)+\frac{1}{kT}D_{cube}^{T}\boldsymbol{F}^{P}(t)\Delta t+\Delta\boldsymbol{r}^{B} \tag{6.9}$$

$$\boldsymbol{n}(t+\Delta t)=\boldsymbol{n}(t)+\frac{1}{kT}D_{cube}^{R}\boldsymbol{T}_{\perp}^{P}(t)\times\boldsymbol{n}\Delta t+\Delta\phi_{\perp 1}^{B}\boldsymbol{e}_{\perp 1}(t)+\Delta\phi_{\perp 2}^{B}\boldsymbol{e}_{\perp 2}(t) \tag{6.10}$$

in which Δt is the time interval in a simulation, $\boldsymbol{F}^{P}$ is the total force acting on the particle, $\boldsymbol{T}_{\perp}{}^{P}$ is the torque corresponding to the component perpendicular to the magnetic moment axis direction, $\boldsymbol{e}_{\perp 1}(t)$ and $\boldsymbol{e}_{\perp 2}(t)$ are orthogonal unit vectors normal to the magnetic moment, and D_{cube}^{T} and D_{cube}^{R} are the translational and rotational diffusion coefficients of the cubic particle. are the translational and rotational diffusion coefficients of the cubic particle. Following on from Chapter 5 we employ, as a first approximation, the translational friction coefficient $\xi_{mean}^{T}=3\pi\eta d_{mean}$ and the rotational friction coefficient $\xi_{mean}^{R}=\pi\eta d_{mean}^{3}$ of a sphere with diameter $d_{mean}=(1+\sqrt{3})d/2$. Hence, the diffusion coefficients D_{cube}^{T} and D_{cube}^{R} of a cubic particle are expressed as

$$D_{cube}^{T}=\frac{kT}{\xi_{cube}^{T}}=\frac{kT}{\xi_{mean}^{T}} \tag{6.11}$$

$$D_{cube}^{R}=\frac{kT}{\xi_{cube}^{R}}=\frac{kT}{\xi_{mean}^{R}} \tag{6.12}$$

$\Delta\boldsymbol{r}^{B}$, $\Delta\phi_{\perp 1}^{B}$ and $\Delta\phi_{\perp 2}^{B}$ are the translational and rotational random displacements due to Brownian motion and they have following stochastic characteristics:

$$\left\langle\Delta\boldsymbol{r}^{B}\right\rangle=0,\ \left\langle\Delta\boldsymbol{r}^{B}\Delta\boldsymbol{r}^{B}\right\rangle=2D_{cube}^{T}\Delta t\boldsymbol{I} \tag{6.13}$$

$$\left\langle\Delta\phi_{\perp 1}^{B}\right\rangle=\left\langle\Delta\phi_{\perp 2}^{B}\right\rangle=0,\ \left\langle(\Delta\phi_{\perp 1}^{B})^{2}\right\rangle=\left\langle(\Delta\phi_{\perp 2}^{B})^{2}\right\rangle=2D_{cube}^{R}\Delta t \tag{6.14}$$

in which $\boldsymbol{I}$ is a unit tensor.

In addition, as in the case for non-axisymmetric particles, it is necessary to consider the rotational motion about the magnetic moment of the cubic particle. If we define a unit vector normal to the magnetic moment by the notation $\boldsymbol{n}_{\perp}$, then the equation of motion for the rotational motion about the magnetic moment is expressed as

$$\boldsymbol{n}_{\perp}(t+\Delta t) = \boldsymbol{n}_{\perp}(t) + \frac{1}{kT} D_{cube}^{R} \boldsymbol{T}_{\parallel}^{P}(t) \times \boldsymbol{n}_{\perp} \Delta t + \Delta\phi_{\parallel}^{B} \boldsymbol{n} \times \boldsymbol{n}_{\perp} \tag{6.15}$$

in which $\boldsymbol{T}_{\parallel}^{P}$ is the torque about the magnetic moment axial direction and $\Delta\phi_{\parallel}^{B}$ is a random rotational displacement with the following stochastic characteristics:

$$\left\langle \Delta\phi_{\parallel}^{B} \right\rangle = 0\,, \quad \left\langle (\Delta\phi_{\parallel}^{B})^{2} \right\rangle = 2D_{cube}^{R}\Delta t \tag{6.16}$$

6.4 Quantitative evaluation of the internal structure of the aggregates

In order to quantitatively evaluate the internal structure of the cubic particle aggregates, we define a new orientational pair correlation function $f_{o.c.}^{(e)}(r)$ for the three plane direction vectors $\boldsymbol{e}_1$, $\boldsymbol{e}_2$ and $\boldsymbol{e}_3$ of a cubic particle.

$$f_{o.c.}^{(e)}(r) = \frac{4}{21} \frac{1}{n_0 g(r)} \frac{1}{N} \left\langle \sum_{i=1}^{N} \frac{\sum\nolimits' \sum_{k=1}^{3} \sum_{l=1}^{3} P_4(\cos\psi_{ij}^{(\boldsymbol{e}_k, \boldsymbol{e}_l)})}{4\pi r^2 \Delta r} \right\rangle \tag{6.17}$$

in which n_0 is the number density, N is the number of particles in the system, r is the radial distance from the particle of interest, $g(r)$ is the radial distribution function and $\psi_{ij}^{(\boldsymbol{e}_k, \boldsymbol{e}_l)}$ is the angle between the direction vectors $\boldsymbol{e}_k$ and $\boldsymbol{e}_l$ of the cubic particles i and j. $\sum'$ implies the summation with respect to particles that are located in the infinitesimal shell volume $\Delta V = 4\pi r^2 \Delta r$ at the radial distance r from the particle of interest, $\langle - \rangle$ is the ensemble average, and $P_4(\cos\psi_{ij})$ is the fourth Legendre polynomial, expressed as $P_4(\cos\psi_{ij}) = (35\cos^4\psi_{ij} - 30\cos^2\psi_{ij} + 3)/8$. It is noted that the orientational pair correlation function gives rise to a value $f_{o.c.}^{(e)}(r) = 1$ if the faces of the cubic particles are oriented parallel to each other. The radial distribution function $g(r)$ is defined as

$$g(r) = \frac{1}{n_0 N} \left\langle \sum_{i=1}^{N} \frac{\Delta N_i(r)}{4\pi r^2 \Delta r} \right\rangle \tag{6.18}$$

in which $\Delta N_i(r)$ is the number of particles located in the infinitesimal shell volume ΔV at the radial distance r from the particle i. It is noted that the quantitative evaluation methods described above are valid for a 3D system. In the case of a quasi-2D system, we deal with the infinitesimal area $\Delta S=2\pi r\Delta r$ instead of the infinitesimal shell volume $\Delta V=4\pi r^2\Delta r$ and then $\Delta N_i(r)$ is the number of particles located in the infinitesimal area ΔS at the radial distance r from the particle i.

For reference, the following order parameter $S_4^{(e)}$ is defined in order to quantitatively discuss the internal structure of the aggregates in the system.

$$S_4^{(e)} = \frac{4}{21}\frac{1}{N_{pair}}\left\langle \sum_{i=1}^{N}\sum_{\substack{j=1 \\ j>i}}^{N}\sum_{k=1}^{3}\sum_{l=1}^{3} P_4(\cos\psi_{ij}^{(\boldsymbol{e}_k,\boldsymbol{e}_l)}) \right\rangle \tag{6.19}$$

It is noted that the order parameter gives rise to a value of $S_4^{(e)}=1$ if all the faces of cubic particles in the system are oriented parallel to each other.

6.5 Parameters for simulations

Unless specifically noted, the Brownian dynamics simulations have been performed with the following values. The volumetric fraction of particles ϕ_V is set as $\phi_V=0.05$, the number of particles is $N=490$, the cutoff distance $r_{coff}^* = r_{coff}/d$ of the magnetic interaction between cubic particles is $r_{coff}^*=10$, the thickness $\delta^* = \delta/d$ of the steric layer is $\delta^*=0.15$, the non-dimensional parameter λ_V is taken as $\lambda_V=100$, 115, 150, 225 depending on the steric layer model. The non-dimensional parameters λ and ξ are set in the wide range of $\lambda=0\sim30$ and $\xi=0\sim20$. We employed periodic boundary conditions for the xyz-axis directions. An external magnetic field is applied in the z-axis direction. We have confirmed that the internal structure of the particle aggregates may be dependent on the volumetric fraction. However, the objective of the present study is to verify the validity of implementing the steric interaction model in a Brownian dynamics simulation for a cubic particle suspension. In the present study, we employ a volumetric fraction $\phi_V=0.05$ that is qualitatively straightforward in order to be able to discern the internal structure of particle aggregates. In the Brownian dynamics simulations, the time interval $\Delta t^*=0.00005$, and the total number of time steps per simulation run is N_{timemx} =5,000,000. In the Monte Carlo simulations, the total number of Monte Carlo steps $N_{smplemx}$=1,000,000. In the Brownian dynamics simulations, if the magnetic particles aggregate to form clusters, then the faces of two neighboring cubic particles overlap by around 0.1d. In the Monte Carlo simulations, therefore, solid cubic particles with no steric layer and a side length of 1.2d have been employed in order to yield significant peaks in the pair orientational correlation function at similar separation positions to the Brownian dynamics particles, as will be shown later. It is noted that cubic particles including the steric layer will be shown in the snapshots that follow.

6.6 Results and discussion

6.6.1 Comparison of the present steric layer model with other researchers' models

6.6.1.1 Steric repulsive force

As discussed in section 6.2, we proposed a new steric layer model for evaluating the repulsive interaction due to the overlap of cubic particle steric layers, shown in Fig. 6.1(c). In order to verify the validity of the present steric layer model, we compare it with the results obtained using the models proposed by Donaldson et al. [10].

We first discuss the dependence of the repulsive force on different steric layer models including the Donaldson n et al. model. Figure 6.2 shows the repulsive force $|\boldsymbol{F}^{(V)*}|=|\boldsymbol{F}^{(V)}|/(kT/d)$ acting on the cubic particles as a function of the center-to-center separation distance r^* between the two particles of interest when located along the particle axis line with the neighboring faces of the cubes in a parallel arrangement. Figure 6.2(a) shows the comparison of results for the present steric layer model and the Donaldson models for a common given value of λ_V=150. It is seen from Fig. 6.2(a) that the value of the repulsive force is dependent on the number N_{sph} of spherical particles per cube side in the Donaldson model. This is because the total repulsive force between two particles is evaluated from the summation of the interaction of each pair of constituent spherical particles. The total repulsive force, therefore, has been employed as a criterion for comparison rather than the repulsive interaction strength λ_V itself. Figure 6.2(b) shows results of the repulsive force $|\boldsymbol{F}^{(V)*}|$ for the present model and the three models of Donaldson et al., which were obtained by employing an appropriate value of λ_V in order that the total repulsive force is approximately equivalent to that of the present model that employs λ_V=150. It is seen from Fig. 6.2(b) that a similar repulsive force acts between particles in the range of $1.1\lesssim r^*\lesssim 1.3$ although a relatively significant discrepancy occurs in the range of $1\lesssim r^*\lesssim 1.1$. It will be shown later in the results of the radial and pair orientational correlation functions that two cubic particles overlap in a face-to-face contact manner in the range of $1.2\lesssim r^*\lesssim 1.3$ and clearly implies that the present results for λ_V=150 can be compared with those of the Donaldson et al. models with parameter values λ_V=115, 100 and 225 for the respective values N_{sph}=3, N_{sph}=5 and N_{sph}=7.

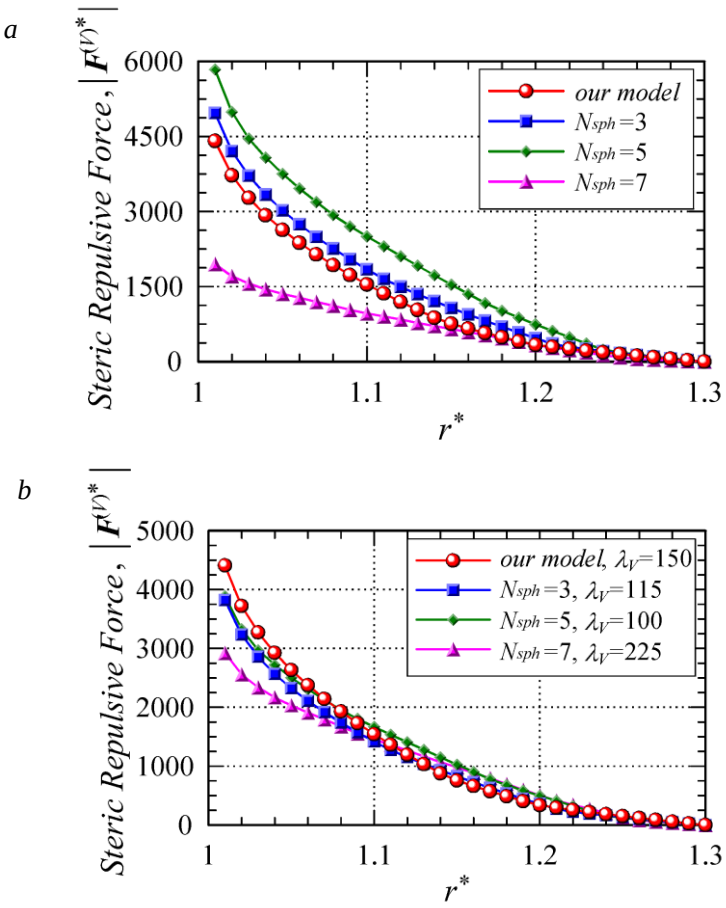

Fig. 6.2 Dependence of the repulsive force $|\boldsymbol{F}(V)^*|$ on the steric layer model and the models proposed by Donaldson et al. [10] as a function of the center-to-center separation distance r^*.

6.6.1.2 Computational time of a simulation

We now discuss the relationship between the computation time, the CPU time, required by each steric layer model. Table 1 shows the CPU time required by one Intel core i5 650 3.20 GHz processor for one complete simulation run for the present model and the Donaldson models [10]. We here focus on the case of ξ=0 and λ=30 that requires the most computation time for the present simulations. It is seen from Table 1 that the models of Donaldson et al. require significantly more computation time as the value of N_{sph} is increased. In particular, in the case of N_{sph}=7, the simulation time is about 20 days and therefore this model may be scarcely practical. Although results with a higher degree of accuracy may be expected from a model with larger values of N_{sph}, from the viewpoint of a reasonable computation time, the model of N_{sph}=5 may be the most appropriate. In

contrast, our model requires only around 12 hours, which is similar to the case of N_{sph}=3 model. Hence, if we can show that our model gives rise to reasonable results with sufficient accuracy, then the usefulness and validity of the present steric layer model for evaluating the steric interaction energy will be reasonably proved.

Table 6.1 CPU time required for one complete simulation run.

	our model	N_{sph}=3 model	N_{sph}=5 model	N_{sph}=7 model
time [hour]	12	12	72	480

6.6.1.3 Validity of the present steric layer model

In the present section, we discuss the validity of the steric layer model by a comparison with the results obtained from Monte Carlo simulations for a 3D system in thermodynamic equilibrium.

Figure 6.3 shows results of the orientational pair correlation function $f_{o.c.}^{(e)}(r)$ for the current model and a comparison with the three models of Donaldson et al. [10] and the Monte Carlo simulation. It is noted that the value of $f_{o.c.}^{(e)}(r)$ is sensitive to changes in particle orientation. Figure 6.4 shows snapshots of the aggregate structures for qualitatively recognizing the discrepancy in the results of $f_{o.c.}^{(e)}(r)$ where Fig. 6.4(a) is a snapshot for the case of the Donaldson model with N_{sph}=3 and Fig. 6.4(b) is a snapshot of our model.

We first discuss results obtained for the models by Donaldson et al. [10], shown in Fig. 6.3(a) where it is seen that the characteristics of the curves for their models approach those of the Monte Carlo simulation with increasing value of N_{sph}. This is because the sides and corners of a cubic particle can be modeled to a higher degree of accuracy with increasing N_{sph} values. In particular, an improvement in the curves from N_{sph}=3 to N_{sph}=5 is remarkably significant, where the curve for N_{sph}=5 model is tending to a good agreement with the Monte Carlo simulation. From the characteristics of the results shown in Fig. 6.3(a), it is clear that all the curves exhibit the first pronounced peak at around the short distance $r^* \simeq 1.2$, which implies that two neighboring particles are in a perfect face-to-face contact configuration. Although the remaining peaks also appear at positions similar to those of the Monte Carlo simulation, in the case of N_{sph}=3 the peaks at increasing distance r^* tend significantly lower than those for N_{sph}=5 and N_{sph}=7. The characteristics shown for the case of N_{sph}=3 quantitatively imply that other types of clusters are formed in the system in addition to the closely-packed clusters that are reasonably expected from the previous study in Chapter 4 by Monte Carlo simulations. Figure 6.4(a) shows a snapshot for the case of N_{sph}=3 model and it is seen that closely-packed clusters with face-to-face contact are formed in the lower area, whilst aggregates with irregular contact are observed in the upper area. From the Monte Carlo simulations in Chapter 4, we confirmed that this kind of large irregular cluster is not observed. Hence, we understand that the aggregates with irregular contact arise via an unsatisfactory modeling

of the edges and corners of a cube in the case of a N_{sph}=3 model. That is, cubes modeled with significantly round edges and corners give rise to the large irregular aggregate shown in Fig. 6.4(a). As discussed above, the curve for N_{sph}=5 in Fig. 6.3(a) is in good agreement with the Monte Carlo simulation and such irregular clusters have not been observed in snapshots similar to that in Fig. 6.4(b) employing the present steric layer model. From these results, we may conclude from the models of Donaldson et al., that the models with at least N_{sph}=5 tend to be more accurate and obtain physically reasonable results for a cubic particle suspension.

We now discuss the validity of the present steric layer model by using the results shown in Figs. 6.3(b) and 6.4(b). It is seen from Fig. 6.3(b) that the curve obtained from our model is in good agreement with that obtained for the models of N_{sph}=7 and N_{sph}=5 by Donaldson et al. Moreover, the agreement with the Monte Carlo model may be regarded as being sufficiently reasonable. Although in our cubic particle model a single cube edge is expressed with three spheres of different diameters, as shown in Fig. 6.1(c), the above discussion exemplifies that our approach is able to give rise to reasonable aggregate structures, which may be qualitatively clarified from the simulation snapshot shown in Fig. 6.4(b). This good agreement arises from our effective modeling whereby spherical particles with a relatively small diameter are arranged at the eight corners of the cube by a method employing inscribed spheres. Hence, although only three particles are used for expressing one cube edge in a similar manner to the model of N_{sph}=3 by Donaldson et al., our model is able to offer more accurate results. We now address the result of the present model shown in the snapshot Fig. 6.4(b) which is in good agreement with the Monte Carlo and the Donaldson et al. models of N_{sph}=5 and 7 although not shown as snapshots. From Fig. 6.4(b), it is seen that, although closely-packed clusters are predominately observed, the large irregular aggregate clusters are not formed, which is in significant contrast to the snapshot shown in Fig. 6.4(a).

From these results, we understand that the present steric layer mode is able to give rise to physically reasonable aggregate structures with sufficient accuracy and in satisfactorily good agreement with the corresponding Monte Carlo simulation. This understanding will be further supported from the following characteristics of the radial distribution function.

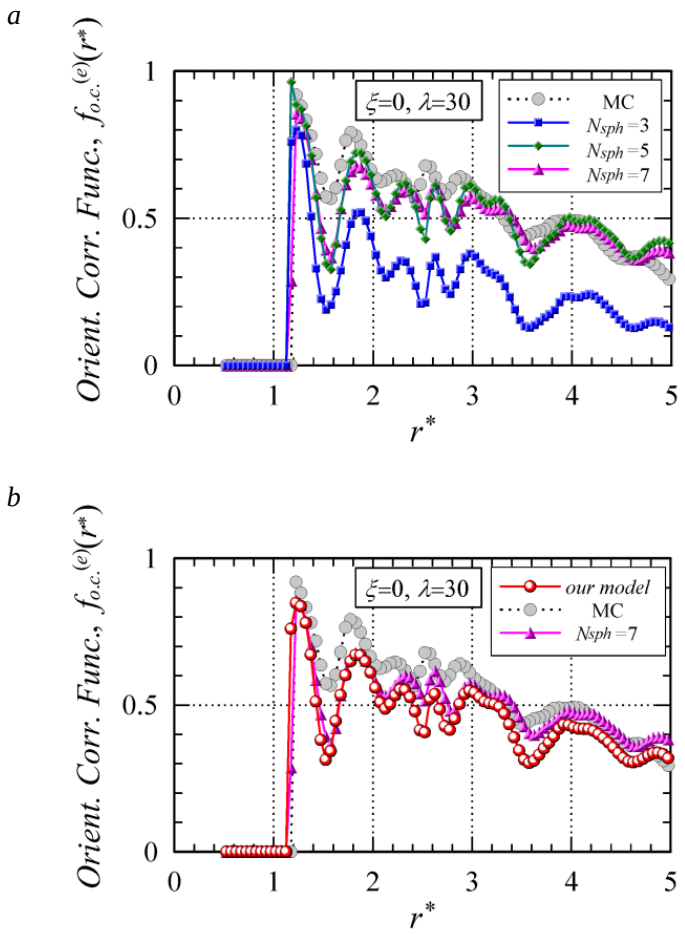

Fig. 6.3 The orientational correlation function $f_{o.c.}^{(e)}(r^*)$ for λ=30 and ξ=0 in a comparison with (a) three models presented by Donaldson et al. and (b) our model.

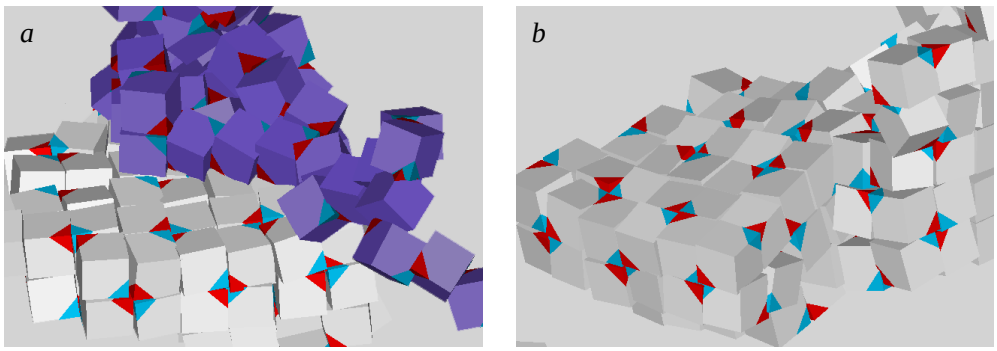

Fig. 6.4 The aggregate structures for λ=30 and ξ=0 for (a) the Donaldson et al. model of N_{sph} =3 and (b) our model.

6.6.2 Brownian dynamics simulation with our repulsive interaction model

In this section, we verify the validity of employing a Brownian dynamics simulation method with the present steric interaction model for cubic particles. We first discuss the dependence of the internal structure of particle aggregates on the magnetic particle-particle interaction strength λ in the absence of the magnetic field ξ=0. Figure 6.5 shows snapshots of particle aggregates with no applied magnetic field for different magnetic particle-particle interaction strengths λ. Figures 6.5(a), 6.5(b) and 6.5(c) are for the values λ=20, λ=25 and λ=30, respectively. For the case of λ=20 as shown in Fig. 6.5(a), it is seen that the particles tend to form a relatively loose aggregate structure where the neighboring particles do not contact each other in a close face-to-face configuration. As the magnetic particle-particle interaction strength is increased, from λ=20 to λ=25 as shown in Fig. 6.5(b), it is seen that particles also tend to form loosely-packed clusters but now there is an increased number of constituent particles in face-to-face contact. In contrast, for the case of a strong magnetic particle-particle interaction strength λ=30 shown in Fig. 6.5(c), large closely-packed aggregate structures are formed in the system. We have already discussed that the results of the radial distribution function shown in Fig. 5.6 in Chapter 5, and the pair correlation function shown in Fig. 6.3(b) are in good agreement with the corresponding Monte Carlo simulation.

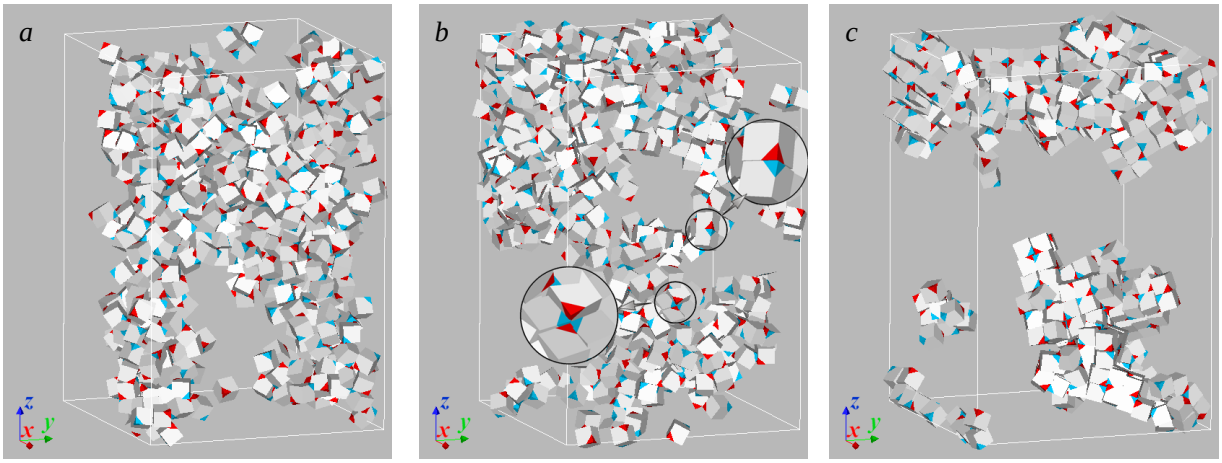

Fig. 6.5 Dependence of the aggregate structures on the magnetic particle-particle interaction strengths (a) λ=20, (b) λ=25 and (c) λ=30 in no applied magnetic field ξ=0.

We next discuss a phase change in the aggregate structure due to the influence of an external magnetic field. In Chapter 4, by means of Monte Carlo simulations, we clarified that the large closely-packed clusters shown in Fig. 6.5(c) are transformed into wall-like clusters due to the influence of a magnetic field. Therefore, we here investigate whether the same regime change occurs during Brownian dynamics simulations that employ our steric interaction model. Figure 6.6 shows snapshots of aggregate structures in the case of a strong magnetic particle-particle interaction strength λ=30. Figures 6.6(a) and 6.6(b) are for magnetic particle-field interaction strengths ξ=5 and ξ=10. It is noted that the smaller snapshot on the right-hand side is viewed from the *z*-axis direction of the external magnetic field in order to discern the aggregate structures more clearly. For the case of the relatively weak magnetic particle-field interaction strength of ξ=5, shown in Fig. 6.6(a), the closely-packed clusters are transformed into wall-like clusters. However, it is seen from the snapshot on the right-hand side of Fig. 6.6(a) that the small closely-packed clusters do not completely collapse. For the case of a strong magnetic particle-field interaction strength ξ=10, shown in Fig. 6.6(b), it is clearly seen that the magnetic moment of a particle tends to incline in the magnetic field direction and the closely-packed clusters have completely collapsed and transformed into wall-like clusters. This regime change is quantitatively supported by the results of the magnetization curve shown in Fig. 6.7, where the Langevin function is also shown for reference. In the range of $\xi \lesssim 5$ where the magnetic particle-field interaction strength is relatively weak, the magnetization curve shows smaller values than that of the Langevin function. This characteristic quantitatively suggested that the aggregate structures are not completely transformed into the wall-like clusters in this range. In contrast, in the range of $\xi \gtrsim 10$ where the magnetic particle-field interaction strength is relatively strong, the curve exhibits larger values than that of the Langevin function. This is because the orientation of the magnetic moments of constituent particles in wall-like clusters is strongly restricted due to the magnetic interaction between the neighboring particles. That is, the magnetization curve is able to discern a regime change in the aggregate structures. Moreover, the results obtained by our model from Brownian dynamics simulations are in good agreement with the Monte Carlo simulations.

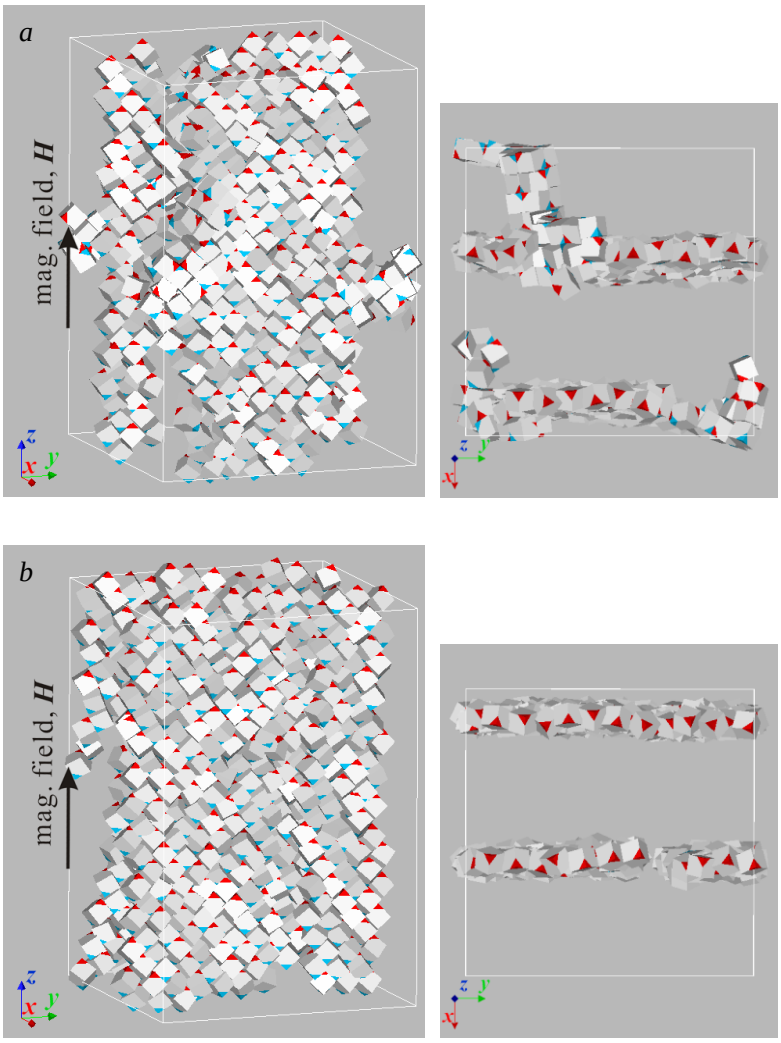

Fig. 6.6 Dependence of the aggregate structures on the magnetic particle-field interaction strength of (a) ξ=5 and (b) ξ=10 for the magnetic particle-particle interaction strength λ=30.

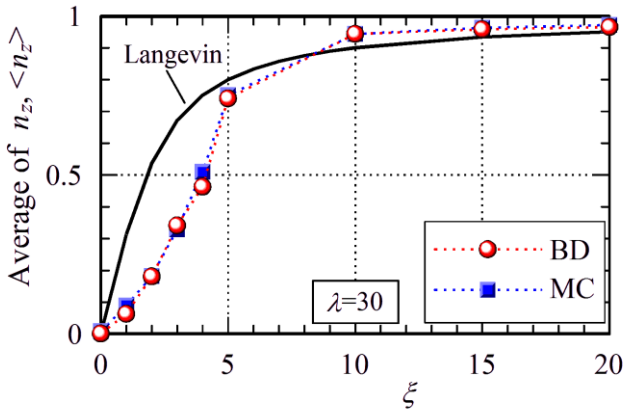

Fig. 6.7 The normalized magnetization curve in a comparison with the Langevin function.

Finally, we consider the radial distribution function for a wide range of the non-dimensional parameters λ=0~30 and ξ=0~20 in order to quantitatively discuss the accuracy of the results obtained from the present steric layer model. Since the first and second peaks in the radial distribution function are significantly sensitive to the internal structure of aggregates, we here discuss these initial peaks rather than the full radial distribution function. Figure 6.8 shows the height of the first and second peaks where in Figs. 6.8(a) is shown the height of the initial peaks as a function of the magnetic particle-particle interaction strength λ for no applied magnetic field ξ=0 and then in Fig. 6.8(a) the peaks are shown as a function of the magnetic particle-field interaction strength ξ for a relatively large magnetic particle-particle interaction strength λ=30. In these figures, the results obtained from a corresponding Monte Carlo simulation are also shown for comparison.

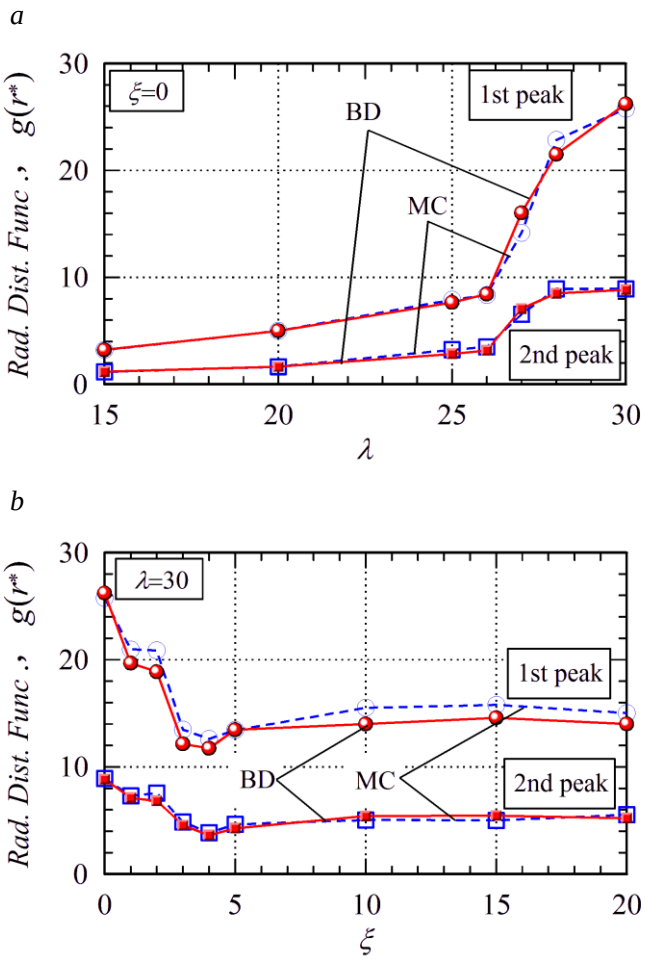

Fig. 6.8 Dependence of the first and second peak of the radial distribution function on (a) the magnetic particle-particle interaction strength λ and (b) the magnetic particle-field interaction strength ξ.

It is seen from Fig. 6.8(a) that the heights of the first and second peaks have a gradual increase with increasing magnetic particle-particle interaction strength λ until both peaks begin to increase more steeply in the region around $\lambda \simeq 26$. These characteristics are in significantly good agreement with results from the Monte Carlo simulations that are also shown. The steep increase in the height of each peak arises from the formation of the closely-packed clusters shown in Fig. 6.4(b). This type of regime change in the internal structure of particle aggregates has already been discussed in Chapter 4 in regard to a Monte Carlo simulation for a suspension composed of magnetic solid cubic particles. An increase in the value of the first peak implies that neighboring particles tend to combine with each other in perfect face-to-face contact to form a cluster and the increase in the second peak implies the expansion of the closely-packed clusters. As previously discussed, the closely-packed clusters shown in Fig. 6.4(b) are transformed into wall-like clusters with increasing magnetic particle-field interaction strength ξ. This regime change in the aggregate structures is also supported by the characteristics of the first and second peaks of the radial distribution function shown in Fig. 6.8(b). Since stable closely-packed clusters are formed in the system in the absence of a magnetic field, $\xi=0$, it is reasonable that the heights of each peak exhibit the larger values shown in Figs. 6.8(a) and 6.8(b) where $\xi=0$. As the magnetic particle-field interaction strength is increased within the range $0 \lesssim \xi \lesssim 4$, the closely-packed clusters are transformed into wall-like clusters. This leads to a decrease in the value of the two peaks because the wall-like clusters are formed with a weaker face-to-face contact configuration than the closely-packed clusters. For a further increase in the magnetic particle-field interaction strength within the range $4 \lesssim \xi \lesssim 10$, the closely-packed clusters completely collapse and wall-like clusters expand into the whole simulation region, where the neighboring particles in a wall-like cluster are stably combined in an offset face-to-face configuration [7]. This gives rise to the slight increase in both curves with increasing magnetic particle-field interaction strength. In the range of $\xi \gtrsim 10$, the values of each peak remain approximately constant, which implies that the formation of wall-like structures is almost complete at $\xi \simeq 10$. Moreover, it is seen that the results from the current model are in good agreement with the Monte Carlo simulations.

From the above-mentioned characteristics obtained from the radial distribution function in regard to the particle configuration in the aggregates, we may conclude that Brownian dynamics simulations employing our steric layer model are able to give rise to physically reasonable results with sufficient accuracy.

6.7 Conclusion

In the present study, we proposed a new technique for the treatment of steric interactions between cubic particles and showed the validity of this interaction model by performing Brownian dynamics simulations for a 3D system for comparison with the corresponding Monte Carlo simulation for a system in thermodynamic equilibrium. The results that have been obtained here are summarized in the following. In our model, a cubic particle with a uniform steric layer is idealized as a sphere-connected model where three spheres with different diameters are used for constructing the geometry of a cubic particle. Each sphere is coated with a uniform steric layer and the interaction energy is evaluated by a summation of the interaction energy arising from the overlap of the steric layers of all the pairs of spheres belonging to the two particles of interest. From a comparison with the radial distribution function of a corresponding Monte Carlo simulation, the treatment of the steric interaction by the present model gives rise to physically reasonable results with sufficient accuracy. This clearly verifies that for Brownian dynamics simulations, the present steric layer model is a potential technique for expressing the steric interaction energy between cubic particles coated by a uniform repulsive layer.

References

[1] A. M. Schmidt, Thermoresponsive magnetic colloids, Colloid Polym. Sci. 285 (2007) 953-966.

[2] C. S. S. R. Kumar and F. Mohammad, Magnetic nanomaterials for hyperthermia-based therapy and controlled drug delivery, Adv. Drug Delivery Rev. 63 (2011) 789-808.

[3] Y. L. Golovin, S. L. Gribanovsky, D. Y. Golovin, N. L. Klyachko, A. G. Majouga, A. M. Master, S. Marina and A. V. Kabanov, Towards nanomedicines of the future: Remote magneto-mechanical actuation of nanomedicines by alternating magnetic fields, J. Controlled Release 219 (2015) 43-60.

[4] S. Suzuki and A. Satoh, Influence of the cluster formation in a magnetic particle suspension on heat production effect in an alternating magnetic field, Colloid Polym. Sci. 297 (2019) 1265-1273.

[5] Z. Zhao and C. Rinaldi, Magnetization dynamics and energy dissipation of interacting magnetic nanoparticles in alternating magnetic fields with and without a static bias field, J. Phys. Chem. C 122 (2018) 21018-21030.

[6] D. Soto-Aquino and C. Rinaldi, Nonlinear energy dissipation of magnetic nanoparticles in oscillating magnetic fields, J. Magn. Magn. Mater. 393 (2015) 46-55.

[7] A. Satoh, *Modeling of Magnetic Particle Suspensions for Simulations* (CRC Press, Boca Laton, 2017).

[8] B. S. John, A. Stroock and F. A. Escobedo, Cubatic liquid-crystalline behavior in a system of hard cuboids, The Journal of chemical physics, J. Chem. Phys. 120 (2004) 9383-9389.

[9] B. S. John and F. A. Escobedo, Phase behavior of colloidal hard tetragonal parallelepipeds (cuboids): A Monte Carlo simulation study, J. Phys. Chem. B 109 (2005) 23008-23015.

[10] J. G. Donaldson and S. S. Kantrovich, Directional self-assembly of permanently magnetised nanocubes in quasi two dimensional layers, Nanoscale 7 (2015) 3217-3228.

[11] E.S. Pyanzina, A.V. Gudkova, J.G. Donaldson and S.S. Kantrovich, Cluster analysis in systems of magnetic spheres and cubes, J. Magn. Magn. Mater. 431 (2017) 201-204.

[12] J.G. Donaldson, E.S. Pyanzina and S.S. Kantrovich, Nanoparticle shape influences the magnetic response of ferro-colloids, ACS Nano 11 (2017) 8153-8166.

[13] S. Suzuki, A. Satoh and S. Wada, Monte Carlo simulations of magnetic particle suspensions with a simple assessment method for the particle overlap between magnetic spheroids, Mol. Phys. 118 (2019) e1607915.

Chapter 7 Magnetorheological characteristics of a cubic hematite particle suspension by means of Brownian dynamics simulations

7.1 Introduction

As previously mentioned in Chapter 1, the magnetorheological effect is employed in the field of fluid engineering in the design of mechanical devices [1-3] and in past studies, many researchers have addressed a suspension composed of magnetic spherical particles. Nowadays, many researchers are able to synthesize magnetic particles with a variety of geometric shapes which include rod-like, disk-like and cube-like particles [4-8]. The geometrical shape of a magnetic particle has a significant influence on the formation of aggregate structures and therefore a non-spherical particle or non axisymetric particle suspension is expected to exhibit a more complex magnetorheological effect. In a previous study [9], our research group treated a suspension composed of ferromagnetic rod-like particles in order to investigate the relationship between the magnetorheological characteristics and the particle aggregates by means of Monte Carlo and Brownian dynamics simulations. In Monte Carlo simulations, we understood that an increase in the magnetic particle-field interaction strength induces a significant regime change in the aggregate structure of rod-like particles. In the Brownian dynamics simulations, it was clarified that the magnetorheological properties are strongly dependent on the type of aggregate structure formed in the system.

In the case of spherical and rod-like particles, neighboring particles in clusters contact with each other in a point-to-point contact configuration. In contrast, in the case of cubic particles, clusters are formed with a face-to-face configuration between the neighboring particles as shown in the previous Chapters employing Monte Carlo and Brownian dynamics simulations in a system in thermodynamic equilibrium. These studies clearly exemplify that cube-like particle suspensions are expected to have the potential to exhibit different characteristics regarding their magnetorheological properties in comparison with those of spherical or rod-like particles. From the viewpoint of an application in the field of mechanical devices such as dampers and actuators, it is significantly desirable to investigate the dependence of the magnetorheological properties of cubic magnetic particles on the regime of particle aggregates in a flow field.

From this background, in the present study we treat a suspension composed of cubic magnetic particles in a simple shear flow, and investigate the relationship between the magnetorheological properties and the particle aggregates. In the first instance, we discuss the aggregation phenomena of cubic particles in a simple shear flow, and then, we elucidate the dependence of magnetorheological characteristics on the various factors such as the magnetic particle-particle interaction, the magnetic field interaction and the Peclet number. In order to investigate the magnetorheological effect in detail, as will be shown later, the net viscosity is decomposed into three viscosity components.

7.2 Particle model

In the present study, we employ the simple model of cubic hematite particles shown in Fig. 7.1. The hematite cube with side length d, and a magnetic dipole moment $\boldsymbol{m}=m\boldsymbol{n}$ is assumed to be coated by a uniform steric layer with a thickness δ. A simple shear flow is applied in the x-axis direction and a magnetic field $\boldsymbol{H}$ ($H=|\boldsymbol{H}|$) is applied in y-axis direction.

If the position vector of particle i is denoted by $\boldsymbol{r}_i$ and the magnetic moment of particle i is denoted by $\boldsymbol{m}_i=m\boldsymbol{n}_i$, then the magnetic force $\boldsymbol{F}_{ij}^{(m)}$ and torque $\boldsymbol{T}_{ij}^{(m)}$ due to the magnetic interaction of particles i and j and the magnetic torque $\boldsymbol{T}_i^{(H)}$ acting on particle i due to the applied magnetic field are expressed as

$$\boldsymbol{F}_{ij}^{(m)}=-\frac{3\mu_0 m^2}{4\pi d^4}\cdot\frac{1}{(r_{ij}/d)^4}\left[-(\boldsymbol{n}_i\cdot\boldsymbol{n}_j)\boldsymbol{t}_{ij}+5(\boldsymbol{n}_i\cdot\boldsymbol{t}_{ij})(\boldsymbol{n}_j\cdot\boldsymbol{t}_{ij})-\left\{(\boldsymbol{n}_j\cdot\boldsymbol{t}_{ij})\boldsymbol{n}_i+(\boldsymbol{n}_i\cdot\boldsymbol{t}_{ij})\boldsymbol{n}_j\right\}\right] \tag{7.1}$$

$$\boldsymbol{T}_{ij}^{(m)}=\frac{\mu_0 m^2}{4\pi d^3}\cdot\frac{1}{(r_{ij}/d)^3}\left\{3(\boldsymbol{n}_j\cdot\boldsymbol{t}_{ij})\boldsymbol{n}_i\times\boldsymbol{t}_{ij}-\boldsymbol{n}_i\times\boldsymbol{n}_j\right\} \tag{7.2}$$

$$\boldsymbol{T}_i^{(H)}=\mu_0 mH\,\boldsymbol{n}_i\times\boldsymbol{H}/H \tag{7.3}$$

in which, $\boldsymbol{t}_{ij}$ is the unit vector denoting the direction of particle i relative to particle j, expressed as $\boldsymbol{t}_{ij}=\boldsymbol{r}_{ij}/r_{ij}$, where $\boldsymbol{r}_{ij}=\boldsymbol{r}_i-\boldsymbol{r}_j$ and $r_{ij}=|\boldsymbol{r}_{ij}|$. From the non-dimensionalization procedure, we obtain two non-dimensional parameters λ and ξ which imply respectively the strengths of the magnetic particle-particle interaction and the magnetic particle-field interaction. The non-dimensional parameters λ and ξ are expressed as $\lambda=\mu_0 m^2/(4\pi d^3 kT)$ and $\xi=\mu_0 mH/(kT)$, where k is the Boltzmann's constant, T is the absolute temperature of the liquid and μ_0 is the permeability of free space.

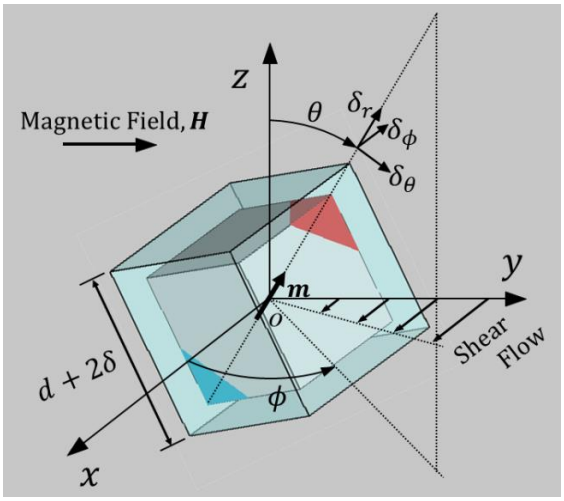

Fig. 7.1 Particle model and the coordinate system.

In order to obtain a more stable dispersion, the particles suspended in a base liquid are generally coated by a repulsive layer such as an electric double layer or steric layer. Molecular dynamics and Brownian dynamics simulations can not be adequately performed unless an expression for the repulsive interaction between particles is known. In Chapter 6, we have proposed a sphere-constituted model in order to consider the repulsive interaction between cubic particles. We have already discussed the repulsive force $\boldsymbol{F}_{ij}^{(V)}$ and torque $\boldsymbol{T}_{ij}^{(V)}$ due to the overlap of the steric layers in Chapter 6, therefore in this chapter omit the equations for the repulsive force and torque. It is noted that the strength of the repulsive interaction is characterized by the non-dimensional parameter $\lambda_V=\pi n_s d_0^2/2$, where n_s is the number of surfactant molecules per unit area on the surface of a spherical particle and d_0 is the diameter of a representative spherical particle and in the case of the present study, the side length d of the cubic particle is employed.

7.3 Brownian dynamics simulation

In the present study, the simulated cubic particles move with transrational and rotational Brownian motion in a simple shear flow $\boldsymbol{U}$ which is characterized by the angular velocity vector $\boldsymbol{\Omega}$. The angular velocity vector $\boldsymbol{\Omega}$ and the simple shear flow $\boldsymbol{U}$ are expressed as $\boldsymbol{\Omega}$= (0, 0, $-\dot{\gamma}/2$) and $\boldsymbol{U}$ =($\dot{\gamma} y$, 0, 0) with the shear rate $\dot{\gamma}$. If the position vector of a cubic particle is $\boldsymbol{r}$ and the unit vector of the magnetic moment $\boldsymbol{m}=m\boldsymbol{n}$ is $\boldsymbol{n}$, then the equations of translational and rotational motion are expressed as the following expressions. It is noted that the components normal to the magnetic moment direction are represented by the subscript $\perp$, and the components parallel to the magnetic moment direction are represented by the subscript | |.

$$\boldsymbol{r}(t+\Delta t)=\boldsymbol{r}(t)+\boldsymbol{U}\Delta t+\frac{1}{kT}D_{cube}^{T}\boldsymbol{F}^{P}(t)\Delta t+\Delta\boldsymbol{r}^{B} \tag{7.4}$$

$$\boldsymbol{n}(t+\Delta t)=\boldsymbol{n}(t)+\boldsymbol{\Omega}_{\perp}\times\boldsymbol{n}\Delta t+\frac{1}{kT}D_{cube}^{R}\boldsymbol{T}_{\perp}^{P}(t)\times\boldsymbol{n}\Delta t+\Delta\phi_{\perp 1}^{B}\boldsymbol{e}_{\perp 1}(t)+\Delta\phi_{\perp 2}^{B}\boldsymbol{e}_{\perp 2}(t) \tag{7.5}$$

$$\boldsymbol{n}_{\perp}(t+\Delta t)=\boldsymbol{n}_{\perp}(t)+\boldsymbol{\Omega}_{\parallel}\times\boldsymbol{n}_{\perp}\Delta t+\frac{1}{kT}D_{cube}^{R}\boldsymbol{T}_{\parallel}^{P}(t)\times\boldsymbol{n}_{\perp}\Delta t+\Delta\phi_{\parallel}^{B}\boldsymbol{n}\times\boldsymbol{n}_{\perp} \tag{7.6}$$

in which, Δt is the time interval. $\boldsymbol{F}^{P}$ is the magnetic force acting on the cubic particle, $\boldsymbol{T}_{\perp}^{P}$ and $\boldsymbol{T}_{\parallel}^{P}$ are the torques which correspond to components perpendicular and parallel to the direction of the magnetic moment axis. $\boldsymbol{e}_{\perp 1}(t)$ and $\boldsymbol{e}_{\perp 2}(t)$ are orthogonal unit vectors normal to the magnetic moment, and D_{cube}^{T} and D_{cube}^{R} are the translational and rotational diffusion coefficients of the cubic particle. $\Delta\boldsymbol{r}^{B}$, $\Delta\phi_{\perp 1}^{B}$, $\Delta\phi_{\perp 2}^{B}$ and $\Delta\phi_{\parallel}^{B}$ are the random displacements inducing the translational and rotational Brownian motion.

From the analysis of the flow field around a cube in a simple shear flow with a sufficiently low Reynolds number undertaken with the commercial software ANSYS CFX, we have confirmed that the force acting on a cube can be regarded as the force acting on a sphere with the mean diameter d_{mean} of the inscribed and the circumscribed sphere of the cube. That is, even in the situation of a simple shear flow, we have confirmed that the friction and diffusion coefficients of a cube can be expressed by the friction and diffusion coefficients of a sphere with the mean diameter d_{mean}. It is noted that this approximation is not valid for simulations under a simple shear flow with a Reynolds number larger than unity.

The present physical phenomenon is governed by the four non-dimensional parameters λ, ξ, λ_V and Pe, where $Pe = D_{cube}^{R}/\dot{\gamma}$ is the Peclet number and implies the strength of the shear flow. In order to discuss the magnetorheological characteristics in detail, the net viscosity $\eta_{yx}^{total}=\eta_{yx}^{F}+\eta_{yx}^{TH}+\eta_{yx}^{FT}$ is decomposed into three viscosity components η_{yx}^{F}, η_{yx}^{TH} and η_{yx}^{FT}. These components imply that η_{yx}^{TH} is the contribution to the net viscosity from the torque arising from the magnetic particle-field interaction, and η_{yx}^{F} and η_{yx}^{FT} are the contributions to the net viscosity from the force and the torque arising from the magnetic particle-particle interaction. Moreover, the net viscosity η_{yx}^{total} is defined as $\eta_{yx}^{total}=\tau_{yx}^{total}/\dot{\gamma}$ with the shear stress τ_{yx}^{total}. The total shear stress τ_{yx}^{total} is expressed as the sum of three components

$$\tau_{yx}^{total} = -n_0\left\langle \sum_{i=1}^{N}\sum_{\substack{j=1\\(j>i)}}^{N} y_{ij}F_{ijx}^{(m)} \right\rangle + \frac{n_0}{2}\left\langle \sum_{i=1}^{N} T_{iz}^{(H)} \right\rangle + \frac{n_0}{2}\left\langle \sum_{i=1}^{N}\sum_{\substack{j=1\\(j>i)}}^{N} T_{ijz}^{(m)} \right\rangle \tag{7.7}$$

in which, n_0 is the particle number density, N is the number of particles, y_{ij} is the y-component of the relative position vector $\boldsymbol{r}_{ij}$, $F_{ijx}^{(m)}$ is the x-component of the magnetic force $\boldsymbol{F}_{ij}^{(m)}$, $T_{iz}^{(H)}$ is the z-component of the magnetic torque $\boldsymbol{T}_{i}^{(H)}$ and $T_{ijz}^{(m)}$ is the z-component of the magnetic torque $\boldsymbol{T}_{ij}^{(m)}$. In the results section, the value of each viscosity is divided by the viscosity η of the base liquid and the volumetric fraction ϕ_V. The viscosity components η_{yx}^{F}, η_{yx}^{TH} and η_{yx}^{FT} are calculated by using the shear stress of each term in Eq.(7.7).

7.4 Results and discussion

7.4.1 Parameters for simulations

Unless specifically noted, Brownian dynamics simulations were performed by employing the following values. The volumetric fraction of cubic particles, ϕ_V, is set as ϕ_V =0.05, the number of particles in the system, N, is N=490, the cutoff distance $r_{coff}^{*}=r_{coff}/d$ of the magnetic particle-particle interaction between particles is r_{coff}^{*}=10, the thickness $\delta^{*}=\delta/d$ of the steric layer δ^{*}=0.15, the non-dimensional parameter λ_V is λ_V =150. The other non-dimensional parameters λ, ξ and Pe are set in a range of λ=10~50, ξ=1~20, Pe=1. We employed the Lees-Edwards boundary condition. A simple shear flow and a magnetic field are applied in the x-axis and y-axis direction, respectively. The size of the simulation box (L_x, L_y, L_z) is set as L_x= 2L_y and L_x=L_z. Moreover, the time interval Δt^{*} is Δt^{*}=0.00002, and the total number of time steps per simulation run is N_{timemx}=5,000,000. We employed the final 50% of the simulation data for the averaging procedure. It is noted that we have confirmed that aggregate structures are stably formed in the system within the initial 50%.

From the previous studies in Chapters 4 and 6, it has been clarified that cubic particles aggregate to form the closely-packed clusters shown in Fig. 7.2(a), and the closely-packed clusters are transformed into the chain-like clusters shown in Fig. 7.2(b) and wall-like clusters shown in Fig. 7.2(c) may arise due to the influence of the magnetic field. Hence, in the present study, we discuss the characteristics of the magnetorheological effects arising from the regime change in the internal structure of the particle aggregates. In the sections 7.4.2 and 7.4.3, we will focus on results for the case of λ=30 and λ=50, and Pe=1, for which a regime change significantly occurs.

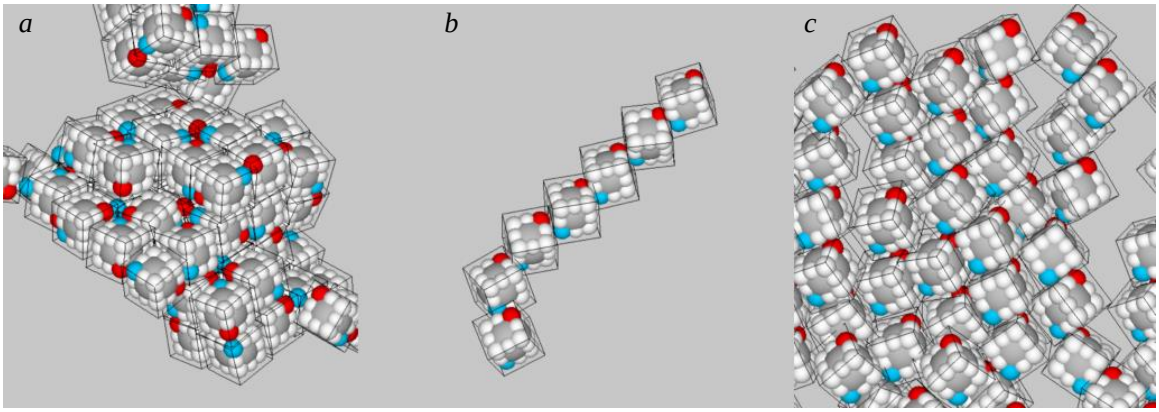

Fig. 7.2 Types of clusters formed in the system: (a) closely-packed clusters, (b) chain-like clusters and (c) wall-like clusters.

7.4.2 Influence of the magnetic particle-field interaction strength

Figure 7.3 shows the snapshots for the relatively large magnetic particle-particle interaction strength λ=30 and Peclet number *Pe*=1 where Figures 7.3(a) and 7.3(b) are for the cases of the external magnetic particle-field interaction strength ξ=10 and ξ=20. It is noted that a smaller snapshot on the right-hand side shows only particles located on a certain *xy*-plane in order to discern the internal structure more clearly. Figure 7.4 shows the characteristics of the orientational distribution function. For the case of ξ=1, cubic particles aggregate to form the closely-packed clusters with a perfect face-to-face contact configuration, as shown in Fig. 7.2(a). For the case of ξ=10 shown in Fig. 7.3(a), the closely-packed clusters are transformed into chain-like clusters inclined in the direction of the flow field. The orientational characteristics of the magnetic moments of the constituent particles in the chain-like clusters are quantitatively evaluated by the orientational distribution function shown in Fig. 7.4(a). It is seen from Fig. 7.4(a) that the peak appears in the region (θ, ϕ)≃(90°, 65°) and is a characteristic that implies that the magnetic moments of the constituent particles incline in the flow field direction and away from the magnetic field direction.

For the case of ξ=20 shown in Fig. 7.3(b), the magnetic moments of each particle are strongly restricted to the magnetic field direction, and wall-like aggregate structures are formed in the system. From the results shown in Fig. 7.4(b), it is seen that the peak has become stronger and the peak position is shifted toward the region of (θ, ϕ)=(90°, 90°) with increasing magnetic particle-field interaction strength. This is because the magnetic moments of the constituent particles are significantly restricted to the magnetic field direction due to the formation of the wall-like clusters. In the following, we will discuss the internal structure of chain-like and wall-like clusters in more detail.

Under shear flow conditions, in the situation of a strong magnetic field, chain-like clusters formed in the system may exhibit the two different particle configurations shown in Fig. 7.5 where Fig. 7.5(a) shows a chain-like cluster (*cluster* 1) inclined from the magnetic field direction into the flow field direction and Fig. 7.5(b) shows a chain-like cluster (*cluster* 2) inclined from the magnetic field direction toward the opposite direction to the flow field. It is seen from the snapshots on the right-hand side of Figs. 7.3(a) and 7.3(b) that chain-like clusters based on the particle configurations of the *cluster* 1 and *cluster* 2 are simultaneously formed in the system. In particular, it is seen from the detail of the snapshot on the right-hand side of Fig. 7.3(b) that wall-like clusters are based on the chain-like clusters with the particle configuration of *cluster* 2. The formation mechanism for *cluster* 1 and *cluster* 2 may be explained as follows. In the situation of a relatively weak magnetic field, as shown in Fig. 7.3(a), chain-like clusters tend to incline in the flow field direction from the magnetic field direction due to the influence of the shear flow. In the situation of a strong magnetic field, we may expect the formation of chain-like clusters where the orientation of the magnetic moments of the particles is strongly restricted in the magnetic field direction, as shown in Fig. 7.5. The resultant

magnetic force arising from the magnetic particle-particle interaction between the constituent particles in the *cluster* 1 shown in Fig. 7.5(a) acts in the opposite direction to the shear flow. In contrast, in the case of *cluster* 2 shown in Fig. 7.5(b), the resultant magnetic force acts in the same direction to the shear flow. Hence, when the orientation of the magnetic moments of particles is strongly restricted to the magnetic field direction, chain-like clusters with the particle configuration of the *cluster* 2 are stably formed in the system. We will discuss the dependence of the magnetorheological properties on the internal structure of particle aggregates in the following section.

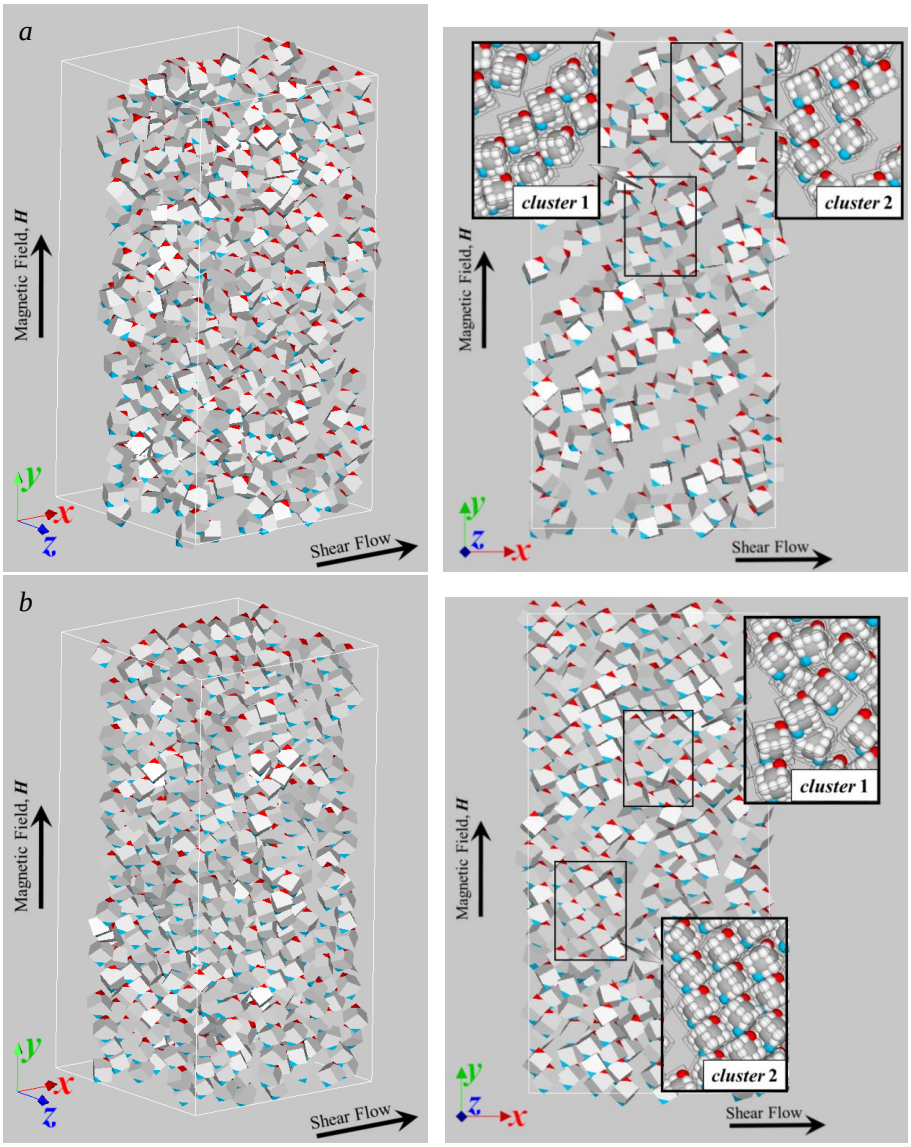

Fig. 7.3 Dependence of the aggregate structures on the magnetic particle-field interaction strength of (a) ξ=10 and (b) ξ=20 in the situation of a magnetic particle-particle interaction strength λ=30 and a Peclet number *Pe*=1.

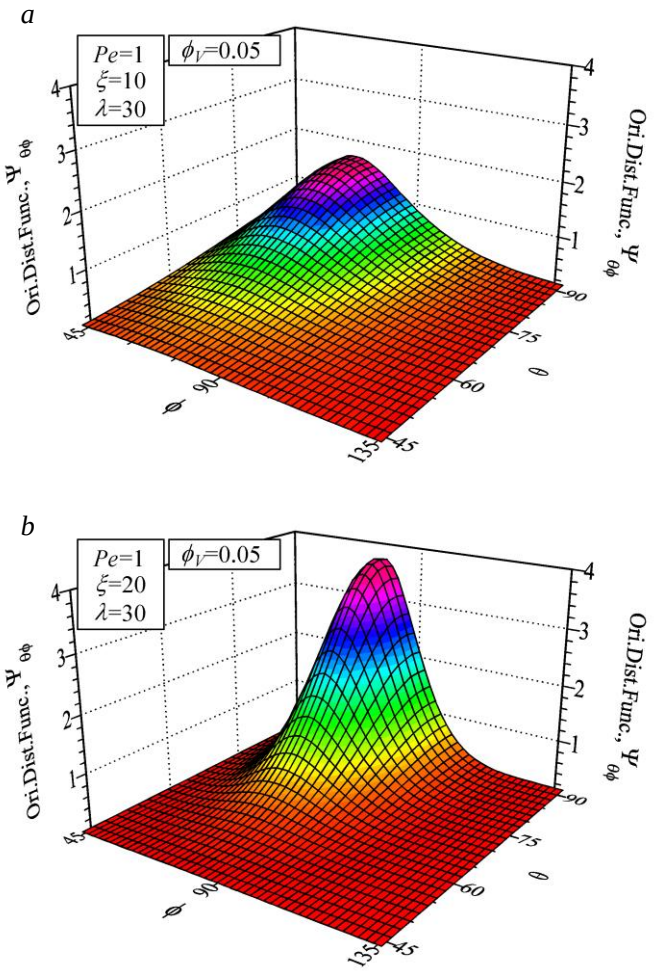

Fig. 7.4 Dependence of the orientational distribution function on the magnetic particle-field interaction strength for ξ=10 and (b) ξ=20 in the situation of the magnetic particle-particle interaction strength λ=30 and the Peclet number *Pe*=1.

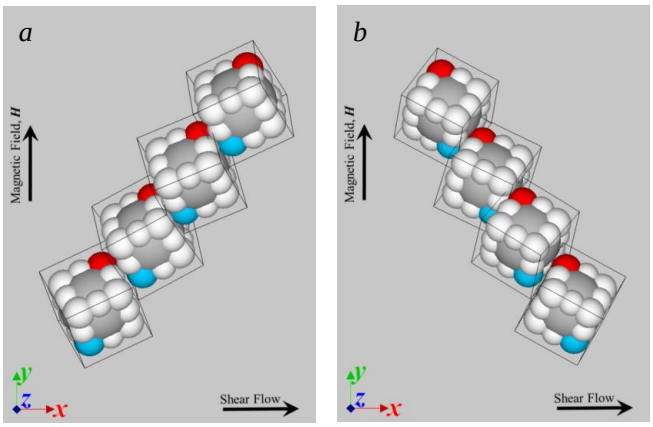

Fig. 7.5 Two chain-like clusters, (a) *cluster* 1 and (b) *cluster* 2, in the situation of a strong magnetic field.

7.4.3 The relationship between magnetorheological effects and particle aggregates

In this section, we discuss the effect of a difference in the internal structure of particle aggregates described in section 7.4.2 on the magnetorheological characteristics. Figure 7.6 shows the dependence of the viscosity on the magnetic particle-field interaction strength ξ for the case of a weak shear flow Pe=1: Figs. 7.6(a), 7.6(b) and 7.6(c) show respectively the net viscosity η_{yx}^{total}, the viscosity component η_{yx}^{TH}, and in combination the viscosity components η_{yx}^{F} and η_{yx}^{FT}. Each figure shows results for the three cases of magnetic particle-particle interaction strength, λ=10, λ=30 and λ=50.

First, we discuss results of the net viscosity shown in Fig. 7.6(a). For the case of λ=30 and λ=50 where there are significant aggregate structures formed in the system, it is seen that all the curves tend to increase with the magnetic particle-field interaction strength until around $\xi \approx 10$. However, the curve for λ=50 then continues to increase with increasing magnetic particle-field interaction strength whilst the curve for λ=30 starts to decrease significantly in the range of $\xi \gtrapprox 10$. The characteristic of the curve for λ=30 may imply a regime change in the aggregate structure, as shown in Fig. 7.3. That is, the net viscosity η_{yx}^{total} increases until around $\xi \lessapprox 10$ where the chain-like clusters that trend to incline from the magnetic field direction toward the flow field direction are formed in the system, but it significantly decreases in the range of $\xi \gtrapprox 10$ where wall-like clusters are then formed in the system. In contrast, for the case of λ=50, particle aggregates do not transform into wall-like clusters due to the influence of the relatively large magnetic particle-particle interaction strength, even in the case of the strong magnetic particle-field interaction strength $10 \lessapprox \xi \lessapprox 20$.
That is, chain-like clusters that incline in the flow field direction are predominately formed in the system, which leads to an increase in the net viscosity. However, in the range of $\xi \gtrapprox 20$, it may be expected that a regime change occurs, and therefore the curve for λ=50 is expected to decrease with increasing magnetic field.

Next, we focus on the three viscosity components η_{yx}^{F}, η_{yx}^{TH} and η_{yx}^{FT} in order to elucidate the dependence of the internal structures of the clusters on the viscosity more clearly. In the following discussion, we focus only on the case of λ=30 where a significant regime change in the particle aggregates occurs due to the influence of the applied magnetic field.

We first discuss the viscosity component η_{yx}^{TH} shown in Fig. 7.6(b). For the case of λ=30, it is seen from Fig. 7.6(b) that the viscosity component η_{yx}^{TH} shows a significantly small value in the range of $\xi \lessapprox 3$. This arises because the effect of strength of the magnetic particle-particle interaction is more dominant than that of the magnetic particle-field interaction. That is, the torque due to the influence of the weak magnetic field does not significantly affect the closely-packed clusters shown in Fig. 7.2(a). However, as the magnetic field is increased with $3 \lessapprox \xi \lessapprox 10$, the closely-packed clusters collapse and are transformed into the chain-like clusters shown in Fig. 7.3(a). The chain-like clusters tend to incline towards the magnetic field direction with increasing magnetic particle-field

interaction strength, which leads to a large resistance to the shear flow. Therefore, in the range of $3 \lesssim \xi \lesssim 10$, the viscosity component η_{yx}^{TH} increase with the magnetic particle-field interaction strength. As the interaction strength is further increased with $10 \lesssim \xi \lesssim 20$, the aggregate structures are completely transformed into the wall-like clusters, as shown in Fig. 7.3(b). In the region of $10 \lesssim \xi \lesssim 20$, since there is no significant change in the internal structures of the aggregates, the viscosity component η_{yx}^{TH} tends to an asymptotic limit. From the above characteristics, we understand that the viscosity component η_{yx}^{TH} significantly increases during the regime change from closely-packed clusters into chain-like clusters that occurs due to the influence of the magnetic field.

We next discuss results of the viscosity component η_{yx}^{F} shown in Fig. 7.6(c). It is seen from Fig. 7.6(c) that the curve for λ=30 increases with increasing magnetic particle-field interaction strength in the region of $1 \lesssim \xi \lesssim 5$. However, in the region of $10 \lesssim \xi \lesssim 20$, the viscosity component η_{yx}^{F} decreases with the magnetic particle-field interaction strength, and then acquires a negative value. This characteristic arises from a regime change caused by the external magnetic field. That is, if the chain-like clusters as shown in Fig. 7.5(a) are predominately formed in the system, the resulting magnetic force acts in the opposite direction to the shear flow, which leads to positive values of the viscosity component η_{yx}^{F}. In contrast, if the chain-like clusters as shown in Fig. 7.5(b) are predominately formed in the system, the resulting magnetic force acts in the same direction as the shear flow, and therefore the value of the viscosity component η_{yx}^{F} acquires negative values. Because wall-like clusters are based on the particle configuration of *cluster* 2 shown in Fig. 7.5(b), the curve for λ=30 tends to decrease in the range of $10 \lesssim \xi \lesssim 20$ where the wall-like clusters are predominately formed in the system.

We finally discuss the viscosity component η_{yx}^{FT} that is also shown in Fig. 7.6(c). For the case of λ=30, it is seen that the curve of the viscosity component η_{yx}^{FT} exhibits the opposite characteristic to that of the viscosity component η_{yx}^{F}. That is, in the region of $3 \lesssim \xi \lesssim 5$ where the chain-like clusters based on the particle configuration of *cluster* 1 are predominately formed in the system, the viscosity component η_{yx}^{FT} decreases and tends to negative values. On the other hand, in the range of $10 \lesssim \xi \lesssim 20$ where the aggregate structures are transformed into the wall-like clusters, the viscosity component η_{yx}^{FT} increases and tends to positive values. These features may be explained as follows. In the case that the aggregate structures based on the *cluster* 1 are predominately formed in the system, the magnetic torque functions to accelerate the flow field, which gives rise to negative values of η_{yx}^{FT}. In contrast, in the case that wall-like clusters with a particle arrangement of *cluster* 2 are formed, the magnetic moment of each particle is restricted to the magnetic field direction due to the influence of the magnetic torque acting between neighboring particles. Hence, the magnetic torque gives rise to a resistance to the flow field, and therefore the viscosity component η_{yx}^{FT} tends to positive values. From these characteristics, we understand that the viscosity of a cubic particle suspension exhibits complex dependence on the main clusters formed in the system. Moreover, we

suggest that a cubic magnetic particle suspension may exhibit negative magnetorheological characteristics under certain conditions.

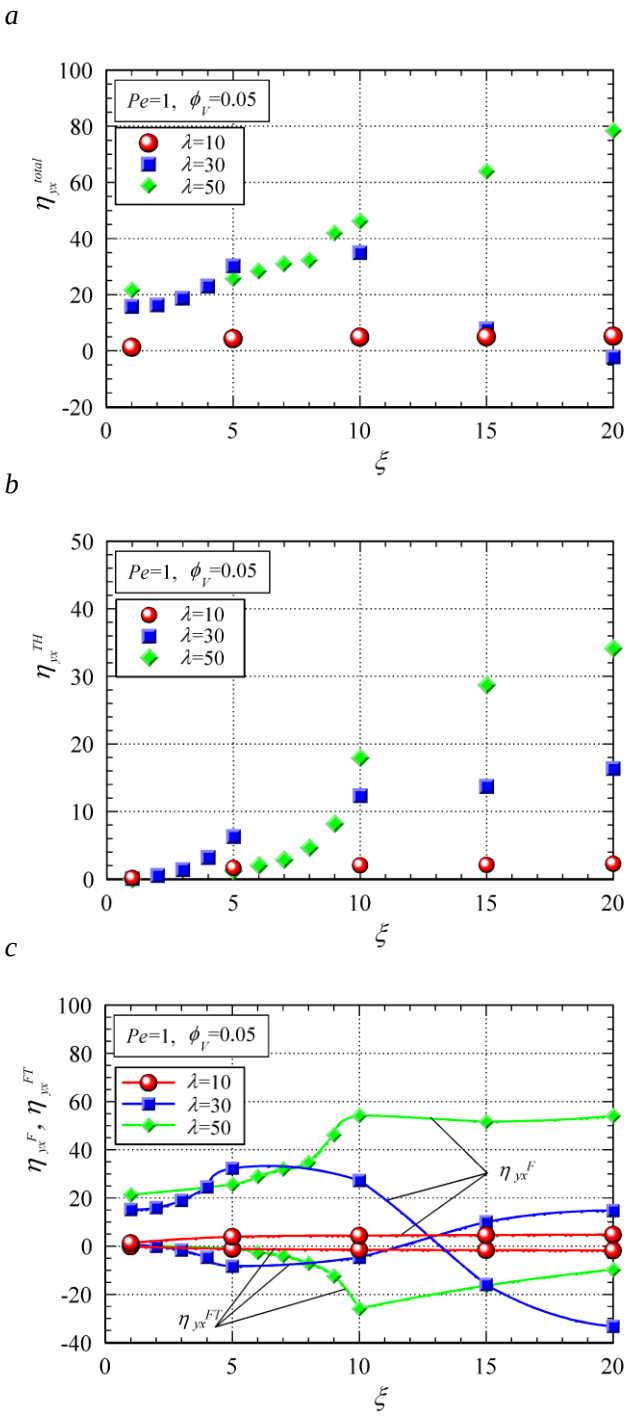

Fig. 7.6 Dependence of (a) the net viscosity η_{yx}^{total}, and the single (b) η_{yx}^{TH} and the combined (c) η_{yx}^{F} and η_{yx}^{FT} viscosity components on the magnetic particle-field interaction strength ξ for the case Pe=1.

7.5 Conclusion

In the present study, we have addressed a suspension composed of cubic hematite particles in a simple shear flow, and investigated the relationship between the magnetorheological characteristics and aggregate structures by means of Brownian dynamics simulations. Brownian dynamics simulations have been performed for the various cases of the magnetic particle-particle interaction strength, the magnetic particle-field interaction strength and the shear rate and where an external magnetic field was applied in a direction normal to the simple shear flow. The main results obtained here are summarized as follows. In a weak applied magnetic field, if the magnetic particle-particle interaction strength is sufficiently strong, the cubic particles tend to aggregate to form closely-packed clusters. As the magnetic particle-field interaction strength is increased, the closely-packed clusters are transformed into chain-like clusters that tend to incline from the magnetic field direction towards the flow field direction. As the magnetic field is further increased, the aggregate structures grow into wall-like structures where the orientations of the magnetic moments of constituent particles are strongly restricted to the magnetic field direction. If the predominant clusters formed in the system are chain-like clusters inclined in the flow field direction, the net viscosity is increased because the chain-like clusters give rise to a large resistance to the flow field. However, if the wall-like clusters are the predominant clusters, a force that tends to accelerate the flow field arises due to the characteristic of the particle arrangement in the wall-like clusters, and therefore the net viscosity is decreased. From these results, we conclude that the viscosity of a cubic particle suspension exhibits complex dependence on the regime of particle aggregates that may arise in the system such as the closely-packed, chain-like and the wall-like clusters. Moreover, we suggest that a cubic magnetic particle suspension may have negative magnetorheological characteristics under certain conditions.

References

[1] W. A. Bullough, (ed.), *Electro-Rheological Fluids, Magneto-Rheological Suspensions and Associated Technology* (World Scientific, Singapore, 1996).

[2] N. M. Wereley, (ed.), *Magnetorheology: Advances and Applications* (Royal Society of Chemistry, London. 2013).

[3] R. E. Rosensweig, *Ferrohydrodynamics* (Cambridge University Press, Cambridge, 1985).

[4] E. Matijevic and P. Scheiner, Ferric hydrous oxide sols: III. Preparation of uniform particles by hydrolysis of Fe(III)-chloride, -nitrate, and -perchlorate solutions, J. Colloid Interface Sci. 63 (1978) 509-524.

[5] M. Ozaki, S. Kratohvil and E. Matijević, Formation of monodispersed spindle-type hematite particles, J. Colloid Interface Sci. 102 (1984) 146-151.

[6] T. Sugimoto, H. Itoh and T. Mochida, Shape control of monodisperse hematite particles by organic additives in the gel-sol system, J. Colloid Interface Sci. 205 (1998) 42-52.

[7] M. Aoshima, M. Ozaki and A. Satoh, Structural analysis of self-assembled lattice structures composed of cubic hematite particles, J. Phys. Chem. C 116 (2012) 17862-17871.

[8] T. Sugimoto and K. Sakata, Preparation of monodisperse pseudocubic α-Fe2O3 particles from condensed ferric hydroxide gel, J. Colloid Interface Sci. 152 (1992) 587-590.

[9] K. Okada and A. Satoh, Regime of aggregate structures and magneto-rheological characteristics of a magnetic rod-like particle suspension: Monte Carlo and Brownian dynamics simulations, J. Magn. Magn. Mater. 437 (2017) 29-41.

Chapter 8 Summary and concluding remarks

8.1 Summary of the present paper

In the present paper, we addressed a suspension composed of magnetic particles with a cubic geometry and investigated the dependence of the internal structure of particle aggregates and rheology characteristics on the various factors such as the magnetic particle-particle interaction strength, the magnetic particle-field interaction strength and the volumetric fraction of particles. Monte Carlo simulations and Brownian dynamics simulations have been employed as simulation methods. The present paper consists of three pillars: (1) basic research for the application to surface modification technology, (2) the development of a Brownian dynamics simulation technique for a cubic particle suspension, and (3) basic research for the application to magnetically-controlled fluid devices. The main appealing points of the present paper are as follows:

1. We have investigated the phase change in the aggregate structures of magnetic cubic particles on a material surface by means of Monte Carlo simulations.
2. We have estimated the translational and rotational diffusion coefficients of a cube particle that are required for developing a new Brownian dynamics simulation method.
3. We have elucidated the coupling characteristics of the translational and the rotational motion of a cube in the situation of the Reynolds number being sufficiently smaller than unity.
4. We have proposed a new steric layer model, which is expected to obtain results with a reasonably high degree of accuracy with less computation time than other researchers' models.
5. We have developed a Brownian dynamics simulation technique for a suspension composed of cubic particles, which has not been presented until the present.
6. We have elucidated the relationship between magnetorheological characteristics and aggregate structures of a cubic particle suspension by means of our Brownian dynamics simulation method.

8.1.1 Summary of Chapter 2

We investigated the aggregate structures of a suspension composed of cubic hematite particles by means of Monte Carlo simulations. From the viewpoint of application in the field of surface modification technology, we have treated a quasi-2D suspension in thermodynamic equilibrium. As the magnetic particle-particle interaction strength is increased, the effects of the thermal energy are reduced and particles tend to aggregate together. Such aggregates of cubic particles are designated as closely-packed clusters. An external magnetic field tends to enhance the formation of elongated clusters in the direction of the magnetic field. Our simulations indicate that larger closely-packed clusters are formed with an increasing volumetric fraction of particles. However, the internal

structure of the closely-packed clusters is not found to be significantly influenced by a change in the volumetric fraction.

8.1.2 Summary of Chapter 3

In Chapter 2, we focused on the situation where half the ensemble particles have a magnetic moment pointing in the upward diagonal direction relative to the material surface whilst the others point in the downward diagonal direction. We have expanded the study in Chapter 2 to consider a variety of situations of ensemble ratios in regard to the number of particles with upward and downward magnetic moment directions relative to the material surface. From quasi-2D Monte Carlo simulations, we understand that the orientation ratio of the cubic particles has a significant effect on the regime of the particle aggregates. That is, as the composition ratio is decreased, the size of closely-packed aggregates becomes smaller, and the formation of thin linear clusters tend to be preferred in the situation of a strong magnetic field. Furthermore, a decrease in the composition ratio tends to dull the occurrence of a regime change in the particle aggregates with a change in the magnetic particle-particle interaction strength. Hence, the composition ratio may be used as a technique for controlling the cluster formation and the size of closely-packed clusters of cubic hematite particles, even in the situation of a strong magnetic particle-field interaction strength.

8.1.3 Summary of Chapter 4

In Chapters 2 and 3, from the viewpoint of a surface modification technology, we considered a quasi-2D suspension in thermodynamic equilibrium in order to investigate the characteristics of magnetic cubic particles on a material surface. In Chapter 4, we have expanded our investigation to include 3D Monte Carlo simulations of a suspension of cubic hematite particles in order to discuss a regime change in the structure of the particle aggregates. If the magnetic particle-particle interaction strength is sufficiently large, closely-packed clusters are formed by a repetition and expansion of a basic cluster unit composed of 8 particles, which may be a strongly preferred configuration as it gives rise to a minimum energy. As the magnetic particle-particle interaction strength is increased, closely-packed clusters tend to collapse and transform into wall-like clusters that align along the magnetic field direction. This is because the magnetic moment of each particle has a strong tendency to incline towards the magnetic field direction in a strong magnetic field. An increase in the volumetric fraction of particles induces a regime change from thick chain-like clusters to the formation of wall-like clusters.

8.1.4 Summary of Chapter 5

We analyzed the flow field around a cube in a Stokes flow regime in order to estimate the diffusion or friction coefficients of cube-like particles that are required in order to conduct Brownian

dynamics simulations for a cubic particle suspension. In the situation of a uniform flow field with a Reynolds number sufficiently smaller than unity, the resulting force acts on the cube only in the flow field direction, and the resulting torque acting on the cube may be regarded as negligible. In the situation of a rotational flow field with a sufficiently low Reynolds number, the resulting torque acts on the cube only in the direction of the angular velocity of the rotational flow field, and the resulting force acting on the cube is negligible. These characteristics are similar to those for the case of a sphere in a Stokes flow. From these results, we may conclude that the diffusion or friction coefficients of cubic particles may be expressed by introducing a correction factor to those applicable for spherical particles.

8.1.5 Summary of Chapter 6

We propose a new repulsive layer model for treating the interaction between the steric layers of coated cubic particles. This approach is an effective technique applicable to particle-based simulations such as a Brownian dynamics simulation of a suspension composed of cubic particles. 3D Brownian dynamics simulations employing this repulsive interaction model have been performed in order to investigate the equilibrium aggregate structures of a suspension composed of cubic hematite particles. From a comparison with the radial distribution function of a corresponding Monte Carlo simulation, the present model treatment of the steric interaction is found to give rise to physically reasonable results with sufficient accuracy. Hence, we have verified that the present steric layer model is a potential technique for expressing the steric interaction energy between cubic particles coated by a uniform repulsive layer.

8.1.6 Summary of Chapter 7

We treated a suspension composed of magnetic cubic particles in a simple shear flow field by means of Brownian dynamics simulations in order to investigate the dependence of the magnetorheological characteristics on the cluster formation. We assumed that an external magnetic field is applied in the direction normal to the simple shear flow. In a weak magnetic particle-field interaction strength, the cubic particles tend to aggregate to form closely-packed clusters if the magnetic particle-particle interaction strength is sufficiently large. As the magnetic particle-field interaction strength is increased, the closely-packed clusters are transformed into chain-like clusters that tend to incline from the magnetic field direction towards the flow field direction. The chain-like clusters give rise to a large resistance to the flow field, and therefore, the net viscosity is increased. As the magnetic field strength is further increased, wall-like clusters are formed in the system. In this situation, a force to accelerate the flow field arises due to the characteristic of the particle arrangement within the wall-like clusters and this tends to induce a decrease in the net viscosity. Hence, we understand that the magnetorheological properties significantly depend on the internal structure of the particle aggregates formed in the system.

8.2 Topics for future research

In order to develop a Brownian dynamics method for a cubic particle suspension, it is required to solve the problem for the modeling of the repulsive layer of the coated cubic particles and clarify the relationship between the components of the friction or diffusion tensor. In the present paper, we have approached such problems and developed a Brownian dynamics simulation for a cubic particle suspension. Finally, based on the results obtained in the present paper, the future research direction of cubic magnetic particle suspensions is suggested.

8.2.1 Brownian dynamics simulations on the behavior of cubic hematite particles on a material surface in time-dependent magnetic fields

In the previous Chapters 2 and 3, we treated a suspension composed of cubic hematite particles on a material surface, and investigated a regime change in the aggregate structure by means of Monte Carlo simulations. In order to control the aggregate structure of cubic particles more efficiently, investigating the effect of time-dependent magnetic fields may be a desirable path to follow the investigation of the uniform magnetic field. It is possible to investigate the behavior of a cubic magnetic suspension in a time-changing magnetic field, such as an alternating magnetic field or a rotating magnetic field, by employing the Brownian dynamics method as a simulation tool. Petrichenko et al., [1] have conducted an experimental study regarding the swarming of hematite cubes in a rotating magnetic field, where they investigated the dependence of swarm size and angular velocity on the rotating magnetic field strength and frequency. Further simulation studies are required to elucidate more clearly the mechanism for the formation of particle aggregates in a rotating magnetic field.

8.2.2 Brownian dynamics simulations on the heat production effect of a cubic magnetic particle suspension in an alternating and rotating magnetic field

It is well established that magnetic particles exhibit heat generation characteristics in an alternating magnetic field and a rotating magnetic field. Therefore, a variety of studies regarding the potential application to a magnetic hyperthermia treatment have been actively conducted [2-4]. Hyperthermia treatment is a medical therapy for killing tumor or cancer cells by means of the heating effect of magnetic particles. There are several simulation studies that investigate the relationship between the characteristics of the heating effect and the aggregate structures of magnetic particles in the situation of an alternating magnetic field [5-7]. However, since these studies treat a suspension composed of spherical particles, it may be desirable to further study suspensions of non-spherical particles and non-axisymetric particles such as rod-like, disk-like and cube-like particles. If we employ the Brownian dynamics method for a cubic particle suspension that has been

developed in this paper, we then have the potential to investigate the relationship between the heating effects and particle aggregates in an alternating and rotating magnetic field. It has been clarified that the aggregate structures formed in the system depend on the shape of the magnetic particles, and therefore it may be possible to expand on the knowledge of heat generation characteristics obtained from spherical particles by investigating suspensions of non-spherical particles.

8.2.3 Developing new simulation methods for a cubic particle suspension

It is not possible to consider Hydrodynamic interactions with the Brownian dynamics simulation techniques developed in this paper. In order to obtain more accurate simulation results, it may be required to establish more advanced simulation techniques where hydrodynamic interactions are taken into consideration. There are several micro-analysis simulation methods that can solve both the particle motion and the ambient flow field simultaneously that include the Lattice Boltzmann method [8-10], the multi-particle collision dynamics method [11, 12] and the dissipative particle dynamics method [13, 14]. In the case of a three-dimensional system, the lattice Boltzmann method requires a significantly high computational cost, and therefore it may be necessary to develop a multi-particle collision dynamics method in order to investigate a cubic particle suspension.

References

[1] O. Petrichenko, G. Kitenbergs, M. Brics, E. Duboids, R. Perzynski and A. Cēbers, Swarming of micron-sized hematite cubes in a rotating magnetic field - Experiments, J. Magn. Magn. Mater. 500 (2020) 166404.

[2] A. M. Schmidt, Thermoresponsive magnetic colloids, Colloid Polym. Sci. 285 (2007) 953-966.

[3] C. S. S. R. Kumar and F. Mohammad, Magnetic nanomaterials for hyperthermia-based therapy and controlled drug delivery, Adv. Drug Delivery Rev. 63 (2011) 789-808.

[4] Y. L. Golovin, S. L. Gribanovsky, D. Y. Golovin, N. L. Klyachko, A. G. Majouga, A. M. Master, S. Marina and A. V. Kabanov, Towards nanomedicines of the future: Remote magneto-mechanical actuation of nanomedicines by alternating magnetic fields, J. Controlled Release 219 (2015) 43-60.

[5] S. Suzuki and A. Satoh, Influence of the cluster formation in a magnetic particle suspension on heat production effect in an alternating magnetic field, Colloid Polym. Sci. 297 (2019) 1265-1273.

[6] Z. Zhao and C. Rinaldi, Magnetization dynamics and energy dissipation of interacting magnetic nanoparticles in alternating magnetic fields with and without a static bias field, J. Phys. Chem. C 122 (2018) 21018-21030.

[7] D. Soto-Aquino and C. Rinaldi, Nonlinear energy dissipation of magnetic nanoparticles in oscillating magnetic fields, J. Magn. Magn. Mater. 393 (2015) 46-55.

[8] A. Satoh and R. W. Chantrell, Application of the lattice Boltzmann method to many particle dispersions, J. Fluid Sci. Tech. 6 (2011) 114-127.

[9] Y. Ido, H. Sumiyoshi and H. Tsutsumi, Simulations of behavior of magnetic particles in magnetic functional fluids using a hybrid method of lattice Boltzmann method, immersed boundary method and discrete particle method, Comput. Fluids 142 (2017) 86-95.

[10] K. Han, Y. T. Feng and D. R. J. Owen, Three-dimensional modelling and simulation of magnetorheological fluids, Int. J. Numer. Meth. Engng. 84 (2010) 1273-1302.

[11] A. Satoh, Feasibility of the multi-particle collision dynamics method as a simulation technique for a magnetic particle suspension, Mol. Simul. 46 (2020) 213-223.

[12] D. Zablotsky, Field effect in the viscosity of magnetic colloids studied by multi-particle collision dynamics, J. Magn. Magn. Mater. 474 (2019) 462-466.

[13] A. Satoh and R. W. Chantrell, Application of the dissipative particle dynamics method to magnetic colloidal dispersions, Mol. Phys. 104 (2006) 3287-3302.

[14] A. J. Gharibvand, M. Norouzi and M. M. Shahmardan, Dissipative particle dynamics simulation of magnetorheological fluids in shear flow, J. Braz. Soc. Mech. Sci. Eng. 41 (2019) 103.

Research performances regarding the present study

Journal papers

1. K. Okada and A. Satoh, Quasi-2D Monte Carlo simulations of the regime change in the aggregates of magnetic cubic particles on a material surface, Mol. Phys. 115 (2017) 683-701. (IF=1.704)
2. K. Okada and A. Satoh, Dependence of the regime change in particle aggregates on the composition ratio of magnetic particles with different magnetic moment directions, Colloids Surf., A 557 (2018) 146-154. (IF=2.829)
3. K. Okada and A. Satoh, 3D Monte Carlo simulations on the aggregate structures of a suspension composed of cubic hematite particles, Mol. Phys. 116 (2018) 2300-2309. (IF=1.704)
4. K. Okada and A. Satoh, Evaluation of the translational and rotational diffusion coefficients of a cubic particle (for the application to Brownian dynamics simulations), Mol. Phys. 118 (2019) e1631498. (IF=1.51)
5. K. Okada and A. Satoh, Brownian dynamics simulations of a cubic haematite particle suspension with a more effective treatment of steric layer interactions, Mol. Phys. 118 (2020) e1740806. (IF=1.51)

International conference (Oral presentation in English)

1. K. Okada and A. Satoh, Phase change in aggregate structures of magnetic cube-like particles on a plane surface by means of Monte Carlo simulations, ECIS 2016, Roma, (Italy), September, 2016, (Oral presentation).
2. K. Okada and A. Satoh, Monte Carlo simulations on the aggregate structures in a suspension composed of magnetic cubic particles on a material surface, AIChE2017, Minneapolis, (America), November, 2017, (Oral presentation).
3. K. Okada and A. Satoh, 3D Monte Carlo simulations on the preferred configuration of cubic hematite particles in the aggregate structures, IMECE2018, Pittsburgh, (America), November, 2018. (Oral presentation).
4. K. Okada and A. Satoh, Analysis of a stokes flow past a cube (Friction and diffusion coefficients for Brownian dynamics simulations), IMECE2019, Salt Lake City, (America), November, 2019. (Oral presentation).

International conference (Poster presentation in English)

1. K. Okada and A. Satoh, 3D Monte Carlo simulations on a regime change in the internal structure of the aggregates of magnetic cubic particles, ECIS2017, Madrid, (Spain), September, 2017. (Poster presentation).

2. K. Okada and A. Satoh, The aggregate structures of magnetic cubic particles in thermodynamic equilibrium by means of Brownian dynamics simulations, AIChE2019, Hyatt Regency, (Orlando), November, 2019. (Poster presentation).

Transactions of the JSME (in Japanese)

1. A. Satoh and K. Okada, Two-dimensional Monte Carlo simulations on transition of aggregate structures of a suspension composed of cubic hematite particles, Transactions of the JSME (in Japanese), Vol. 81, No.831 (2015), DOI: 10.1299/ transjsme.15-00484.
2. K. Okada and A. Satoh, Aggregate structures of a suspension composed of cubic hematite particles by means of three-dimensional Monte Carlo simulations, Transactions of the JSME (in Japanese), Vol. 83, No.856 (2017), DOI: 10.1299/ transjsme.17-00378.
3. A. Satoh, K. Okada and M. Futamura, 3D Monte Carlo simulations on the control of the aggregate structures of cubic magnetic particles in terms of an external electric field, Transactions of the JSME (in Japanese), Vol.84, No.868 (2018), DOI: 10.1299/transjsme.18-00321.
4. K. Okada and A. Satoh, Diffusion coefficients of cube-like particles for application to Brownian dynamics simulations, Transactions of the JSME (in Japanese), Vol. 85, No.871 (2019), DOI: 10.1299/ transjsme.18-00476.
5. K. Okada and A. Satoh, Application of the Brownian dynamics method to magnetic cube-like particle suspensions, Transactions of the JSME (in Japanese), Vol. 85, No.877 (2019), DOI: 10.1299/ transjsme.19-00236.
6. K. Okada and A. Satoh, Brownian dynamics simulations on the magnetorheological characteristics of a cubic hematite particle suspension, Transactions of the JSME (in Japanese), Vol. 86, No.884 (2020), DOI: 10.1299/transjsme.19-00446.

Internal conference (Oral presentation)

1. K. Okada and A. Satoh, Monte Carlo simulations on the aggregation phenomena and the regime change in the aggregates of cube-like hematite particles on a two-dimensional surface, The 67th Divisional Meeting on Colloid and Interface Chemistry, Hokkaido, (Japan), September, 2016. (Oral presentation in English).
2. K. Okada and A. Satoh, The elucidation of the magnetorheological characteristics of a suspension composed of cubic magnetic particles by means of Brownian dynamics simulations, the 55th congress and meeting on Tohoku affiliate, Miyagi, (Japan), March, 2020. (Oral presentation in Japanese).

Acknowledgement

The present study was conducted under the supervision of Professor Akira Satoh at Akita Prefectural University. This research would not have been possible without the support and encouragement of many people. The author of the present paper would like to acknowledge them.

First of all, I would like to give my sincere gratitude to Professor Akira Satoh for his support, guidance and valuable comments. I had been directly instructed by Professor Satoh for a total of seven years in undergraduate, masters and doctoral courses since I was assigned to Prof. Satoh's laboratory. He provided me with many valuable experiences such as presentations at international conferences and journal paper writing. In addition, he also provided me with an excellent environment for my research. If I had not been assigned to the present research group, I would not have gained such valuable experiences. It is obvious that a meeting with Prof. Satoh has been a turning point in my life. I would like to deeply thank Prof. Satoh for his technical and mental support of my academic life.

Secondly, I would like to express my appreciation to Dr. Noriyuki Hirota, Prof. Tsutomu Ando, and Associate Prof. Satoshi Ogata for their valuable comments and helpful suggestions. Dr. Noriyuki Hirota is a Principal Researcher with the National Institute for Materials Science (NIMS) in Japan. He gave me valuable opinions and comments regarding the magnetic properties and the aggregate structures of a magnetic particle suspension from a materials science perspective. Tsutomu Ando who is Professor at Nihon University and Satoshi Ogata who is Associate Professor at Tokyo Metropolitan University gave me various advice as fluid dynamics experts for improving my thesis and fruitful suggestions for my future research from a simulator's point of view. Their comments and suggestions in the interim presentation were extremely valuable to the author and thus have greatly contributed to the writing of this thesis. I would like to express my deep gratitude to them.

Thirdly, I would like to express my special thanks to Assistant Professor Muneo Futamura at Akita Prefectural University for kindness and cooperation. He gave me some advice for future research and future marriage life. Moreover, he drove us to the venue of an internal conference. I would like to thank Assistant Prof. Futamura for his help in the laboratory.

I would like to thank Rafael Cuadra who is currently a working doctoral student at Akita Prefectural University for inspiring my passion for research. I am grateful to Seiya Suzuki who is currently a doctoral student. He has been instrumental in maintaining my mental and emotional health. I wish to thank all members of the present laboratory for their cooperation.

Finally, I would like to acknowledge the financial support from Grant-in-Aid for JSPS Fellows (18J21020). I also received financial supports from the Marubun Research Promotion Foundation, the Yoshida Foundation for Science and Technology, the Foundation for the Promotion of Engineering Research, and The Murata Science Foundation in order to attend some international conferences.